

THESIS ON MECHANICAL ENGINEERING E87

**Design and Technology of
Oxides-Containing Ceramic-Based
Composites**

NIKOLAI VOLTŠIHHIN

TUT
PRESS

TALLINN UNIVERSITY OF TECHNOLOGY

Faculty of Mechanical Engineering
Department of Materials Engineering

Dissertation was accepted for the defence of the degree of Doctor of Philosophy in Engineering on October 28, 2014.

Supervisors: Leading research scientist, Dr.Sci. Irina Hussainova,
Department of Materials Engineering, Tallinn University of
Technology, Estonia

Senior researcher, PhD. Maksim Antonov, Department of
Materials Engineering, Tallinn University of Technology,
Estonia

Opponents: Prof. Michael Gasik, AALTO University Foundation, School of
Chemical Technology, Finland

PhD. Kaupo Kukli, University of Tartu, Institute of Physics,
Estonia

**Defence of the thesis: December 8, 2014 at 11.00, Tallinn University of
Technology, Ehitajate tee 5, room U06-220.**

Declaration:

*Hereby I declare that this doctoral thesis, my original investigation and
achievement, submitted for the doctoral degree at Tallinn University of
Technology has not been submitted for any academic degree.*

/Nikolai Voltšihhin/



European Union
European Social Fund



Investing in your future

Copyright: Nikolai Voltšihhin, 2014

ISSN 1406-4758

ISBN 978-9949-23-703-6 (publication)

ISBN 978-9949-23-704-3 (PDF)

MEHHANOTEHNIKA E87

**Oksiide sisaldava
komposiitkeraamika tehnoloogia**

NIKOLAI VOLTŠIHHIN

CONTENTS

LIST OF PUBLICATIONS.....	7
INTRODUCTION.....	8
APPROBATION.....	9
ABBREVIATIONS.....	10
1 REVIEW OF THE LITERATURE.....	11
1.1 Ceramics and ceramic-based composite materials.....	11
1.1.1 Zirconia.....	12
1.1.2 Hardmetals.....	13
1.1.3 Ceramic matrix composites.....	16
1.1.3.1 ZrC-based ceramic matrix composites.....	16
1.1.3.2 Alumina nanofibers added zirconia.....	19
1.2 Consolidation techniques.....	20
1.2.1 Pressureless sintering.....	20
1.2.2 Hot isostatic pressing.....	21
1.2.3 Spark plasma sintering.....	22
1.3 Objectives of the study.....	25
2 EXPERIMENTAL AND MATERIALS.....	26
2.1 Precursor materials and designed systems.....	26
2.2 Processing and methods.....	27
2.3 Sintering.....	28
2.4 Characterization of raw materials and produced specimens.....	30
2.4.1 Phase analysis and microstructure examination.....	30
2.4.2 Density and mechanical properties.....	31
2.4.3 Erosive and abrasive wear testing.....	31
3 PROCESSING AND PROPERTIES OF THE DESIGNED COMPOSITES.....	33
3.1 WC-Ni-ZrO ₂ hardmetal.....	33

3.1.1 Sintering features	33
3.1.2 Phase composition and microstructure.....	34
3.1.3 Properties of the produced materials.....	36
3.1.4 Results of wear testing	38
3.2 ZrC-ZrO ₂ ceramic	40
3.2.1 Processing of the materials.....	40
3.2.2 Microstructural characterization of composites	41
3.2.3 Properties of the produced composites	42
3.3 Alumina toughened zirconia composite material	44
3.3.1 Sintering of the produced mixture.....	44
3.3.2 Microstructure and properties characterization.....	44
4 CONCLUSIONS	47
REFERENCES	49
OTHER PUBLICATIONS BY THE AUTHOR.....	54
ACKNOWLEDGEMENTS	56
ABSTRACT	57
KOKKUVÕTE	58
CURRICULUM VITAE	59
ELULOOKIRJELDUS.....	61

LIST OF PUBLICATIONS

The present dissertation is based on the following papers, which are referred in the text by the Roman numerals I–IV.

- I. Hussainova, I., Antonov, M., **Voltšihhin, N.**, Kübarsepp, J., Wear behavior of Co-free hardmetals doped by zirconia and produced by conventional PM and SPS routines. *Wear* 312 (2014) 83–90.
DOI: <http://dx.doi.org/10.1016/j.wear.2014.01.014>
- II. **Voltšihhin, N.**, Hussainova, I., Cura, E., Hannula, S-P., Traksmaa, R., Densification and microstructure development in zirconia toughened hardmetals. *Key Engineering Materials* 527 (2013) 50–55.
DOI: <http://dx.doi.org/10.1016/j.ceramint.2013.12.063>
- III. Hussainova, I., **Voltšihhin, N.**, Cura, E., Hannula, S-P., Densification and characterization of spark plasma sintered ZrC-ZrO₂ composites. *Materials Science & Engineering A* 597 (2014) 75–81.
DOI: <http://dx.doi.org/10.1016/j.msea.2013.12.058>
- IV. **Voltšihhin, N.**, Rodríguez, M., Hussainova, I., Aghayan, M., Low temperature, spark plasma sintering behavior of zirconia added by a novel type of alumina nanofibers. *Ceramics International* 40 (2014) 7235–7244.
DOI: <http://dx.doi.org/10.1016/j.ceramint.2013.12.063>

INTRODUCTION

Ceramic matrix composites (CMC) and hardmetals are materials with a great potential and very wide application area. CMCs are widely used in almost all areas of our daily life because of unique combination of hardness and toughness; therefore, they are commonly used in tribo-applications. Hardmetals represent the materials with large content of hard phases bonded together by binder metal and mostly used in situations where wear resistance is of paramount importance. Wear is an area, which needs to be constantly developed and thus already functioning materials need to be improved. Materials selection and development of novel grades as well as design of proper technological process for their manufacturing is a major focus for modern industry. The need for composites of high performance is ever growing due to their ability to increase the overall productivity and improve energy efficiency in different applications.

The motivation for the research is the urgent need in a knowledge-based design, development and processing of the industrially applicable materials for decreasing losses related to wear.

Advancement in mechanical and wear resistant properties of the existing materials can be achieved by introducing the additional constituents into the composition of the material. Zirconium dioxide (ZrO_2) is considered as a versatile material being studied today. It has properties that can influence the behavior of already known materials, if it is added in right proportions and composite is produced under needed conditions.

Traditionally, CMCs are produced with the help of powder metallurgy (PM) routes. PM allows fabrication of novel materials components with near net shape, intricate features and good dimensional precision pieces, which are often finished without the need of machining [1]. PM technique gives a number of process variables to improve the materials properties and mechanical behavior. The most important processes used in PM are mixing, pressing and sintering. Sintering is considered the most important and complicated operation. There are different approaches for sintering and each has a significant effect on a final product. Therefore, the technological goal of the study was to select a process and a proper routine for consolidation of CMC and hardmetals with zirconia additives.

The objective of this study is to develop and fabricate the ceramic-based composites of increased indentation fracture toughness (IFT) and reliability by incorporating sintering additives that simultaneously serve as toughening reinforcing components.

To achieve the goal, different consolidation techniques were exploited including such routines as hot isostatic pressing (HIP) and spark plasma sintering (SPS).

APPROBATION

- 1 37th International Conference on Advanced Ceramics & Composites ICACC, Daytona Beach, FL, USA, 2013.
- 2 The 22nd International Baltic Conference of Engineering Materials and Tribology, BALTMATTRIB, Riga, Latvia, 2013.
- 3 The 21st International Baltic Conference on Engineering Materials and Tribology, BALTMATTRIB, Tallinn, Estonia, 2012.
- 4 8th International Conference of DAAAM Baltic Industrial Engineering, Tallinn, Estonia, 2012.
- 5 15th Conference on Composite Materials, ECCM15, Venice, Italy, 2012.
- 6 3rd European Conference on Tribology and 4th Vienna International Conference on Nano Technology, Vienna, Austria, 2011.

ABBREVIATIONS

ANF – Alumina nanofiber

ATZ – Alumina toughened zirconia

AZ – Alumina-zirconia composite

BPR – Ball to powder ratio

CMC – Ceramic matrix composite

FT – Fracture toughness

HIP – Hot isostatic pressing

HTC – High temperature composite

IFT – Indentation fracture toughness

LPS – Liquid phase sintering

PM – Powder metallurgy

PSZ – Partially stabilized zirconia

SEM – Scanning electron microscope

SPS – Spark plasma sintering

VPS – Vacuum pressureless sintering

XRD – X-ray diffraction

YTZ – Yttria stabilized tetragonal zirconia

Y-PSZ – Yttria partially stabilized zirconia

ZTA – Zirconia toughened alumina

wt.% – Weight percentage

kX – Thousand of times magnification in the SEM

1 REVIEW OF THE LITERATURE

1.1 Ceramics and ceramic-based composite materials

Ceramics are chemical compounds of the metallic and nonmetallic elements. Oxides, nitrides and carbides are the most common representatives of this group of materials. In the mechanical behavior, ceramic materials are relatively stiff and strong [2]. In addition, they are typically very hard but exhibit extreme brittleness (lack of ductility) and are highly susceptible to fracture (Figure 1.1 made with CES edupack).

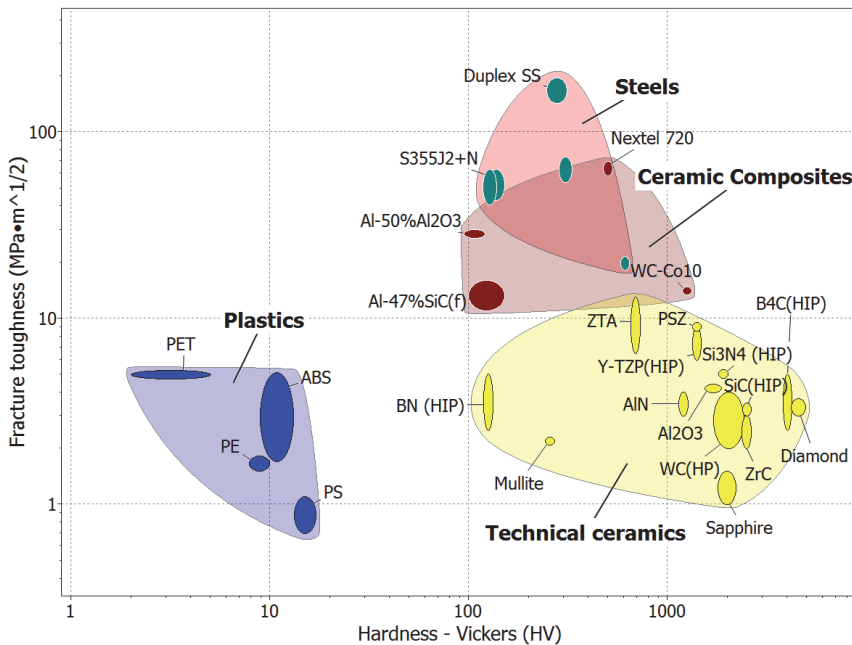


Figure 1.1 Balloon graph of fracture toughness resistance against hardness for various metals, ceramics, and composite materials

The progress in structural ceramics and CMCs requires the development of new design methodologies to produce materials with improved fracture toughness as it measures the resistance of a material to growth of a crack [3].

Among all mechanical properties, low resistance to fracture is considered as one of the most problematic issue for ceramics limiting their application. There are different ways to improve fracture toughness of ceramic materials. From mechanical point of view, any energy dissipation during crack propagation will reduce a driven force for crack growth. Mostly studied mechanisms for improvement in crack growth resistance are [4–6]:

- toughening by metal particles,
- crack deflection toughening,
- toughening by whiskers
- micro-crack toughening,
- crack bridging and

- transformation toughening

Present research is concentrated on obtaining the mechanisms of transformation toughening and toughening by whiskers. These mechanisms (as well as toughening by metal particles) can be obtained by introducing additives to the main composition, thus making it possible to vary the final parameters needed for these mechanisms to occur. The transformation toughening is known as a mechanism that emanates from the additional phase present in the main material matrix. The widely known representative material of transformation toughening is zirconia.

1.1.1 Zirconia

Transformation toughening is now well established mechanism for reducing the brittleness of ceramics [7, 8]. The well-known examples are composites of metastable tetragonal zirconia ($t\text{-ZrO}_2$) precipitates. Such materials represent partially stabilized ZrO_2 , zirconia toughened alumina (ZTA) and tetragonal ZrO_2 polycrystals ($t\text{-ZrO}_2$). The factors controlling the metastability of $t\text{-ZrO}_2$ particles leading to a "particle size effect" are [9]: (a) matrix constraint, (b) chemical composition, (c) the nucleation barrier to transformation as well as (d) stabilizer type, stabilizer amount, (e) grain size and grain size distribution, and (f) residual stresses [10–12] etc. The mechanical properties of the composite, i.e. fracture toughness, bend strength and thermal shock resistance, are significantly improved by the interaction of propagating cracks with ZrO_2 particles. The stress field at the crack tip nucleates the tetragonal to monoclinic transformation in the metastable particles which then undergo a volume increase (Figure 1.2). Some of the crack energy is dissipated in nucleating the transformation. The transformed particles near the edges or tip of the crack exert constraints in crack vicinity. This is responsible for the behavior of the materials, in which the toughness increases with increasing length of the crack [10].

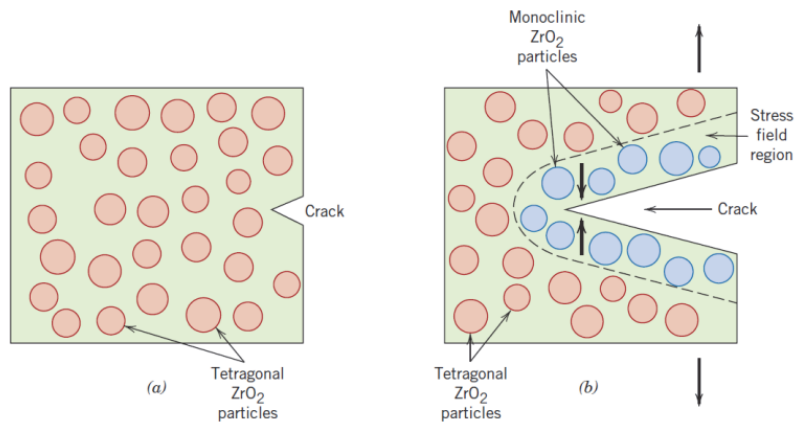


Figure 1.2 Schematic representation of stress-induced tetragonal-to-monoclinic (martensitic) phase transformation of zirconia [3]

The transformation crystallography of confined ZrO_2 particles has been examined both experimentally and theoretically [13–19].

Transformation toughening of materials based on the martensitic phase transition in ZrO_2 systems has been widely studied [20] and results demonstrated a potential for exploitation of stabilized tetragonal zirconia as a toughening agent in different ceramic matrices. Incorporation of potential crack growth inhibitor into the hardmetal matrix with a smart fabrication technology gives a solution for the production of the material with improved tolerance to impact loading.

Tetragonal to monoclinic phase transformation and associated volume change of ZrO_2 is one of the challenges when it is used to modify ceramic matrixes. Thermal residual stresses during sintering process and/or high temperature loads are the most critical parameters influencing transformability of tetragonal ZrO_2 particles located in the carbide material matrix. Wide variety of experiments have been made on zirconia as a toughening component with other ceramic materials, including TiB_2 , TiC, WC, ZrC and others [21].

1.1.2 Hardmetals

WC-Co material is widely used in industrial applications. The variety of WC-based materials is used in a broad range of applications, including metal cutting, mining, construction, rock drilling, metal forming, structural components, and wear parts.

Conventionally hardmetals are produced under liquid phase sintering conditions with cobalt as a binder phase. However, a cheaper and of same or higher quality substitutes for cobalt can be introduced into the WC-based hardmetals as a binder material. Some studies have been performed in order to find the satisfactory alternative binder [22–25]. It has been shown that using Ni as a binder increases resistance to oxidation and corrosion while mechanical properties of the WC-Co composites are slightly higher [26, 27]. Therefore, Ni is used in this study as a binder for WC-based hardmetal.

It is a well-known fact that the homogeneous distribution of phases in composites is a half the battle for designed mechanical, tribological and other properties of multi-phase materials. The structures of hardmetals are optimized for different applications by varying the binder content as well as the composition and grain size of the hard phases [28–30]. Submicron microstructures in WC-Co materials can be achieved by adding some small amounts of tantalum carbide (TaC), niobium carbide (NbC), vanadium carbide (VC), or chromium carbide (Cr_3C_2) with VC being the most efficient for grain growth hindering and Cr_3C_2 also adds enhancement to the mechanical properties [31–34].

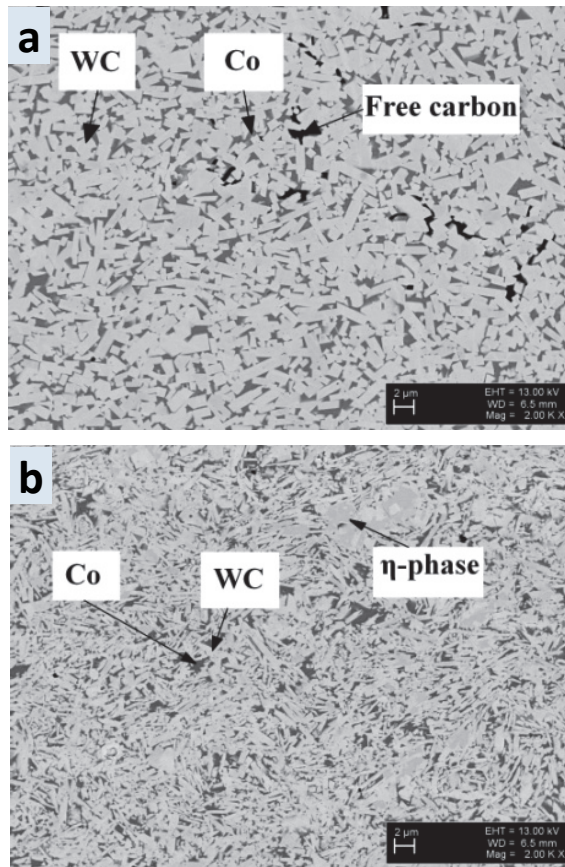


Figure 1.3 Microstructure of a) WC-Co hardmetal with a free carbon inclusions b) eta-phase microstructure [31]

The carbon content in WC-Co hardmetals plays a great role and must be controlled within the narrow limits [35, 31]. Excessive carbon amount results in the appearance in the microstructure of free and finely divided graphite (Figure 1.3 a), which is classified as C-type porosity [36]. Deficiency in carbon amount during formation of WC composite, results in the formation of a series of double carbides such as $\text{Co}_3\text{W}_3\text{C}$ or $\text{Co}_6\text{W}_6\text{C}$. These formations are called η -phase (eta-phase), which are unfavorable because of their high brittleness. The η -phase can be seen in Figure 1.3 b.

The additive carbon content does not only take part in elimination of η -phase while it also influences the growth of WC grains if its amount is increased [37]. However, the carbide grain growth in the WC-Co structures is dependent on the sintering technique used for the production of the material.

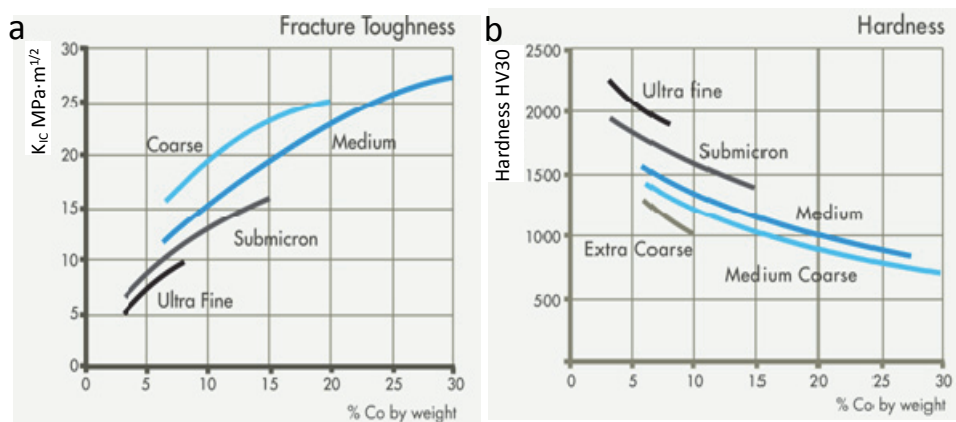


Figure 1.4 Graphs representing a) fracture toughness and b) hardness dependences on the Co content and grain size in the WC-Co hardmetals [38]

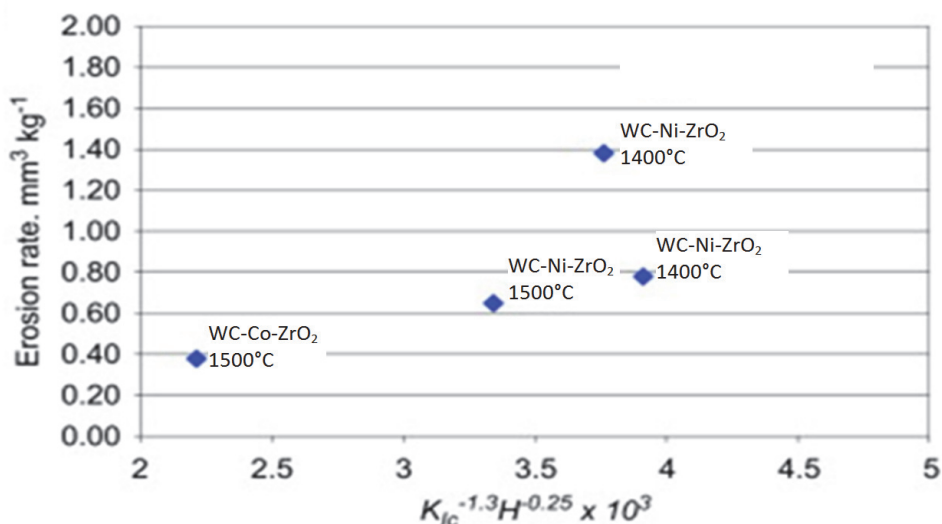


Figure 1.5 Erosion wear as a function of $K_{Ic}^{-1.3} H^{-0.25}$. Compositions and sintering temperatures are indicated [39]

All stated microstructural and compositional parameters, such as grain size and presence of eta-phase, affect the mechanical properties of the bulk materials. Figure 1.4 represents dependence of hardness and fracture toughness on the grain size and the cobalt content of the produced hardmetals. Erosive wear as a function of both fracture toughness and hardness of the product is represented in Figure 1.5 [38–40]. Therefore, properties of these materials are synergistic and are influenced by the fabrication method.

Even though, hardmetals and especially WC-Co have proved their unique properties for almost a century there is still a tendency to develop and improve its' mechanical and wear behavior. In recent decades, research interests have been focused on improvement of composites reliability and durability [41–45].

Zirconia additive to the WC-based composites is leading to a lower hardness while retaining the composite properties under high temperature and oxidative conditions [46]. Zirconia is not capable to provide the same ductility as a metallic binder; however, its unique toughening capability can provide an increased fracture toughness and, if some minimum amount of metal binder is left in the composite, it can provide the composite with some additional ductility as well.

1.1.3 Ceramic matrix composites

The fracture toughness of the CMCs is being developed constantly and there has been a significant improvement in this area because of new types of CMCs, which are based on particulates, fibers, or whiskers of different ceramics added to the matrixes of other ceramics. As a result, some of CMCs have improved their fracture toughness to the values of $70 \text{ MPa}\cdot\text{m}^{1/2}$ (e.g. Nextel720).

1.1.3.1 ZrC-based ceramic matrix composites

Some of the CMCs constituents are refractory materials with high melting points of up to $3000 \text{ }^\circ\text{C}$ and high hardness due to the strong covalent bonding of their atoms. The number of the materials with melting point as high as $3000 \text{ }^\circ\text{C}$ is very limited and one of them is zirconium carbide ZrC.

Zirconium carbide (ZrC) belongs to a class of high temperature ceramics and meets all of the HTC requirements. Zirconium carbide exhibits high hardness ($\sim 25.5 \text{ GPa}$) and modulus of elasticity ($350\text{--}440 \text{ GPa}$) as well as high electrical conductivity (resistivity $78 \times 10^{-6} \text{ } \Omega\cdot\text{cm}$) combined with a high melting point at about $3440 \text{ }^\circ\text{C}$. Representatives of HTC group of materials, including ZrC, are not commonly found in nature. There are different ways of synthesis of such kind of materials; and depending on the production technique used the quality of the final powders can be different [47–49].

Due to the high melting point and strong covalent bonding between atoms of ZrC, it is difficult to sinter this carbide with conventional techniques and without additional pressure during sintering process. To improve mechanical performance and increase sinterability of the structure and tolerance to loading, special additives should be used. Among mostly studied ZrC-based composites, there are ZrC-Mo refractory hardmetals and ZrC-ZrO₂ composites produced by different routines [50–53]. Sciti et. al. [52] prepared ZrC with different MoSi₂ additives and sintered those with the help of SPS. Densities close to the theoretical one have been obtained, Figure 1.6.

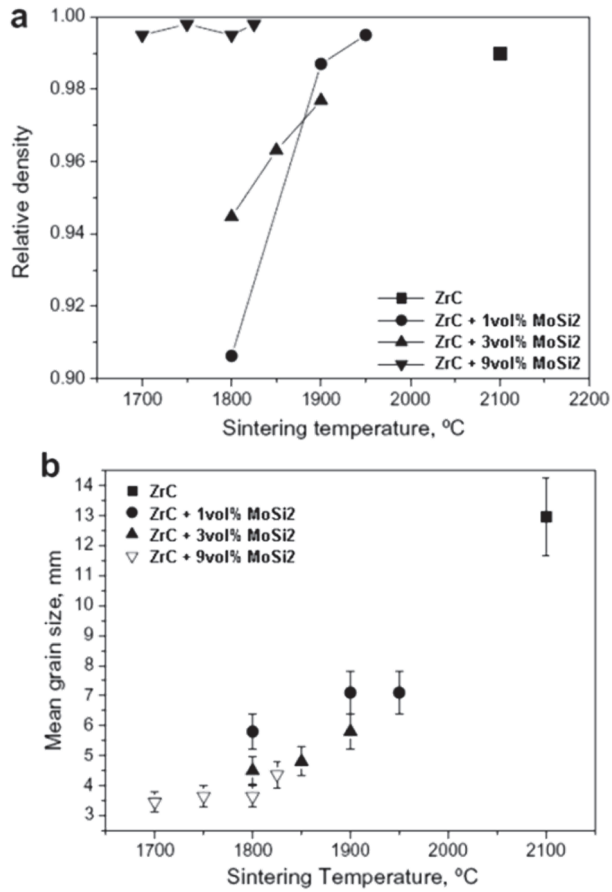


Figure 1.6 Dependence of the a) relative density and b) mean grain size on the sintering temperature [52]

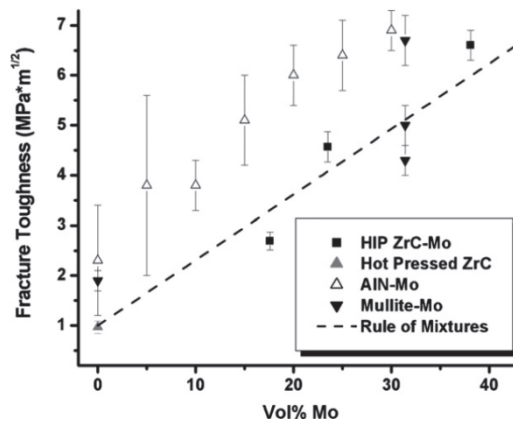


Figure 1.7 Fracture toughness values for different materials, including ZrC-Mo composite [53]

Sintering of ZrC with different amounts of Mo by hot isostatic pressing resulted in densities close to theoretical. Fracture toughness increases with increasing in Mo content, Figure 1.7 [53].

One of the examples of zirconia content influence on the toughness of ZrC ceramic composite is depicted in Figure 1.8a [51]. It has been shown that with increasing content of zirconia in ZrC–ZrO₂ structure, the fracture toughness of ZrC-based composite also increases. The hardness of ZrC–ZrO₂ composite also increases with increasing ZrO₂ content. The main reason for a higher hardness of ZrO₂-added CMC in comparison with pure ZrC is internal porosity of the undoped ZrC.

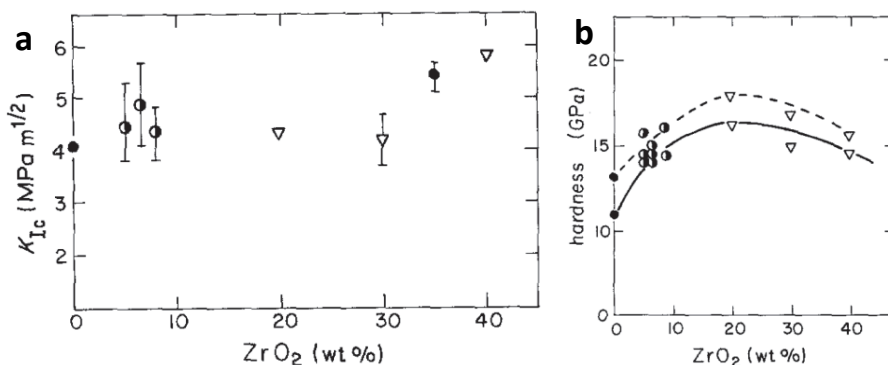


Figure 1.8 Graphs of the ZrC-ZrO₂ representing a) fracture toughness measured by notched beam increases with increasing zirconia content reaching a maximum value of 5.8 MPa m^{1/2} at 40 wt.%. and b) hardness, Vickers (---) and Knoop (-) hardness techniques, (●, ○) Specimens containing Type B ZrO₂, ball milled and pressed. (▽) Type A ZrO₂, dispersed and cast. (▽) 2000 °C (●) 2200 °C (○) 2400 °C [51]

In other study ZrC was combined with TiC in order to improve the sinterability of ZrC. The composite was sintered with SPS technique to obtain material of high hardness. It was revealed that this composite material improves the elasticity modulus with increasing dwell time of sintering for the SPS technique (Figure 1.9).

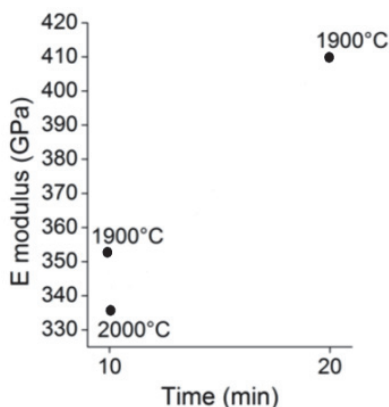


Figure 1.9 Effect of sintering parameters on ZrC-25 vol.% TiC composite properties [IX].

1.1.3.2 Alumina nanofibers added zirconia

One type of composite materials acting under crack bridging and crack deflection mechanisms is called whisker reinforced ceramics in which fiber like particles of some other ceramic material are used for reinforcement of the base ceramic [54, 55]. The main aim of the whisker reinforced ceramics is dedicated to the high strength and stiffness with an advantage in weight over many other groups of materials. Even though, the widely known whiskers to be added to ceramic matrix are SiC or Si₃N₄ more new ceramic whisker types come into play.

Alumina nanofibers (ANF) have been recently developed [56–58]. They can be seen on Figure 2.1. The diameter of the alumina fibers varies between 7 and 40 nm. Due to nanosize, they have a large surface area and highly agglomerated. Therefore, it is a challenge to provide accurate dispersion of the nanofibers throughout the matrix. The fibers are thermally stable at temperatures of up to 1100 °C after which gamma phase may undergo transformation into alpha phase following by fibers decomposition into particles [58]. This property makes these fibers useful for refractory applications, at the same time making them difficult to produce dense ceramic composite material.

Zirconia toughened alumina ZTA is a widely known ceramic composite material. This material main constituent is alumina, which contains different amounts of zirconia. Zirconia is added into alumina as a sintering aid to increase sinterability of the composite and as a toughening agent (for increasing of the fracture toughness) [59–61]. Noted for their mechanical properties, composites are commonly used in structural applications, such as cutting tools, grinding media and in many medical applications. However, there are cases where zirconia is used as the main phase and alumina is serving as a doping additive for increasing properties [62]. In this case, the composite is called alumina toughened zirconia (ATZ).

Using new approaches for well-known materials compositions is always of a scientific interest. This approach can consist of a new production technique or an improved type of the same material or in using different design of the microstructure, or this approach can be a combination of all of the named methods. One of the approaches is based on introduction of a novel type of alumina nanofibers into the zirconia matrix as a toughening agent. Therefore, material containing both zirconia and alumina fibers should act under several toughening mechanisms when fracture conditions are applied.

Conventional sintering temperature for obtaining near full density material from nanosize zirconia and alumina is in the range from 1300 to 1500 °C. This is a challenge for production of material which transforms at 1200 °C and nonstandard, pressure-assisted sintering technologies, such as hot press (HP) or SPS could be used [63]. It has already been shown that nanosized aluminum oxide can be sintered at temperatures as low as 1225 °C and that SPS technology does significantly decrease the densification temperature and dwell time, especially if precursor powders are of nanoscale [64].

1.2 Consolidation techniques

It is well-known that properties of the fabricated product are strongly dependent on the number of input parameters, such as quality of the precursor material (including purity, production method and grain size), addition of grain growth inhibitors and other dopants for controlling unwanted phases formation, fabrication method and so on [65]. Numerous attempts have been made to study a phenomenon of densification and influence of sintering parameters on the final product. However, any novel grade requires specific conditions of sintering and precursor powder preparation including powders mixing, drying, plasticizing and pressing [66–68]. Sintering is a core operation for formation of the final product by PM routines. Depending on sintering technique and parameters of the sintering process, the properties of the output part can widely vary.

There are many different sintering techniques used in PM, which can be divided into 2 big groups: continuous and batch furnaces. The batch furnaces can also be divided into 2 sub-groups, which are schematically depicted on Figure 1.10. As pressure plays a great role in production technology of full density powder materials and products, especially ceramic products, it should be represented as a separate group.

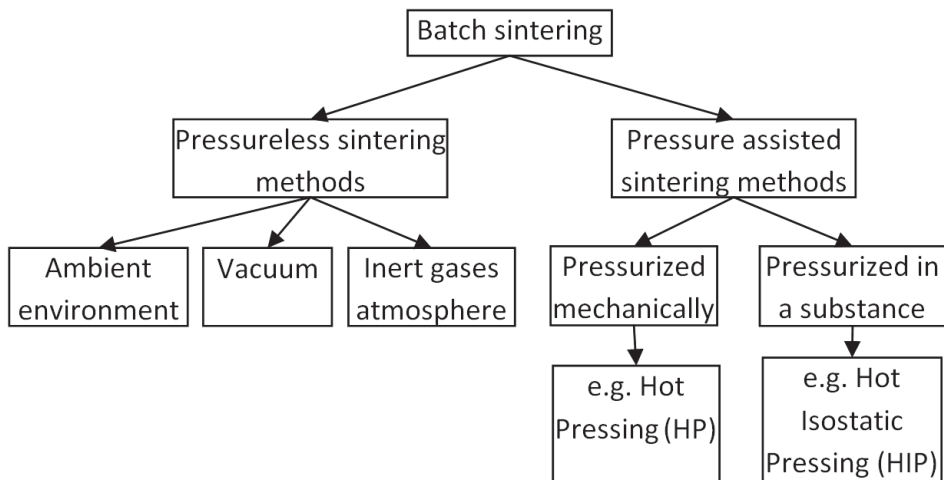


Figure 1.10 Schematic representation of the batch sintering processes

1.2.1 Pressureless sintering

One of the easiest and cheapest PM consolidation methods is sintering of the compacted green bodies in the ambient environment by applying the heat produced by resistance heaters. However, this method can be used only for certain type of materials – mostly oxides, because of air substances can react with most materials at high temperatures. In cases different from sintering of oxides, vacuum or protective environment, such as argon, should be used in order to prevent oxidation and degradation of materials.

Due to high surface energy of the powder particles they seek to decrease their free energy. When the speed of the atoms diffusion is increased by heat, particles reduce their energy by merging with each other and forming single particle. This explanation describes sintering process in common and mostly for solid state sintering. The sintering of at least two components, in which one has lower melting point than another, and sintering temperature is higher than this component' temperature is called liquid phase sintering (LPS) [69].

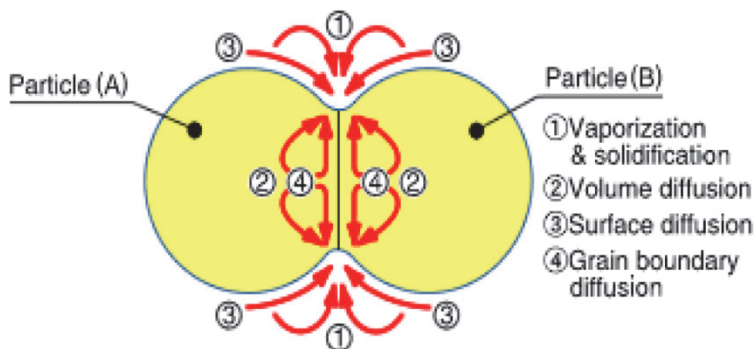


Figure 1.11 Representation of atoms diffusion mechanisms during sintering process [63]

Sintering occurs when atoms start to diffuse through the microstructure. This diffusion is caused by gradient of chemical potential. Some paths for transport of atoms during sintering are schematically represented in Figure 1.11.

Sintering of hardmetals and CMCs is often done using pressureless sintering techniques [70, 71]. However, pressureless sintering is a slow process where all the reactions flow naturally by the influence of heat mainly and sometimes require high temperatures and sintering additives for the near-full densification of the high melting temperature ceramics, which in some cases can deteriorate the properties or lead to the grain growth of the final product [72].

To provide the best interaction between the particles, they have to be compacted to the highest green density before introducing them into the heated furnace. This can be done by cold compaction techniques: uniaxial die compaction, cold pressing in rigid dies or cold isostatic pressing; and by hot compaction techniques such as hot pressing and hot isostatic pressing. Since the hot compaction techniques produce the final product, they are considered as the separate consolidation processes. Unlike the cold compacted–pressureless sintering methods, in the hot compacted–pressure assisted sintering the pressure is applied during the whole process or partially depending on the designed cycle.

1.2.2 Hot isostatic pressing

Hot isostatic pressing (HIP) technique plays an important role in development of ceramics and CMCs. The process consists in applying the high pressure and high temperatures, which may be applied simultaneously in a specially constructed vessel. High temperature and high gas pressure applied to workpiece result in fully isotropic material properties [73–75]. It is also a near-

net shape process, which gives an ability to produce complex shape products and thus gives advantages over other pressure assisted techniques such as hot pressing. Conditions of heat and pressure force internal pores or defects inside a solid body to collapse and provide diffusion bond. Densification of the encapsulated powder or pre-sintered components with HIP results in enhanced mechanical properties and standard deviation of the properties [76].

HIP technique has been studied on the variety of different possible material groups and compositions. One of the examples is a HIP sintered ZrC-MoSi₂ composite [53]. The dispersion processing of SiC whiskers and particles, and the mechanical properties of SiC particles and/or whisker-reinforced Al₂O₃ composites using HIP technology has been studied in [76]. Hardmetals can also be produced by HIP in order to remove different internal defects so that the maximum strength materials can be obtained.

Typical pressures and temperatures for production of different ceramic-based materials by HIP are shown in Table 1.1 [53, 75, 76].

Table 1.1 Parameters for HIP sintering of different materials [53, 75, 76]

Material	T, °C	Pressure, MPa
Al ₂ O ₃	1500	100
Al ₂ O ₃ /TiC	1935	150
Al ₂ O ₃ /ZrO ₂	1500	200
SiC	1850	200
B ₄ C	1850	200
WC/Co	1350	100
ZrC/Mo	1800	200
Y-PSZ	1350–1500	100
TiC	1900	90

1.2.3 Spark plasma sintering

Spark plasma sintering (SPS) or as it is sometimes also called FAST (field assisted sintering technology) or PECS (pulsed electric current sintering) is a pressure assisted sintering technology, which uses a DC pulsed current in a range of 1–10 kA at 10–15 V and a high current intensity to heat up the powder filled up in a graphite (or ceramic) die [77]. The environment is a low vacuum. Pressure is applied by two graphite punches and a force is in the range of 50 to 250 kN. Current flows through the die wall, as well as through the powder and is activating the peculiar heating mechanisms. Schematic representation of the die construction and SPS process can be seen in the Figures 1.12 and 2.3.

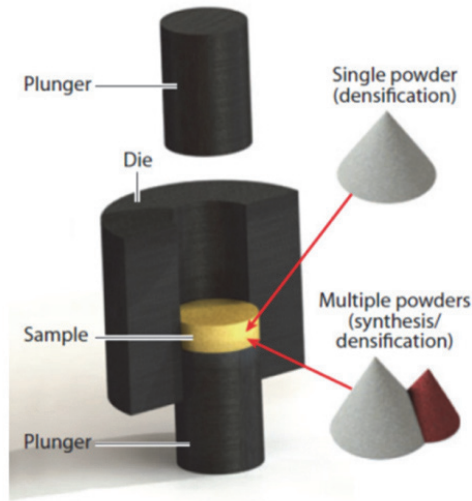


Figure 1.12 Representation of the SPS die [77]

The SPS process allows applying very high heating and cooling rates which enhances the densification through the grain growth stimulating diffusion mechanisms (see Figure 1.13). This allows maintaining the intrinsic properties of the initial powders, when those are already fully densified. This sintering technique is considered as a rapid sintering method, in which the heating power is distributed over the volume of the powder compact homogeneously in a macroscopic scale, but also it dissipates exactly at the locations in the microscopic scale, where energy is required for the sintering process, even at the contact points of the powder particles (see Figure 1.13) [63]. This fact results in a favourable sintering behavior.

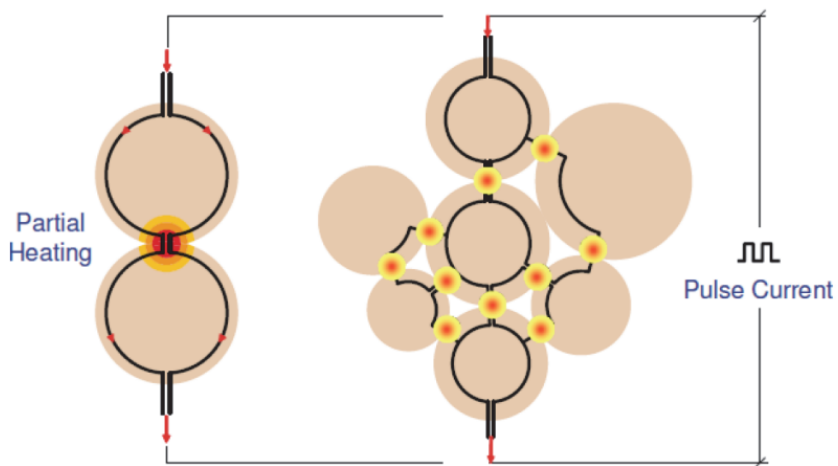


Figure 1.13 Energy dissipation on the microscopic scale [63]

Even though all sintering processes will influence the final product depending on the parameters, in case of SPS this impact is more pronounced.

Heating rate is one of the important parameters of SPS that affects the grain size and densification of materials. Usually SPS heating rate varies between 50 to 600 °C/min. High heating rates helps to obtain fine microstructure by inhibiting significant grain growth. A number of studies have been done on the impact of heating rate on the densification and microstructure of ceramic materials by SPS [78, 79].

The sintering temperature is selected based on the melting point temperature of the material to be sintered [77]. The source of heat production is from the Joule heating produced by the pulsed direct current. Joule heating makes the particle weld together under current passing through them.

Applying pressure together with temperature improves sinterability and results in a better densification of the material. In the earlier stages of sintering pressure helps in rearrangement of the particles and to obtain a compact powder. This helps in eliminating porosity at initial stages of sintering. In later stages of sintering, the applied pressure helps in densification of the material by impacting the driving force of sintering. Xu et al. [80] studied the effect of pressure rate on the densification of zirconia and reported that the rate of densification improved with increase in rate of applied pressure.

Pulsed direct current used in SPS for sintering makes this technique interesting for research as it gives a possibility to change the supply of Joule heating very frequently during sintering cycle and to influence the final product as the result. The impact of pulse variation on the densification of materials has been studied [81]. However, studies indicate that the variation in the pulse rate did not have any significant impact on the densification of materials by SPS.

SPS systems offer many advantages over conventional systems, such as hot press (HP) sintering, hot isostatic pressing or atmospheric furnaces. Some of the advantages include ease of operation and accurate control of sintering energy as well as high sintering speed, high reproducibility, safety and reliability [63]. On the other side SPS has also disadvantages if compared to pressureless or HIP techniques. Those are mainly: problematic production of large size details because of the difficulty in provision of high current intensity and high loads, and impediment in production of net-shaped products, which is common problem for the uniaxial pressing techniques. In addition, control of temperature during SPS cycle is a problematic issue and temperatures measured on the die surface can be significantly different from those at the sample [81]. This can be an obstacle in production of materials with properties change at exact temperatures. However, heating rates as high as 1000 °C/min and very high cooling rates, due to the small heated thermal mass make this technique most attractive.

1.3 Objectives of the study

The overall objective of the work is to design oxides-containing ceramic-based composites and to find and develop the most appropriate technological method for their processing.

The main part of this research relates to improvement of sinterability and enhancement of mechanical properties of commercially known ceramic materials such as WC, Al₂O₃, ZrO₂, and ZrC by using different additives and different PM routines' approaches (mainly sintering) and to reveal the best combination of these variables for the given composite.

The main objective is to process the poreless ceramic-based composites with a homogeneous phase distribution throughout the matrix with increasing reliability of materials to resist fracture propagation. Increase of fracture toughness is to be obtained by means of incorporation of tetragonal zirconia (t-ZrO₂) as a toughening agent in brittle matrix or by introducing fibers into the ceramic matrix.

Throughout the thesis the following technological and scientific sub-goals are addressed:

- Design of the structures of ceramic-based composite containing oxides;
- Development and approval of sintering conditions and selection of the best suited parameters for processing of the abovementioned composites;
- Comprehensive microstructural and mechanical characterization of the materials.

To achieve the goals, the following activities have been performed:

- Studying the effect of the different sintering routines and sintering additives on the process of densification of the composite materials and microstructural parameters;
- Investigation the influence of sintering parameters, such as heating rates, pressure, holding time and nature of heating, on the microstructure development, transformability of tetragonal zirconia, mechanical properties of composite, and their wear resistance, etc.;
- Analysis of materials fracture modes and mechanical/wear properties;
- Stating of general recommendations for parameters of technological process and materials performance under loading.

2 EXPERIMENTAL AND MATERIALS

2.1 Precursor materials and designed systems

Three main composite systems with different amount of constituents were prepared for sintering with the help of different consolidation techniques. The raw materials used are listed in Table 2.1 along with the description.

Table 2.1 Powders for composites preparation

Powder	Particle size μm	Purity %	Designation	Supplier
WC	0.9 ^a	≥ 99.0	WC	Wolfram GmbH
Ni	3.0–7.0 ^b	99.7	Ni	Hunter Chemical LLC
ZrO ₂	0.025 ^a	98.2	PSZ	TOSOH
C	6.5 ^a	100.0	KS6	TIMCAL
ZrC	3.5 ^a	99.0	ZrC	Strategic Metal Investments Ltd.
Al ₂ O ₃ ^c	$\varnothing=0.040$	100.0	γ -phase	Metallurg OÜ

a-suppliers data, b-measured data, c - gamma-alumina nanofibers

Chemical composition of the designed materials is presented in Table 2.2.

WC-Ni material was added by ZrO₂ in order to study the influence of an additive on the mechanical and tribological properties of the hardmetal. The amount of 6 wt.% of ZrO₂ was assumed to be enough to distribute homogeneously in the microstructure and to initiate transformation toughening mechanism. The purpose of adding free carbon (C) to the WC-Ni-ZrO₂ was to avoid formation of η -phase and compare the densification behavior of composite in different sintering conditions using different techniques [37]. Also, 0.2 wt.%C added WC-Ni-ZrO₂ composite was added by 0.3 wt% of Cr₂C₃ in order to reduce grain growth during sintering.

ZrC was added by zirconia in order to increase the fracture toughness of brittle ZrC and to maintain all intrinsic to this material properties at most. Another aim of adding zirconia to ZrC was to decrease the sinterability temperature needed to produce dense material. Even though zirconia has high melting point it can be fully densified at temperatures of 1350 °C or even lower if appropriate technology is used, thus the overall densification temperature of the composite can be decreased [III].

Two compositions were produced with 37 and 23 wt.% of ZrO₂ in order to see the influence of zirconia addition on the behavior of ZrC.

In ZrO₂-Al₂O₃ composite, alumina nanofibers were added as a potential reinforcement agent. The fibers as a raw material are shown in Figure 2.1.

Table 2.2 Chemical composition of the designed composites (given in wt.%)

Grade	WC	Ni	ZrC	ZrO ₂	C	Al ₂ O ₃
WC-Ni-ZrO ₂	85.0–85.8	8.0	-	6.0	0.2–1.0	-
ZrC-ZrO ₂	1	-	-	77.0	23.0	-
	2	-	-	63.0	37.0	-
ZrO ₂ -Al ₂ O ₃	-	-	-	94.0	-	6.0

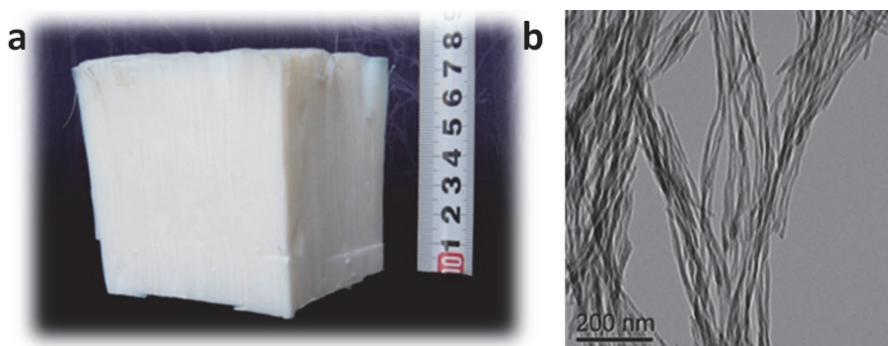


Figure 2.1 ANF precursor fibers on a) macro scale and b) nanoscale [82]

Since gamma-alumina nanofibers exhibit a phase transformation from gamma to alpha polymorph at a relatively low temperature and their following decomposition into the particle state, the idea was to sinter the composite at as low dwell temperature as possible and to leave alumina in the state of fibers [58, IV].

Firstly the alumina fibers were mixed with zirconia powder in amount of 40 wt.%. However, after mixing there were many bundles of fibers agglomerated together in the blend. These compositions could not be sintered to the maximum density. Therefore, 6 wt.% of ANF were added in order to produce a dense material with the fibers distributed evenly throughout the composite.

2.2 Processing and methods

A standard PM procedure was used to produce the abovementioned composite materials. The scheme of the procedure of production and testing of the specimens is schematically depicted in Figure 2.2.

The raw powders were milled/mixed in a ball mill for different periods of time, depending on initial grain size and production routine, dried and sieved. Mostly, ZrO₂ and WC grinding media with a 10:1 ball to powder ratio (BPR) were applied.

After milling, materials to be densified by vacuum pressureless sintering (VPS) route, ambient environment or hot isostatic pressing technique were cold compacted with the help of uniaxial press. The powders to be sintered with SPS technique were introduced into the die of the SPS furnace for the hot consolidation.

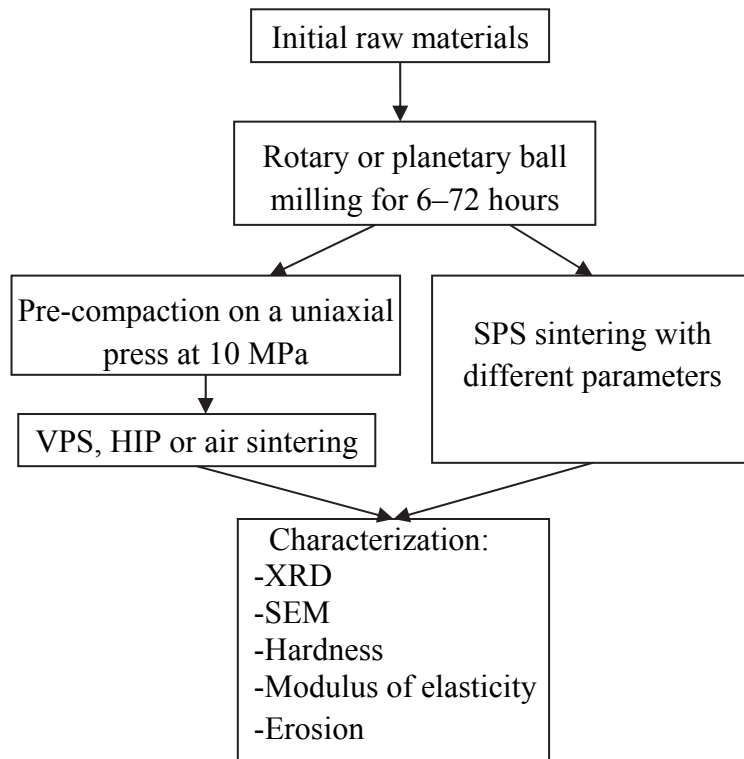


Figure 2.2 Schematic representation of the materials preparation and testing procedure

2.3 Sintering

Composites were sintered by four routines. The VPS, HIP and SPS furnaces used for sintering of the materials are shown in Figure 2.3. Vacuum sintering was performed using the Red Devil furnace (RD WEBB COMPANY, Figure 2.3a) with a vertical located thermocouple and horizontally located pyrometer. Temperatures higher than 1475 °C were measured with a pyrometer. HIP sintering was done using the AIP-HIP 30H furnace (American Isostatic Pressing, Figure 2.3b).

SPS sintering was performed with the help of two different furnaces: in experiment with ATZ composites – Dr. Sinter, SPS-510CE (Japan) was used; and in all other cases – FCT HP D 25-2 (Germany, Figure 2.3c). SPS furnaces have a vertically located pyrometer temperature control and operating at computer controlled regimes that allows data and sintering processes (such as densification behavior, temperatures, electrical parameters etc.) analyzing. The dilatometry sintering of the ATZ composite was done in a dilatometry equipment (Setaram, TMA Setsys 16/18, France). Air sintering was done in a XY-1200N sintering furnace (China).

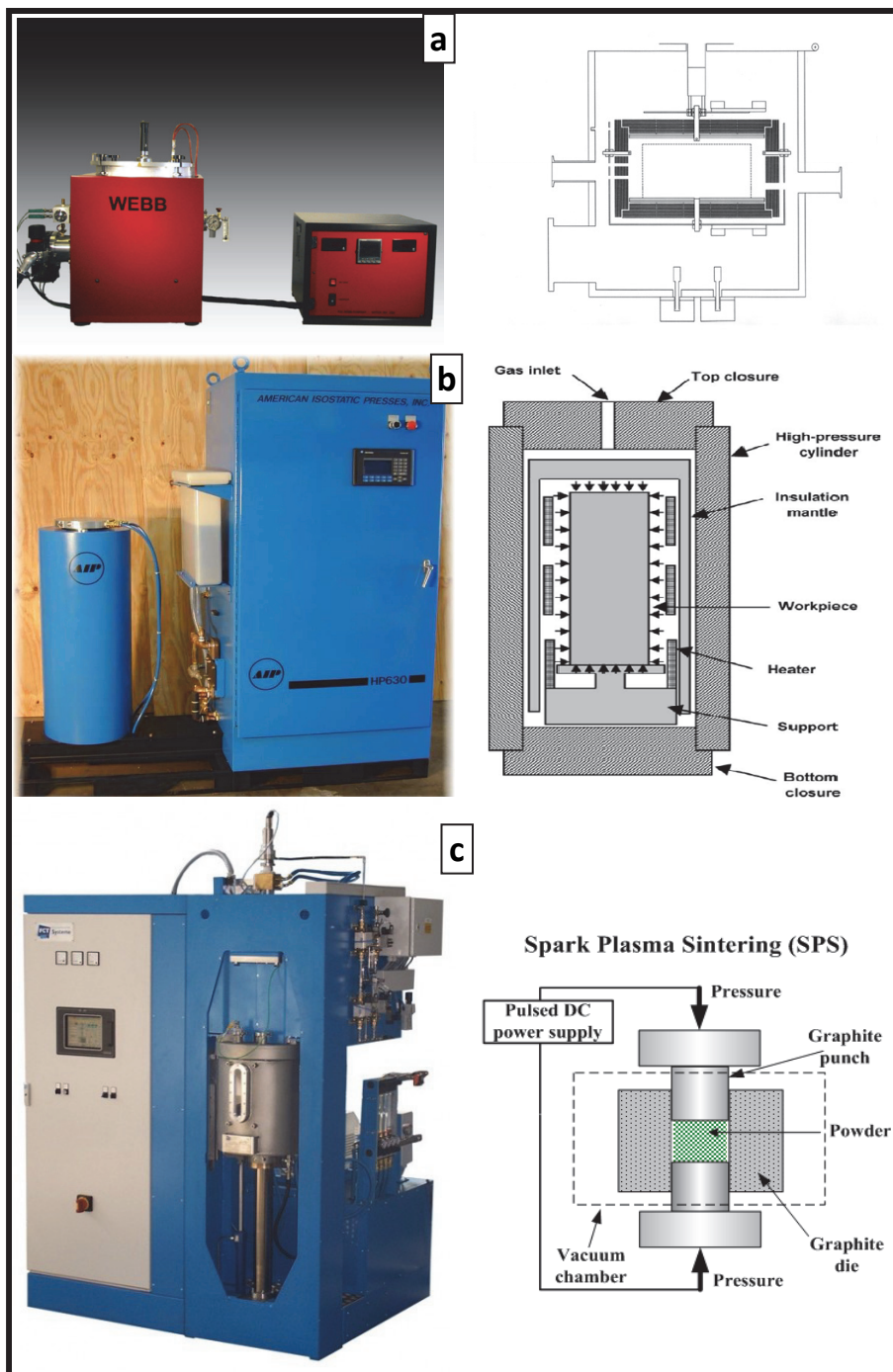


Figure 2.3 Sintering technologies and furnaces used in the study a) VPS; b) HIP; c) SPS [83–87]

A number of experiments were done in order to find a successful consistency of the components and processing parameters needed for stable specimens to be produced.

In Table 2.3 the most appropriate processing parameters are presented. Details on the experimental parameters can be found in the author's publications [I–IV].

Firstly, parameters for the sintering process were chosen theoretically taking into consideration melting points of the compounds. After first experiments, the set of parameters was chosen.

For the WC-Ni-ZrO₂ composite powders were sintered in an interval of 1350–1500 °C and different pressures up 200 MPa for conventional sintering methods. For the SPS method 2 temperatures were tested – 1200 °C and 1275 °C. In case of 1275 °C the grain size of the WC and ZrO₂ particles started to increase while density and other properties stayed on the same level.

Sintering temperatures of ZrC-ZrO₂ composite was varied between 1500–2000 °C and the temperature of 1600 °C was chosen as optimal. Sintering at higher temperatures does not result in better mechanical properties, while requires higher energy consumption.

In case of ZrO₂-ANF composite three different temperatures were studied for the SPS cycle and temperatures equal or above 1300 °C for the other sintering methods. The lowest sintering T °C had to be chosen in order to maintain the ANFs in their fiber state.

Table 2.3 Parameters used for sintering of different materials

Composite	Process	Heating rate °C/min	Cooling rate °C/min	T, °C	Dwell time min	Pressure MPa	Environment
WC-Ni-ZrO ₂ -C	VPS	10	natural	1450	45	5x10 ⁻⁶	high vacuum
	HIP	10	10	1450	45	200	Ar
	SPS	100	500	1200	1	50	Ar
ZrC-23wt.% ZrO ₂	VPS	10	natural	1600	40	5x10 ⁻⁶	high vacuum
	SPS	75	300	1600	10	50	Ar
ZrC-37wt.% ZrO ₂	VPS	10	natural	1600	40	5x10 ⁻⁶	high vacuum
	SPS	100	300	1600	10	50	Ar
ZrO ₂ -Al ₂ O ₃	Air sintering	10	natural	1300	60	ambient	ambient
				1000	5		
	SPS	100	500	1100	5	50	N ₂
				1200	5		

2.4 Characterization of raw materials and produced specimens

2.4.1 Phase analysis and microstructure examination

Phase compositions of the powders mixtures and bulk samples were analyzed with the help of two X-ray diffractometers (XRDs): Philips PW3830 X-ray Generator, 4 kW, Cu-Anode and Siemens Bruker D5005 analyzer with CuK α –radiation. Samples were irradiated with CuK α radiation at 40 kV and 30 mA, in a $\theta - 2\theta$ scan with a step size of 0.02° and a count time of 0.4 s.

Microstructures of the polished bulk surfaces were observed by the scanning electron microscopy (Hitachi S-4700 and EVO Zeis) equipped with EDS. Voltage of up to 20 kV and magnifications up to 20 kX and some cases up to 50 kX was applied for examination of the powders as well as polished and worn surfaces. The samples were studied under different regimes, including secondary and backscattered electrons modes.

2.4.2 Density and mechanical properties

The sintered density was measured by the Archimedes technique using distilled water as the immersion medium.

Hardness was measured on the Indentec 5030 SKV Vickers hardness tester with an indentation load of 10 and 20 kgf. The reported Vickers hardness, HV 10 and HV 20, for each composition is the mean of 10 indents.

Modulus of elasticity was measured using indentation modulus technique with the help of hardness testing machine Zwick Z2.5 [88, 89]. The elastic modulus of the material was determined from the slope of the unloading part of the load – indentation curve obtained using the instrumented hardness measurement method.

The indentation fracture toughness (IFT) approach was chosen as the easiest and effective way to estimate comparative fracture toughness of the composites [90]. The indentation fracture toughness was calculated from the length of radial cracks emanating from the corners of the Vickers indentation imprints using the Palmqvist and median crack approaches [91]. Both of the crack systems were used in order to observe the difference between two IFT methods. The calculation methods were chosen on the basis of the studies in the field and IFT [92–96]. The indenter was pressed into the specimens at a load of 10 kg, which resulted in a well developed cracks formation on the studied surfaces. The IFT definition c/a ratio (in which “ c ” is a half-crack length of a radial crack, and “ a ” is a half-diagonal length of an indent) is less than 3 in most cases. This means that a developed crack system may be considered as the Palmqvist system, while median crack were also taken into consideration in some cases. The surface cracks initiated by the indenter were measured using optical microscopy that gives suitable contrast on the surface for accurate measurements of the crack lengths. The reported values are the mean and standard deviation of at least six indentations. It should be noted that the single-edge V-notch beam (SEVNB) route provides more reliable values of the fracture toughness as compared to the indentation fracture toughness, which often gives the overestimated values. However, difficulties in the sample preparation limit SEVNB method adaptability.

2.4.3 Erosive and abrasive wear testing

Erosion testing was performed with the help of conventional four-channel particles centrifugal accelerator CAK-5m in accordance with the standard method [97]. The principal scheme of the tester is provided in Figure 2.4. It has a feeder for the constant and controlled supply of particles into the system, a rotating disc which has four radial channels to accelerate the particles and a

specimen holding system. During experiment, the sand particles were continuously fed into the central hole of the rotor in which they were accelerated through the radial channels by the centrifugal force and ejected from the open end of the radial channels. The specimen targets are located around the rotating disc in a holding fixtures that can be adjusted under different angles. Silica particles traveling at velocities of 50–80 ms⁻¹ at a normal incident angle were used as erodents in this study. The tests were conducted at room temperature and the erosion rate was determined as volume loss of the target material per mass of the erodent particles.

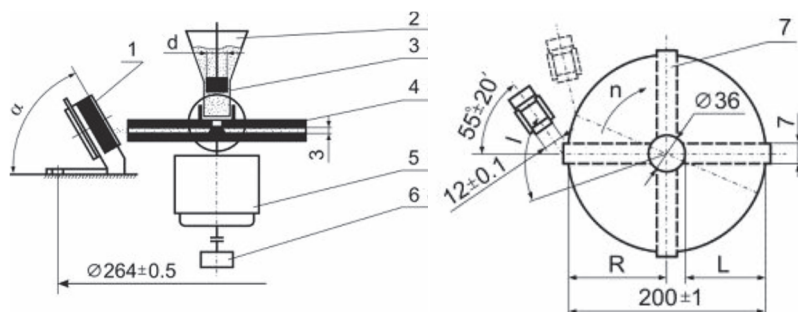


Figure 2.4 Erosion tester for testing materials in abrasive particle jet: 1–specimen, 2–erodent hopper, 3–shield, 4–rotor, 5–drive motor, 6–rotation speed gauge, 7–radial channels

Three-body abrasive testing was performed using the rubber-rimmed rotary wheel machine according to the modified ASTM 65-94 method with reduced diameter of the wheel disk for testing small sized specimens and cutting down expenses during development stage of a new material. Abrasion test results are reported as volume loss in cubic millimeters per load and distance (mm³N⁻¹m⁻¹) for the specified test conditions and are summarized in Table 2.4. Wear tests were repeated at least 3 times.

Table 2.4 Abrasive wear test parameters

Specification	Description
Scheme	Block-on-wheel
Wheel	Ø 80 mm, width 8 mm, steel covered by rubber
Abrasive	SiO ₂ , particle size 0.1–0.3 mm, HV 1100, feeding rate 300 g/min
Circumferential velocity	1 m·s ⁻¹
Number of rotations	1500
Force against specimen	47 N
Atmosphere	Air, relative humidity 50±10 %
Temperature	Room temperature

3 PROCESSING AND PROPERTIES OF THE DESIGNED COMPOSITES

3.1 WC-Ni-ZrO₂ hardmetal

3.1.1 Sintering features

Diagrams of the sintering cycles of the WC-Ni-ZrO₂ hardmetals are illustrated in Figure 3.1

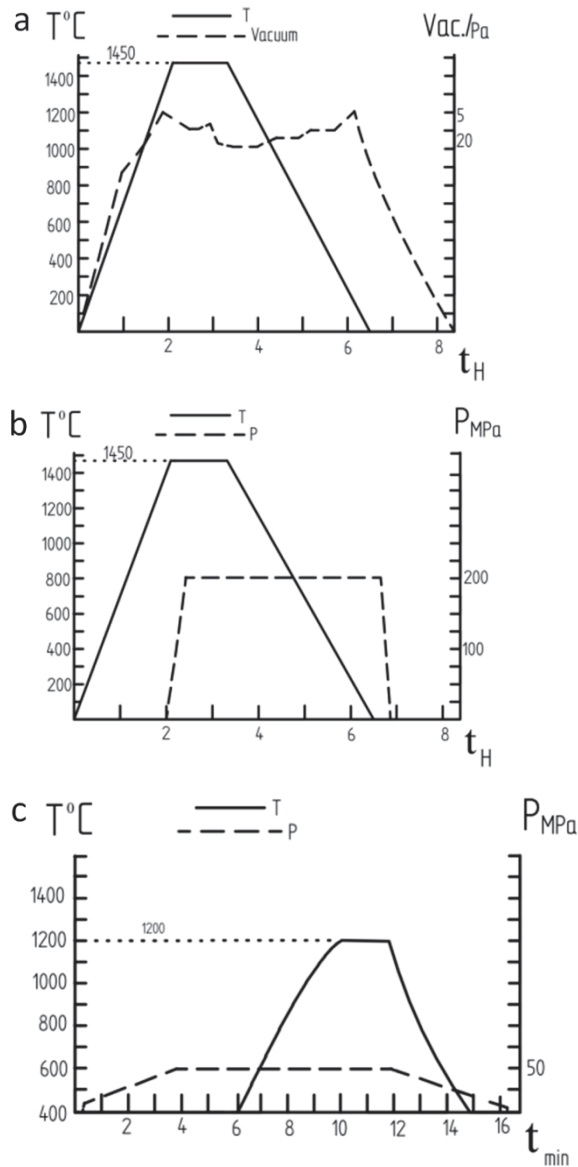


Figure 3.1 Diagrams of the sintering processes a) VPS cycle, b) HIP cycle, c) SPS cycle

Minimum temperature of the SPS cycle was 250 °C lower as compared to HIP and VPS routes and was 1200 °C. Dwell time at this temperature during SPS cycle was 1 min. Because of great difference in sintering cycle time between SPS and conventional sintering techniques, the impact on the microstructure is very well pronounced. The grain growth inhibitors were not added to some of the precursor powders in order to see the influence of the sintering parameters on the microstructure formation.

3.1.2 Phase composition and microstructure

The XRD observation of the WC-Ni-ZrO₂ has revealed presence of so called η-phase when no additive carbon was put into the precursor powder. Observation of the specimen has shown a presence of Ni₂W₄C in HIP or vacuum sintered samples (Figure 3.2a). This carbide phase has a high hardness and is reported in various sources [31], which is known for X_nW_yC type of the structures (X: Ni, Co, Fe, B etc.). Even though it has relatively high hardness, presence of this phase is not favorable, because of extreme brittleness and unpredictable behavior during testing. The formation of η-phase was avoided by prescribed graphite addition. During the XRD studies of the produced specimens the ternary carbon containing phases were not found. In addition, XRD diagrams show presence of tetragonal zirconia in all cases whether sintered by HIP, VPS or SPS.

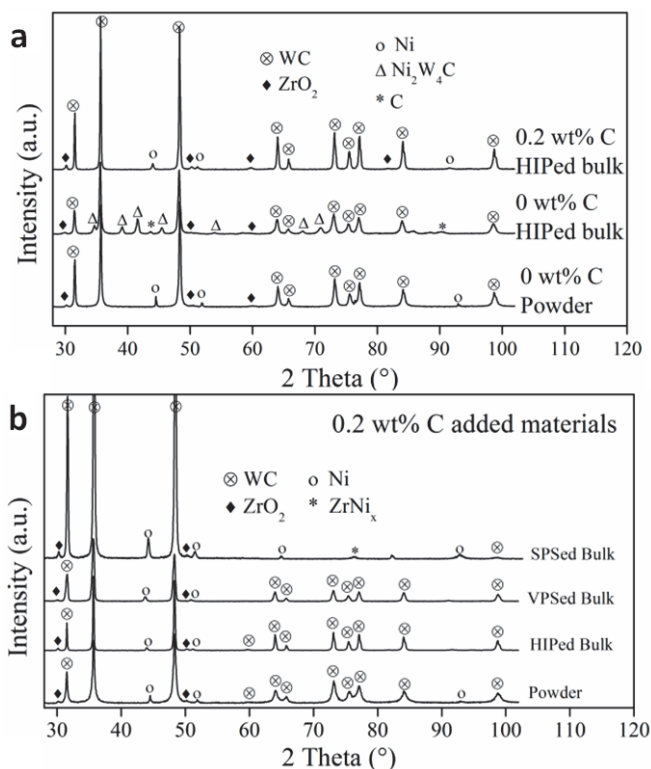


Figure 3.2 The effect of a) C content and b) sintering method on the composition

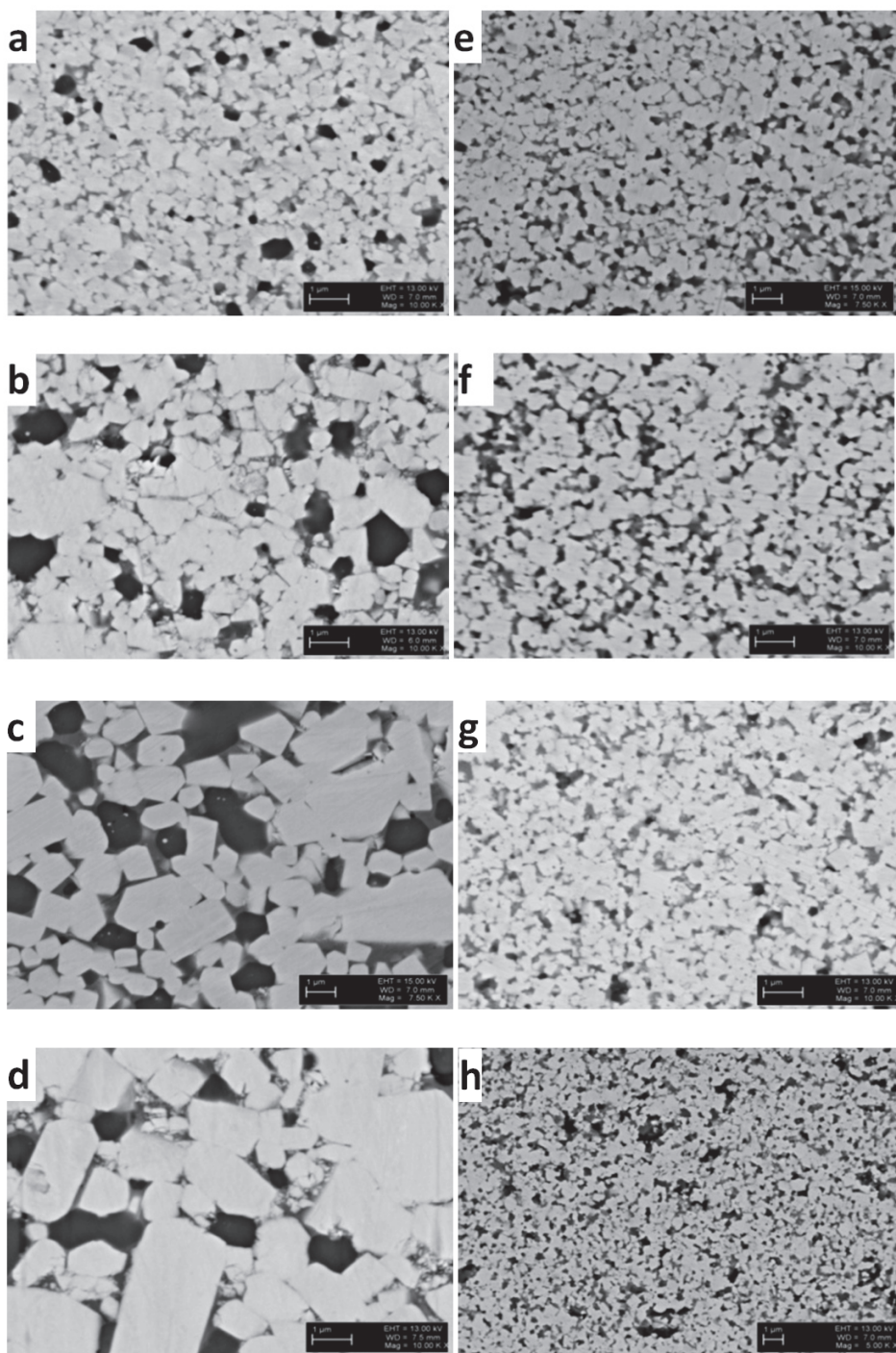


Figure 3.3 SEM images of a) VPS, (0.2 wt.% C) b) VPS, (0.4 wt.% C) c) VPS, (0.7 wt.% C) d) VPS, (1.0 wt.% C) e) SPS, (0.2 wt.% C) f) SPS, (0.4 wt.% C) g) SPS, (0.7 wt.% C) h) SPS, (1.0 wt.% C) [II]

Influence of the carbon content on the microstructure and grain morphology as well as influence of sintering routes were examined by SEM. The images in Figure 3.3 represent the microstructures of the materials with various carbon contents and sintered with different techniques.

The carbon content in Figure 3.3a–d is 0.2–1.0 wt.% of C and the materials were sintered by VPS. Figure 3.3e–h shows materials with the same carbon content but obtained using SPS. The HIPed composites had similar microstructure. The grain growth was observed for both WC and ZrO₂ particles.

The specimens with 0.2 wt.% C were doped by Cr₃C₂ in order to inhibit grain growth during sintering by HIP and VPS. As the result, the grain growth was minimal as compared to other grades. If 0.4, 0.7 and 1.0 wt.% C added microstructures to compare with 0.2 wt.% C added microstructure the difference can be clearly distinguished. Grain size increases proportionally with additional carbon. The coarsest grain size is for the 1.0 wt.% C added composite (Figure 3.3d). This indicates the enhanced discontinuous grain growth namely the effect of carbon addition on the microstructure.

The microstructure of SPSed materials has shown almost none or very little grain growth and seemed to be unaffected by the graphite addition. WC grains were in submicron range and ZrO₂ particles were in the range of ultrafine to nanoscale range for all grades with additional carbon.

The microstructure of Cr₃C₂ containing grade had more homogeneous distribution of the submicron grains for both VPS and HIP samples. WC initially has a rectangular shape and demonstrated a tendency of grain elongation with increase in carbon content (Figure 3.3c, d). This type of morphology was reported for WC–30 wt.% Co composites when the carbon content was increased from 0.1 to 1.0 wt.% [37].

3.1.3 Properties of the produced materials

The hardness and densities together with theoretical densities of the produced specimens are presented in Figure 3.4. As it can be seen, the properties depend on microstructural features, decreasing with increase in carbon content and carbide grain size. Materials with 0.2 wt.% C had the highest hardness among all the materials sintered by different methods. Similar behavior was observed with the density. Hardness of the SPSed samples initially dropped from 1725 HV₂₀ to 1380 HV₂₀ when the C content increased from 0.2 to 0.4 wt.% and then it increased to 1385 HV₂₀ and 1505 HV₂₀ for 0.7 and 1.0 wt.% C, respectively. SPS routine has the unique advantage of suppressing grain growth over other methods. This is probably the main reason for the increase in hardness with higher C content along with better densification as compared to HIPed and VPSed samples.

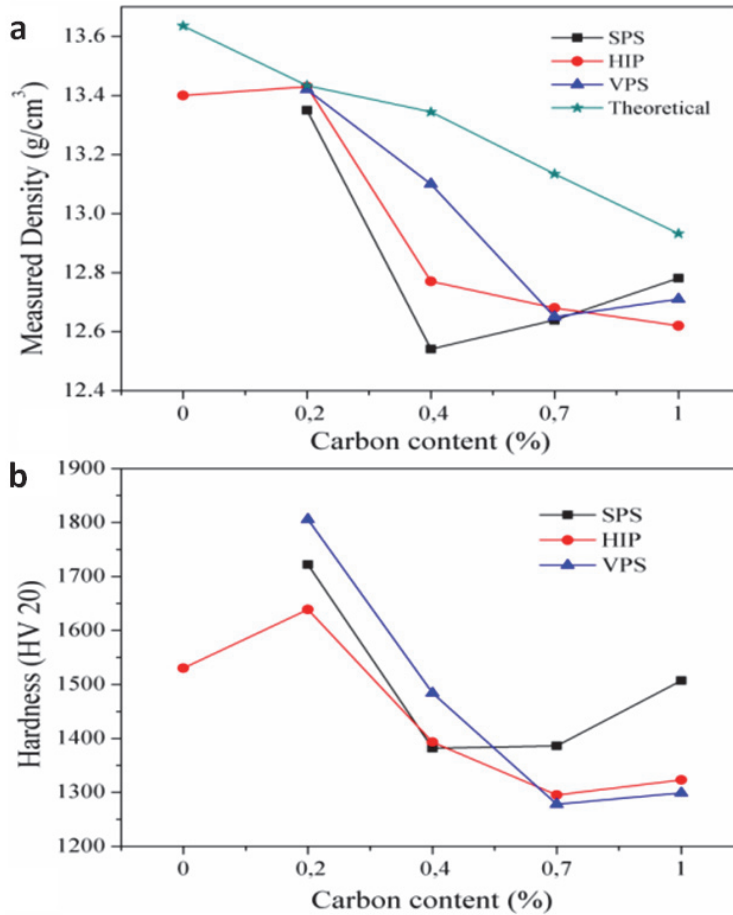


Figure 3.4 Effect of carbon content on the a) density and b) hardness of the samples. Standard deviation of the measurements has not exceeding 5–10 %

The indentation fracture toughness (IFT) of the materials showed evident variations (Figure 3.5) depending on the method of sintering and the procedure of calculations. IFT of HIPed materials decreases with increase in carbon amount. VPSed materials, on the other hand, exhibit an increase in their fracture toughness up to 0.7 wt.% C and decrease when C amount reached 1.0 wt.%. SPSed materials shown almost no difference between IFT calculated for 0.2 and 1.0 wt.% C addition. Fracture toughness had a small increase at 0.4 wt.% C and remained almost the same for 0.7 wt.% C. SPSed materials had an inverse relation between their hardness and fracture toughness. Presence of additional carbon not only hindered η -phase formation but also made some improvement on the densification overall. In the grades produced by HIP IFT was very high especially for low carbon content grades. In general higher fracture toughness is assumed to be a result of synergetic influence of microstructure and zirconia transformation toughening effect.

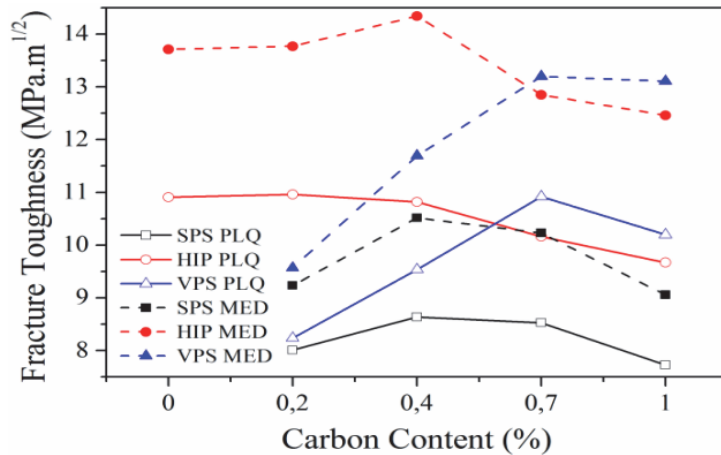


Figure 3.5 Fracture toughness values for Palmquist (PLQ) and median (MED) crack systems. Standard deviation of the measurements has not exceeding 5–10 %

Further optimization of the microstructure through the VPS processing enabled the higher IFT value of 15 MPa·m^{1/2} [I]. The enhanced fracture toughness is considered to be the result of more intensive tetragonal to monoclinic phase transformation of zirconia due to grain size more close to critical grain size needed for the transformation toughening to appear [98].

3.1.4 Results of wear testing

Erosion and abrasion wear rates for the specimens with the optimal microstructure and mechanical properties described in the previous chapters and for the reference WC-Ni material are represented in Figure 3.6. The erosion rate of WC-Ni-ZrO₂ composite is lower as compared to reference WC-Ni specimens produced by the VPS technique under the same laboratory conditions [I].

The better wear resistance of the specimens added by zirconia is related to be an effect of zirconia transformation toughening in the WC-Ni matrix. Wear resistance is strongly dependent on the fracture toughness and hardness. Among materials tested, the reference WC-Ni hardmetal exhibited the lowest mechanical performance; therefore, its lowest wear resistance is expected.

In addition, wear of the specimens caused by the abrasion is represented on the Figure 3.6. The results are similar to those, which were obtained for the erosion testing and are in straight dependence from mechanical properties. The detailed discussion on the topic of wear of given materials can be found in [I, II].

XRD observation of the worn surface shows lowering of intensity of the tetragonal zirconia peaks due to partial transformation into the monoclinic phase during erosion wear (Figure 3.7). Precise analyze and calculation of different zirconia phases in specimens before and after tests revealed the transformability of zirconia in conditions of erosion up to 40 % [I]. Therefore, the effect of possible phase transformation toughening in the hardmetals doped by zirconia can be stated for the conditions of high energy impacts by the erodent particles.

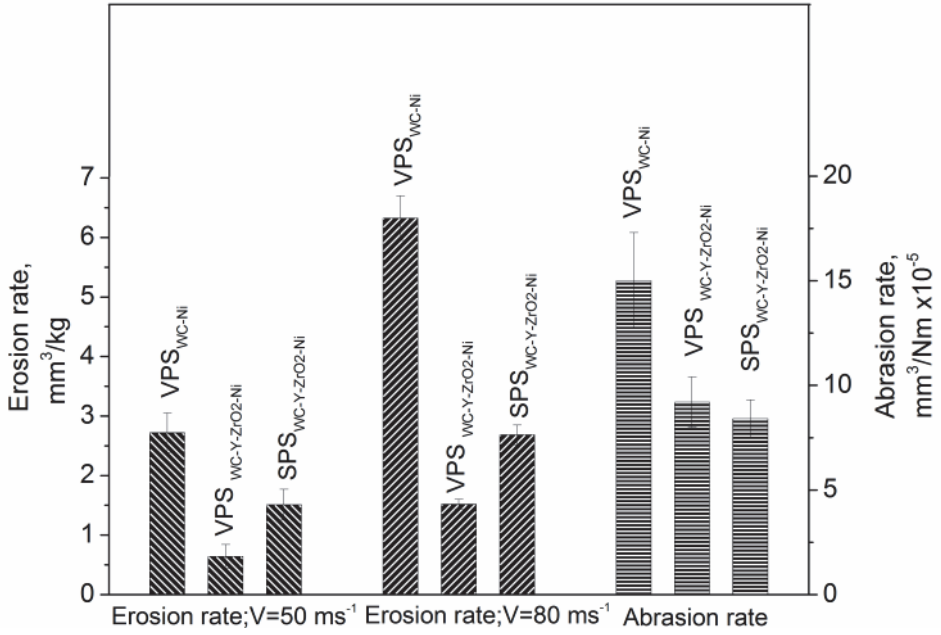


Figure 3.6 Erosion and abrasion rates of the tested specimens [I]

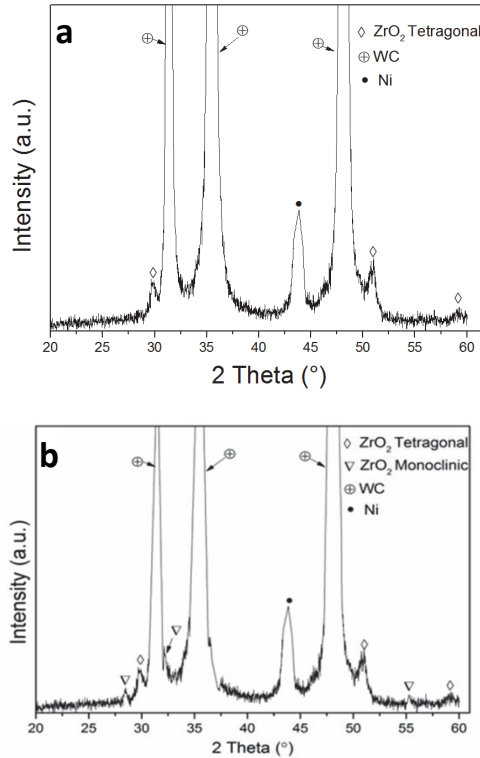


Figure 3.7 XRD pattern of the a) as-sintered and b) eroded surfaces

3.2 ZrC-ZrO₂ ceramic

3.2.1 Processing of the materials

Densification behavior of the ZrC-ZrO₂ composite was analyzed. Displacement rate of the upper electrode against sintering time is demonstrated on Figure 3.8. When the pressure is applied at room temperature, the densification displacement is positive and the powder is compressed to its green density (stage 1). In the heating stage due to the expansion of the graphite molds the displacement is in the opposite direction (stage 2). On the next step, densification occurs and piston movement increases rapidly between 1000 and 1640 °C (stage 3).

During the first stage, densification is caused by rearrangement of particles and plastic deformation under the applied pressure. The densification step has a large rise because of the nanosize of the zirconia particles, which tend to decrease their surface area and rearrange as soon as distance between them is decreased. In second stage, the maximum pressure is applied and pistons movement ends. Also, some negative movement can be observed because of the thermal expansion of the powder and graphite material. Third step indicates densification that is induced by current and concomitant joule heating. Densification starts between 1000 and 1100 °C. Densification now occurs by mass transfer mechanism. Necking between ZrO₂ particles is expected. Neck formation leads to initiation of grain boundaries. There is some negative slope after major densification is finished indicating thermal expansion of the material. Detailed analysis of the SPS densification of Zr-ZrO₂ can be found in [III].

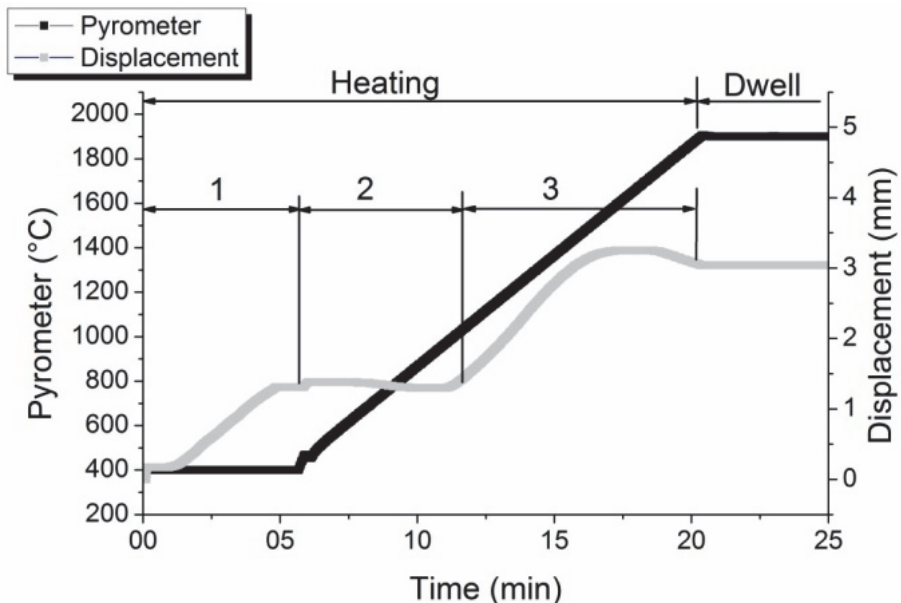


Figure 3.8 Change of piston position during sintering of the ZrC-37 wt.% ZrO₂ [III]

3.2.2 Microstructural characterization of composites

XRD observation of the VPS and SPS produced specimens revealed no significant influence of the sintering routine on the constituents of the composite: both ZrC and ZrO₂ phases were retained in their initial state. The XRD patterns are presented in Figure 3.9 It should be also mentioned that zirconia has retained its tetragonal phase.

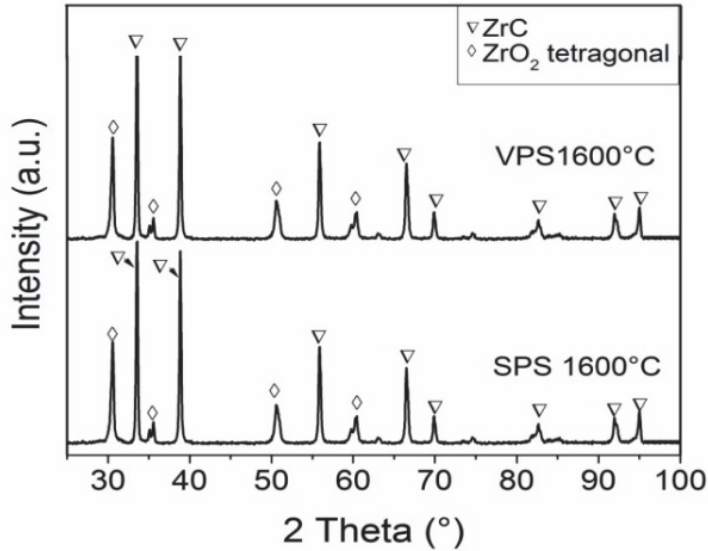


Figure 3.9 XRD graph of the samples obtain by SPS and VPS

The microstructures of the SPS and VPS sintered samples are demonstrated in Figure 3.10. Two phases are well distinguished on the micrographs: the light areas represent ZrC and the dark areas are yttria stabilized zirconia. Zirconia is found in the well-dispersed clusters that increase in size with the increase of YTZ content. Zirconia seems to form an interconnected phase in the composites. Some individual grains can be distinguished and their average size does not exceed the size of the starting ZrC particles, suggesting that ZrC grain growth is minimal during the process of densification.

It can be observed that there is no difference between the microstructures of the specimens produced by different routes. The VPSed specimen resulted in lower densification degree, while mechanical properties were on the same level. Nevertheless, densities of both VPS and SPS samples are about in the same range, having 98 % of theoretical density Table 3.1.

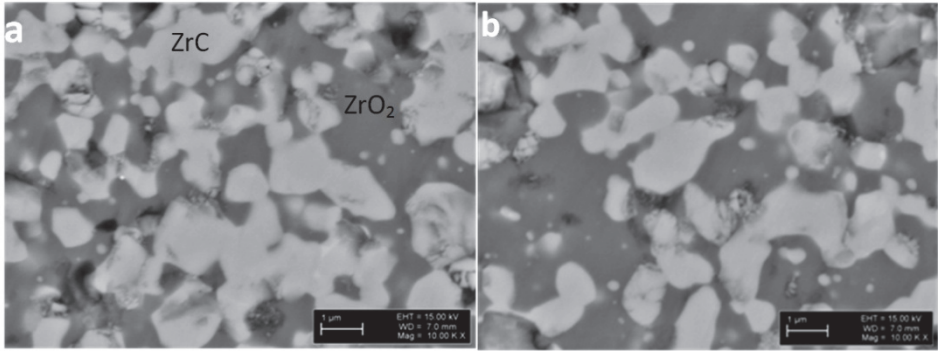


Figure 3.10 Microstructure images of the samples obtained by a) VPS and b) SPS

Sintering of pure ZrC requires temperatures higher than 2000 °C. The presence of zirconium dioxide enhances the densification kinetics during SPS and VPS treatment. Additional oxygen vacancies influence the mass transfer by diffusion of atoms, and consequently, the process of sintering [50–53]. Another reason for enhancing sintering kinetics can be related to the size effect [10]. Well dispersed nano-sized YTZ particles with a high specific surface area promote greater grain boundary diffusion.

3.2.3 Properties of the produced composites

Density and mechanical properties of the ZrC-ZrO₂ composites are listed in Table 3.1.

Table 3.1 Mechanical properties of the ZrC-ZrO₂ composites

Specimen	Density g/cm ³	Hardness HV10	Bulk modulus GPa	IFT MPa·m ^{1/2}
VPS 37 wt.%ZrO ₂	6.20	1520±22	255±11	7.25±1.3
SPS 37 wt.%ZrO ₂	6.35	1550±58	260±23	7.15±4.0
SPS 23 wt.%ZrO ₂	6.30	1515±82	250±27	8.90±3.2

From analysis of the properties it can be concluded that increasing of zirconia content improves sinterability and homogeneity in properties, while specimens with higher ZrC content do not demonstrate any advantages in hardness for example. ZrC is difficult to sinter alone and therefore an additional phase such as nano sized zirconia enhances sinterability noticeably and lowers the sintering temperature of ZrC.

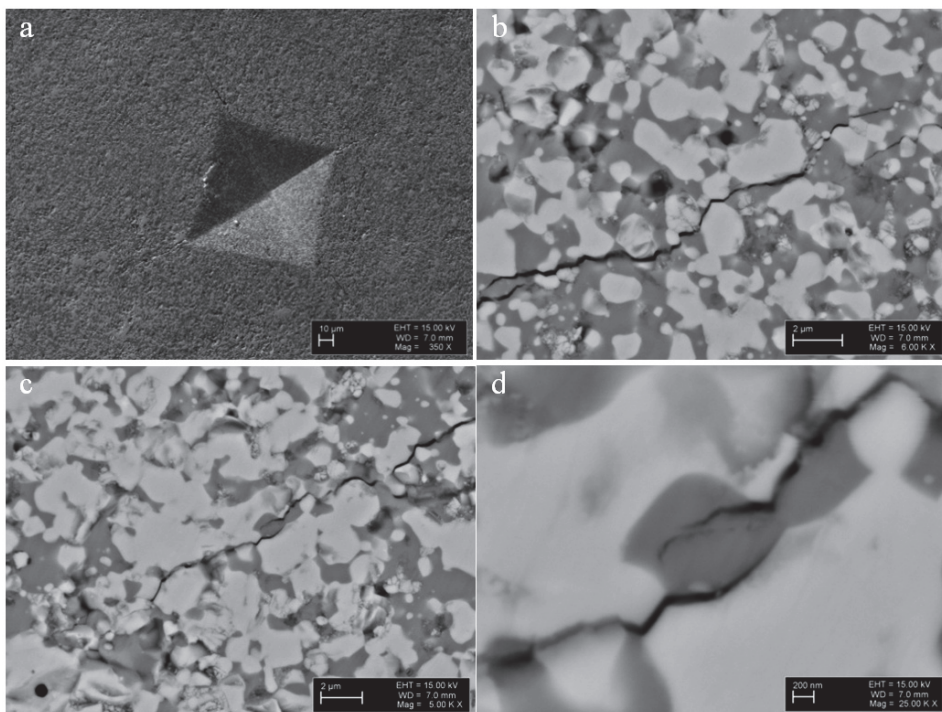


Figure 3.11 Representative SEM images of a) indentation imprint; and b, c, d) cracks propagating from the corner of indent taken from the surface of the ZrC-37 wt.% YTZ composite [III]

SEM micrographs of the crack propagating from the corners of the Vickers indent are shown in Figure 3.11. In all probability, the advanced crack transforms some of the zirconia particles in vicinity of the path of a crack tip, leaving behind regions of permanently transformed material. The crack propagates predominantly along the grain boundaries, indicating an intergranular character of cracking; ZrC grains tend to deflect the crack. Therefore, the multiplicative interactions such as crack deflection and branching combined with transformation toughening are evident and can be regarded as operating toughening mechanisms in the composites.

In order to assess zirconia transformability, the difference in monoclinic phase content of the polished and fractured surfaces, i.e., the fraction of stabilized zirconia transformed into monoclinic phase during fracture, was determined with the XRD measurement.

The transformability of the tetragonal zirconia decreased from 36 % in 23 wt.% ZrO₂ containing composite down to 32 % in the composite with 37 wt.% ZrO₂ of yttria stabilized zirconia. Reducing transformability in the 37 wt.% ZrO₂ grade explains the similar values of the indentation fracture toughness of the composites despite the relatively large difference in zirconia content: toughness increases with increase in transformability, indicating that the stress-induced phase transformation can constitute one of the mechanisms responsible for toughening [III].

3.3 Alumina toughened zirconia composite material

3.3.1 Sintering of the produced mixture

In order to study the densification behavior of the fibers dilatometry sintering at a constant shrinkage rate in pressureless conditions was conducted. The dilatometry graphs can be found in IV.

Zirconia is densified at a temperature of around 1350 °C. However, at temperature of 1200–1250 °C gamma-alumina undergoes transformation to alpha phase accompanied by fibers decomposing into the particles [58]. Therefore, sintering should be conducted at temperatures lower than 1200 °C. It was shown [IV] that at 1000 °C there is almost no densification. Densification starts between 1000 °C and 1100 °C, which agrees with the dilatometry sintering experiment, where the main densification step starts at 1070 °C.

Figure 3.12 represents 3 pistons movement curves which describe densification behavior during SPS cycle. It can be observed that 1100 °C sintering regime is optimal, because at 1000 °C there is almost no densification and at 1200 °C no additional densification occur.

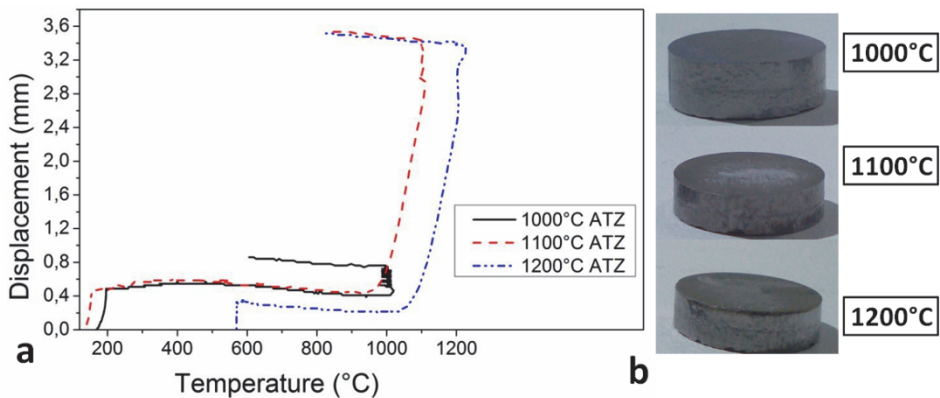


Figure 3.12 Dilatometry graphs of the samples produced by the SPS [IV]

3.3.2 Microstructure and properties characterization

Five different XRD patterns of the studied materials are represented in Figure 3.13. The patterns of the samples sintered at 1100 °C and 1200 °C look similar to PSZ pattern while some important distinctions can be found. Monoclinic zirconia has undergone the transformation into the tetragonal modification after the 700–900 °C and no monoclinic zirconia is left in the bulk specimen. This also explains the densification step during dilatometry sintering where densification occurs at 780 °C. There are no gamma alumina peaks, which are present on the initial pattern of the ANFs.

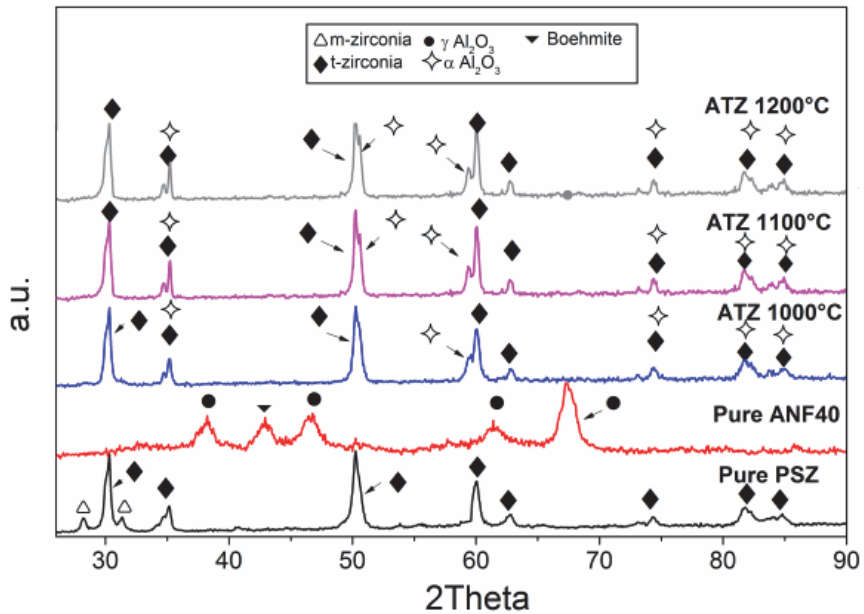


Figure 3.13 XRD pattern of the precursor and sintered materials [IV]

Microstructures of the specimens produced by different sintering methods can be seen on the Figure 3.14. It must be noticed that in case of SPS sintering the ANFs are retained in their initial bundle or whisker state while in case of air sintering those are completely decomposed.

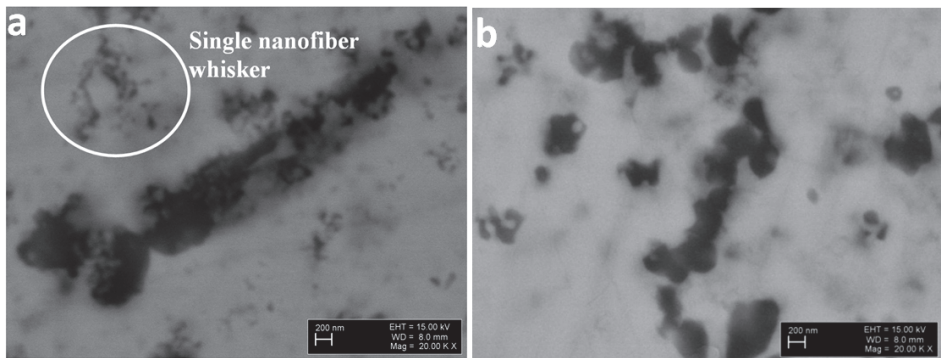


Figure 3.14 Microstructures of the Zirconia-Alumina composite a) sintered at 1100° SPS, b) sintered at 1300 °C Air [IV]

The mechanism of whiskers transformation into the rounded cluster is depicted in IV.

The properties of the produced specimens can be seen from the Table 3.2. It is clear that specimen sintered at 1000 °C has the lowest density and hardness. The 1300 °C air sintered specimen has also very low density and mechanical characteristics. In this case a noticeable difference between the SPS and conventional air sintering processes can be seen. Even though SPS process for this material has been performed at 200 °C lower than air sintering its' density is 20 % higher which is a significant improvement. Also the hardness of the sample sintered at 1100 °C is 1054 HV which is high enough for further testing experiments with this sample.

Table 3.2 Properties of the produced specimens

Technology	Density g/cm³	Densification %	Hardness HV10	Modulus of elasticity, GPa
1000 °C SPS	3.15	54	75±5	-
1100 °C SPS	5.50	93	1035±60	130±24
1200 °C SPS	5.50	93	755±15	150±18
1300 °C air	4.35	74	545±25	90±15

Introduction of tough whiskers into particulate matrix is done to increase its ability to oppose fracture propagation. In paper IV the crack obtained from the Vickers indentation measurement moving through the matrix and then passing through the whisker-like bundle of ANFs can be seen. It should be noticed that movement of the crack is not affected by the ANF inclusion and no crack stopping mechanism take place, whether crack bridging or deflection. Therefore, the IFT measurements were not done on this specimen.

4 CONCLUSIONS

Different oxides-containing ceramic-based composite materials were designed and produced throughout this study with the help of different PM methods with a special emphasis on the sintering technology. Based on this study the following conclusions can be outlined:

1. Production of the dense and poreless WC-Ni-ZrO₂ hardmetal is possible with both: conventional sintering methods (HIP, VPS) and non-conventional SPS method. However, production conditions and produced material characteristics are dependent on the method of fabrication. Sintering time needed for the production of dense WC-Ni-ZrO₂ hardmetals is 20 times faster in case of the SPS technique as compared with VPS and HIP techniques and temperature needed to obtain dense material is almost 20% lower than in case of conventional sintering techniques.

Production of ZrC-ZrO₂ composite with SPS technique is also 10 times faster than in case of VPS, while temperature needed to produce dense sample is the same for both technologies.

Dense ATZ (alumina toughened zirconia) composite can be produced with the help of the SPS technique at low sintering temperature of 1100 °C, while in case of conventional air sintering no dense composite can be obtained at temperature 200 °C higher than mentioned. Low temperature SPS cycle gives an ability to retain the new type of ANF fibers in their whisker like state.

2. Final microstructure of the WC-Ni-ZrO₂ hardmetals produced by conventional sintering methods is dependent on the carbon content in the powder mixture: the optimal carbon content is 0.2 wt.%. However, there is no influence of additive carbon content on the grain growth of the SPS produced specimens.

There is no influence of the sintering technique on the microstructure of the ZrC-ZrO₂ composite. Microstructures of ZrC-ZrO₂ material produced by VPS and SPS are the same.

Microstructure of the ATZ composite produced with SPS has ANF inclusions in form of whiskers while in case of microstructures produced in air at higher temperature all the ANF whiskers are transformed into the rounded clusters.

3. Introduction of ZrO₂ into composites has resulted in a positive result to the toughness properties.

All the mechanical behavior characteristics: IFT, hardness, abrasion and erosion wear resistance are higher for the WC-Ni-ZrO₂ composite as compared to the WC-Ni hardmetal produced under same conditions. Improved fracture toughness and wear resistance are attributed to the addition of ZrO₂ and observed tetragonal to monoclinic phase transformation.

Phase transformation was also observed for the ZrC-ZrO₂ composite. Fracture toughness of pure ZrC was noticeably increased by the addition of ZrO₂.

Hardness of ZrC decreased after adding ZrO₂, while remained on a high level.

Addition of ANF to zirconia matrix and remaining them in whisker like state did not result in crack stopping mechanisms for the bundle inclusion. The hardness of the ATZ composite is high enough for further evaluation.

Materials studied in this work will be processed in future. WC-Ni-ZrO₂ composite is being studied for the underground tunneling project. ATZ composite will be developed in order to produce reliable whiskers containing composite. Tribological and oxidation observations will be performed on the ZrC-ZrO₂ composites.

Novelty of the present work is described as follows:

- Advanced CMC systems exploiting the transformation toughening of tetragonal zirconia have been produced and the technological parameters for their fabrication by different sintering techniques have been proposed.
- Pressureless and pressure assisted sintering techniques, including spark plasma sintering, have been used for fabrication of the composites and the microstructural features and the mechanical properties of the produced materials have been compared.
- The novel type of reinforcement (namely, alumina nanofibers) have been tested for the first time and the produced alumina bulks have been found the perspective choice for the future development of composites with nano-reinforcement.

Present work gives inception to a number of other researches for further development and testing of the materials produced. Technology obtained allows production of dense CMCs with improved IFT and using the novel types of reinforcements (such as ANF).

REFERENCES

1. *European Powder Metallurgy Association (EPMA) Website*.
<http://www.epma.com/what-is-powder-metallurgy> (29.10.2014)
2. M. W. Barsoum, *Fundamentals of Ceramics*, McGraw-Hill, 1997.
3. W. D. Callister, G. D. Rethwisch, *Materials Science Engineering Introduction 8th edition*, John Wiley & Sons, 2010.
4. K.T. Faber, A.G. Evans, Crack Deflection Processes, *Acta Metall.* 31 (1983) 565-576.
5. S.W. Freiman, Brittle Fracture Behavior of Ceramics, *Am. Ceram. Soc. Bull.* 67 (1988) 392-402.
6. John W. Hutchinson, *Mechanisms of toughening in Ceramics*, Elsevier Science Publishers, 1989.
7. H. Heuer, L. W. Hobbs (eds.), *Science and Technology of Zirconia*, American Ceramic Society, 1981.
8. N. Claussen, Fracture Toughness of Al₂O₃ with an Unstabilized ZrO₂ Dispersed Phase, *J. Am. Ceram. Soc.* 59 (1976) 49–51.
9. A. H. Heuer, N. Claussen, W. M. Kriven and M. Ruhle, Stability of Tetragonal Zirconia Particles in Ceramic Matrices, *J. Am. Ceram. Soc.* 65 (1982) 642–650.
10. R. H. J. Hannink, M. V. Swain, Progress In Transformation Toughening of Ceramics, *Annu. Rev. Mater. Sci.* 24 (1994) 359–408.
11. A. B. Yuichiro Morikawa, M. Kawahara, M. J. Mayo, Fracture Toughness of Nanocrystalline Tetragonal Zirconia with Low Yttria Content, *Acta. Mater.* 50 (2002) 4555–4562.
12. A. Krell, A. Teresiak, D. Schläfer, Grain Size Dependent Residual Microstresses in Submicron Al₂O₃ and ZrO₂, *J. Eur. Ceram. Soc.* 16 (1996) 803–811.
13. M. F. Ashby, D. R. H. Jones, *Engineering Materials 1: An Introduction to Properties, Applications and Design*, Butterworth-Heinemann Ltd, 2005.
14. G. K. Bansal and A. H. Heuer, Precipitation in Partially Stabilized Zirconia, *J. Am. Ceram. Soc.* 58 (1975) 235–238.
15. E. Bischoff and M. Ruhle, Twin Boundaries in Monoclinic ZrO₂ Particles Confined in a Mullite Matrix, *J. Am. Ceram. Soc.* 66 (1983) 123–127.
16. W. M. Kriven, The Transformation Mechanism of Spherical Zirconia Particles in Alumina, *Adv. Ceram.* 12 (1984) 64–77.
17. M. Ruhle and D. Waidelich, In Situ Observations of the Martensitic Transformation in Enclosed t-ZrO₂, Proc. *International Symposium on In Situ Experiments with HVEM*, Osaka University, Osaka, (1985) 157–168.
18. B. C. Muddle and R. H. J. Hannink, Crystallography of the Tetragonal to Monoclinic Transformation in MgO-Partially Stabilized Zirconia, *J. Am. Ceram. Soc.* 69 (1986) 547–555.
19. P. M. Kelly, C. J. Ball, Crystallography of Stress-Induced Martensitic Transformations in Partially Stabilized Zirconia, *J. Am. Ceram. Soc.* 69 (1986) 259–264.
20. B. Basu, Toughening Of Yttria-Stabilized Tetragonal Zirconia Ceramics, *Int. Mater. Rev.* 50 (2005) 239–256.

21. J. Vleugels, O. Van der Biest, Development and Characterization of Y₂O₃-stabilized ZrO₂ (Y-TZP) Composites with TiB₂, TiN, TiC, and TiC_{0.5}N, *J. Am. Ceram. Soc.* 82 (1999) 2717–2720.
22. J.K. Yoon, J. M. Doh, Z.A. Munir, H. C. Kima, I. J. Shona, Rapid Sintering of Ultrafine WC–Ni Hardmetals, *Int. J. Refract. Met. Hard. Mater.* 24 (2006) 427–431.
23. X. Yuan, C. Wei, D. Zhang, J. Zhu, X. Gao, Characterization and comparison of grain boundary character distributions in hardmetals with different binder phases, *Comp. Mater. Sci.* 93 (2014) 144–150.
24. G. Gille, J. Bredthauer, B. Gries, B. Mende, W. Heinrich, Advanced and New Grades of WC and Binder Powder—Their Properties and Application, *Int. J. Refract. Met. Hard. Mater.* 18 (2000) 87–102.
25. P. Goeuriot, F. Thevenot, Boron as Sintering Additive in Cemented WC–Co (or Ni) alloys, *Ceram. Int.* 13 (1987) 99–103.
26. S. Imasato, K. Tokumoto, T. Kitada, S. Sakaguchi, Properties of Ultra-Fine Grain Binderless Hardmetal, *Int. J. Refract. Met. Hard. Mater.* 13 (1995) 305–312.
27. E.A. Almond, B. Roebuck, Identification of Optimum Binder Phase Compositions For Improved WC Hardmetals, *Mat. Sci. Eng. A.* 105 (1988), 237–248.
28. J. Russias, S.Y. Aguni, G. Fantozzi, K. Bienvenu, J. Fontaine, Influence of Titanium Nitride Addition on the Microstructure and Mechanical Properties of TiC-Based Hardmetals, *Int. J. Refract. Met. Hard. Mater.* 23 (2005) 358–362.
29. A. Lin, H. Jingtao, C. Jun, Microstructure and Mechanical Properties of WC-20 wt.% Co/ZrO₂(3Y) Hardmetal Composites, *J. Univ. Sci. Technol. B.* 13 (2006) 174–177.
30. I. Hussainova, M. Antonov, I. Jasiuk, X. Du, Characterization of Microstructure And Mechanical Properties of Hardmetals at Micro-and Nanoscales, *Int. J. Mater. Prod. Tec.* 40 (2011) 58–74.
31. K. Juhani, J. Pirso, M. Viljus, S. Letunovits, M. Tarraste, The Influence of Cr₃C₂ and VC as Alloying Additives on the Microstructure and Properties of Reactive Sintered WC-Co Hardmetals, *Mater. Sci.* 18 (2012) 79–83.
32. F. Arenas, I.B. de Arenas, J. Ochoa, S.A. Cho, Influence of VC on the Microstructure and Mechanical Properties of WC-Co Sintered Hardmetals, *Int. J. Refract. Met. Hard. Mater.* 17 (1999) 91–97.
33. S.A. Cho, A. Hernandez, J. Ochoa, J. Lira-Olivares, Phase Relations, Microstructure and Mechanical Properties of VC Substituted WC-10Co Hardmetal Alloys, *Int. J. Refract. Met. Hard. Mater.* 15 (1997) 205–214.
34. C. Lin, E. Kny, G. Yuan, B. Gjuricic, Microstructure and Properties of Ultrafine WC-0,6VC-10Co Hardmetals Densified by Pressure-assisted Critical Liquid Phase Sintering, *J. Alloy. Compd.* 383 (2004) 98–102.
35. *ASM HandBook Volume 07 Powder Metal Technologies and Applications*, ASM, Materials Park OH, 1998.
36. ISO 4505:1978 Hardmetals—*Metallographic determination of porosity and uncombined carbon.*

37. S. Kim, S-K. Han, J-K. Park, H-E. Kim, Variation of WC Grain Shape With Carbon Content in the WC–Co Alloys During Liquid-Phase Sintering, *Scripta Mater.* 48 (2003) 635–639.
38. *Informative website about cemented carbides*
http://www.allaboutcementedcarbide.com/02_02.html (29.10.2014)
39. I. Hussainova, M. Antonov, A. Zikin, Erosive Wear of Advanced Composites Based on WC, *Tribol. Int.* 46 (2012) 254–260
40. A Evans, M Golden, M. Rosenblatt, Impact Damage in Brittle Materials, *Proc. R. Soc.* A36 (1978) 343–353.
41. O. Malek, B. Lauwers, Y. Perez, P. De Baets, J. Vleugels, Processing of Ultrafine ZrO₂ Toughened WC Composites, *J. Eur. Ceram. Soc.* 29 (2009) 3371–3378.
42. Z. H. Qiao, X. F. Ma, W. Zhao, Fabrication, Microstructure and Mechanical Properties of Novel Cemented Hard Alloy Obtained by Mechanical Alloying and Hot-Pressing Sintering, *Mater. Sci. Eng. A* 460 (2007) 46–49.
43. W. Wan, J. Xiong, Z. Guo, H. Du, L. Tang, Erosive Wear Behavior of Ti(C,N)-Based Hardmetals Containing Different Cr₃C₂ Addition in Slurry Conditions, *Int. J. Refract. Met. Hard Mater* 45 (2014) 86–94.
44. B. Basu, T. Venkateswaran, D. Sarkar, Pressureless Sintering and tribological properties of WC–ZrO₂ composites, *J. Eur. Ceram. Soc.* 25 (2005) 1603–1610.
45. D. Jiang, O. der Biest, J. Vleugels, ZrO₂–WC nanocomposites with superior properties, *J. Eur. Ceram. Soc.* 27 (2007) 1247–1251.
46. B. Basu, J. H. Lee, D. Y. Kim, Processing of Nanoceramics and Nanoceramic Composites: New Results, *Key Eng. Mat.* 268 (2004) 2293–2296.
47. H. O. Pierson, *Handbook of Refractory Carbides and Nitrides*, Noyes, Westwood, 1996.
48. D. Yung, L. Kollo, I. Hussainova, A. Zikin, Reactive Sintering of Zirconium Carbide Based Systems, *Proceedings of 8th International DAAAM Baltic Conference Industrial Engineering*, Tallinn, Estonia, 2012, 783–788.
49. M. Umalas, V. Reedo, A. Lõhmus, I. Hussainova, K. Juhani, Synthesis of ZrC-TiC Blend by Novel Combination of Sol-gel Method and Carbothermal Reduction, *Proceedings of 8th International DAAAM Baltic Conference Industrial engineering*, Tallinn, Estonia, 2012, 753–758.
50. S. E. Landwehr, G. E. Hilmas, W. G. Fahrenholtz, I. G. Talmy, Processing of ZrC–Mo Hardmetals for High-Temperature Applications, part I: Chemical Interactions in the ZrC–Mo system, *J. Am. Ceram. Soc.* 90 (2007) 1998–2002.
51. E. Min-Haga, W. D. Scott, Sintering and Mechanical Properties of ZrC–ZrO₂ Composites, *J. Mater. Sci.* 23 (1988) 2865–2870.
52. D. Sciti, S. Guicciardi, M. Nygren, Spark Plasma Sintering and Mechanical Behavior of ZrC-Based Composites, *Scr. Mater.* 59 (2008) 638–641.
53. S. E. Landwehra, G. E. Hilmasa, W.G. Fahrenholtz, I. G. Talmy, S. G. Di Pietroc, Microstructure and Mechanical Characterization of ZrC–Mo Hardmetals Produced By Hot Isostatic Pressing, *Mater. Sci. Eng. A*, 497 (2008) 79–86.

54. C. Wang, H. Yong, Z. Hongxiang, The Effect Of Whisker Orientation In Sic Whisker-Reinforced Si₃N₄ Ceramic Matrix Composites, *J. Eur. Ceram. Soc* 19 (1999) 1903–1909.
55. J. Homeny and W. L. Vaughn, Whisker-Reinforced Ceramic Matrix Composites, *MRS Bulletin* 12 (1987) 66–72.
56. Alumina Nanomaterial: An Interview with Tim Ferland and Aleksandr Rakitin at ANF Technology, *AzoNano*, <http://www.azonano.com/article.aspx?ArticleID=3241> (29.10.2014).
57. V. Su, M. Terehov and B. Clyne, Filtration Performance of Membranes Produced Using Nanoscale Alumina Fibers (NAF,) *Adv. Mater. Eng.* 14 (2012) 1088–1096.
58. M. Aghayan, I. Hussainova, M. Gasik, M. Kutuzov, M. Friman, Coupled Thermal Analysis of Novel Alumina Nanofibers with Ultrahigh Aspect Ratio, *Thermochim. Acta* 574 (2013) 140–144.
59. H. P. Cahoon, C. J. Cristensen, Sintering And Grain Growth Of Alpha-Alumina, *J. Am. Ceram. Soc.* 39 (1956) 337–344.
60. A. H. De Aza, J. Chevalier, G. Fantozzi, M. Schehl, R. Torrecillas, Crack Growth Resistance Of Alumina, Zirconia And Zirconia Toughened Alumina Ceramics for Joint Prostheses, *Biomaterials* 23 (2002) 937–945.
61. R. Benzaid, J. Chevalier, M. Saa Daoui, G. Fantozzi, M. Nawa, L.A. Diaz, R. Torrecillas, Fracture Toughness, Strength And Slow Crack Growth In A Ceria Stabilized Zirconia–Alumina Nanocomposite For Medical Applications, *Biomaterials* 29 (2008) 3636–3641.
62. P. Bansal Narottam, R. Choi Sung, Processing of Alumina-Toughened Zirconia Composites, *National Aeronautics and Space Administration Glenn Research Center*, Cleveland, 2003.
63. M. Suarez, A. Fernandez, J.L. Menendez, R. Torrecillas, H. U. Kessel, J. Hennicke, R. Kirchner and T. Kessel, Challenges and Opportunities for Spark Plasma Sintering: A Key Technology for a New Generation of Materials, *Sintering Applications*, Edited by Burcu Ertug, InTech, 2013.
64. E. Kannisto, E. Cura, E. Levänen, S.-P. Hannula, Mechanical Properties of Alumina Based Nanocomposites, *Key. Eng. Mat.* 527 (2012) 101–106.
65. N. P. Bansal and A. R. Boccaccini, *Ceramics and Composites Processing Methods*, Wiley, 2012.
66. E. Kimmari, I. Hussainova, A. Smirnov, R. Traksmaa, I. Preis, Processing and Microstructural Characterization of WC Based Hardmetals Doped by ZrO₂, *Est. J. Eng.* 15 (2009) 275–282.
67. El-Eskandarany, *Mechanical Alloying for Fabrication of Advanced Engineering Materials*, William Andrew Publishing, Noyes 2001.
68. X. Zhang, et.al Preparation of Zirconium Diboride Powders by Co-pyrolysis of a Zirconium-Containing Organic Precursor and Polyborazine Using a Solution Based Method, *Cer. Int.* 40 (2014) 15207–15214.
69. M. Randall, E. German, E. Pavan Suri, Seong Jin Park, Review: Liquid Phase Sintering, *J. Mater. Sci.* 44 (2009) 1–39.
70. E. R. Maddrell, Pressureless Sintering of Silicon Carbide, *J. Mater. Sci. Lett.* 6 (1987) 486–488.

71. C. Subramanian, T. K. Roy, T. S. R. Ch. Murthy, P. Sengupta, G. B. Kale, M. V. Krishnaiah, A. K. Suri, Effect of Zirconia Addition on Pressureless Sintering of Boron Carbide, *Ceram. Int.* 34 (2008) 1543–1549.
72. L. Zhao, D. J. X. Duan, Z. Yang, Y. Zhou, Pressureless Sintering of ZrC-Based Ceramics by Enhancing Powder Sinterability, *International Int. J. Refract. Met. Hard. Mater.* 29 (2011) 516–521.
73. G. Ziegler Heinrich and G. Wotting, Relationship Between Processing and Properties of Dense and Reaction-Bonded Silicon Nitride, *J. Mater. Sci.* 22 (1987) 3041–3086.
74. M. H. Bocanegra-Bernal, Review Hot Isostatic Pressing (HIP) Technology and its Applications to Metals and Ceramics, *J. Mater. Sci.* 39 (2004) 6399–6420.
75. H.V. Atkinson, S. Davies, Fundamental Aspects of Hot Isostatic Pressing: An Overview, *Metallurgia* 31 (2000) 2981–3000.
76. D. L. Jiang and Z. R. Huang, SiC Whiskers and Particles Reinforced Al₂O₃ Matrix Composites and N₂-HIP Post-Treatment, *Key.Eng. Mat.* (1997) 379–387.
77. J.E. Garay, Current-Activated, Pressure-Assisted Densification of Materials, *Annu. Rev. Mater. Res.* 40 (2010) 445–469.
78. S. Q. Guo, J. M. Yang, H. Tanaka, Y. Kagawa, Effect of Thermal Exposure on Strength of ZrB₂-Based Composites with Nano-Sized SiC Particles, *Comp. Sci. Technol.* 68 (2008) 3033–3040.
79. W. M. Guo, J. Vleugels, G. J. Zhang, P. L. Wang, O. V. Biest, Effect of heating rate on densification, microstructure and strength of spark plasma sintered ZrB₂-based ceramics, *Scripta Mater.* 62 (2010) 802–805.
80. J. Xu, S. R. Casolco, J. E. Garay, Effect of Varying Displacement Rates on the Densification of Nanostructured Zirconia by Current Activation, *J. Am. Ceram. Soc.* 92 (2009) 1506–1513.
81. W. Chen, U. A. Tamburini, J. E. Garay, J. R. Groza, Z. A. Munir, Fundamental Investigations on the Spark Plasma Sintering/Synthesis Process. II. Modeling of Current and Temperature Distributions, *Mater. Sci. Eng. A*, 394 (2005) 139–148.
82. Official website of the ANF production company, <http://www.nafen.eu> (29.10.2014)
83. Official website of the Red Devil vacuum furnace producer <http://www.rdwebb.com/> (29.10.2014)
84. Official website of the AIP HIP furnace producer <http://aiphp.com/> (29.10.2014)
85. Official website of the SPS furnace producer <http://www.fct-systeme.de/> (29.10.2014)
86. Knowledge source of materials engineering website <http://www.substech.com/> (29.10.2014)
87. Kobe Steel, Ltd., Advanced Products & Technologies Dept. Machinery Company, Technical Literature, <http://www.kobelco.co.jp> (29.10.2014)
88. W. C. Oliver, G. M. Pharr, Improved Technique for Determining Hardness and Elastic Modulus Using Load and Displacement Sensing Indentation Experiments, *J. Mater. Res.* (1992) 1564–1583.

89. W. C. Oliver and G. M. Pharr, Measurement of Hardness and Elastic Modulus by Instrumented Indentation: Advances in Understanding and Refinements to Methodology, *J. Mater. Res.* 19 (2004) 3–20.
90. C. B. Ponton, R. D. Rawlings, Vickers Indentation Fracture Toughness, Part 1: Test review of literature and formulation of standardised indentation toughness equations, *J. Mater. Sci. Tech.* (1989) 865–872.
91. J. Lankford, Indentation Microfracture in the Palmqvist Crack Regime: for by the Implications Fracture Toughness Evaluation Indentation Method, *J. Mater. Sci. Lett.* 1 (1982) 493–495.
92. F. Sergejev, M. Antonov, Comparative Study on Indentation Fracture Toughness Measurements of Hardmetals, *Proc. Estonian Acad. Sci. Eng.* 12 (2006) 388–398.
93. H. R. Lawn, E. R. Fuller, Equilibrium Penny-Like Cracks in Indentation Fracture, *J. Mater. Sci.* 10 (1975) 2016–2024.
94. A. G. Evans, T. R. Wilshaw, Quasi-Static Solid Particle Damage in Brittle Solids, I. Observations, analysis and implications, *Acta. Metall.* 24 (1976) 939–956.
95. A. G. Evans, E. A. Charles, Fracture Toughness Determinations by Indentation, *J. Am. Ceram. Soc.* 59 (1976) 371–372.
96. K. Tanaka, Elastic/Plastic Indentation Hardness and Indentation Fracture Toughness: the Inclusion Core Model, *J. Mater. Sci.* 22 (1987) 1501–1508.
97. GOST 23.201– 78, *Products Wear Resistance Assurance. Gas abrasive wear Testing of Materials and Coatings with Centrifugal Accelerator*, Moscow: Publishing House of Standards, 1987 (in Russian).
98. R. Filippov, A. B. Freidin, I. Hussainova, L. Vilchevskaja, Critical Radius of Zirconia Inclusions for the Effect of Transformation Toughening in Ceramics, *Phys. Mesomech.* 17 (2014) 55–64 (in Russian).

OTHER PUBLICATIONS BY THE AUTHOR:

- V. Antonov, M., Goljandin, D., Andreev, A., Voltšihhin, N., Hussainova, I., Sliding wear behaviour of basalt containing composites with additions of either metallic and/or ceramic phases. *Proceedings of BaltTrib VII International Scientific Conference*, Kaunas, Lithuania, 2013, 67–72.
- VI. Voltšihhin, N., Hussainova, I., Kübarsepp, J., Traksmäa, R., Processing and mechanical properties of ZrC-ZrO₂ composites, *Key Engineering Materials* 604 (2014) 258–261.
- VII. Hussainova, I., Antonov, M., Voltšihhin, N., Assessment of zirconia doped hardmetals as tribomaterials, *Wear* 271 (2011) 1909–1915.
- VIII. Voltšihhin, N., Cura, M.E., Hussainova, I., Hannula, S-P. Sintering routes for zirconia doped hardmetals, *Proceedings of 8th International DAAAM Baltic Conference Industrial Engineering*, Tallinn, Estonia 2012, 765–770.
- IX. Voltšihhin, N., Hussainova I., Hannula, S-P., Viljus, M., Influence of precursor zirconium carbide powders on the properties of the spark plasma sintered ceramic composite materials, W. M. Kriven, *Ceramic Engineering*

and Science Proceedings, Developments in Strategic Materials and Computational Design IV, 2013.

- X. Cura, M.E., Voltšihhin, N., Hussainova I., Viljus, M., Hannula, S-P., Effect of carbon content on sinterability and properties of ZrO₂ doped WC-hardmetals, *Proceedings of 8th international conference of DAAAM Baltic industrial engineering*, Tallinn, Estonia, 2012, 771–776.
- XI. Voltšihhin, N., Hussainova, I., Traksmaa, R., Juhani, K., Optimization of WC-Ni-ZrO₂ structure, *Proceedings of 15th Conference on Composite Materials: ECCM15*, Venice, Italy, 2012, 1–8.
- XII. Hussainova, I., Yung, D.L., Voltšihhin, N., Traksmaa, R., Hannula, S-P., Toward high temperature tough ceramics, *Proceedings of 15th Conference on Composite Materials: ECCM15*, Venice, Italy, 2012, 1–8.
- XIII. Yung, D. L., Voltšihhin, N., Hussainova, I., Kollo, L., Traksmaa, R., Sintering of zirconium carbide-based composites, In: *Proceedings of EuroPM2012–Hardmetals: Hardmetals and Ceramics: European Congress and Exhibition on Powder Materials*, Basel, Switzerland, 2012, 83–88.
- XIV. Hussainova, I., Voltšihhin, N., Cura, E., Hannula, S.-P., Processing and properties of zirconia toughened WC-based hardmetals, *Proceedings of the 37th Int'l Conf & Expo on Advanced Ceramics & Composites ICACC*, Daytona Beach, USA, 2013, 1–7.
- XV. Aghayan, M., Voltšihhin, N., Rodríguez, M.A., Marcos, F.R., Dong, M., Hussainova, I., Functionalization of gamma-alumina nanofibers by alpha-alumina via solution combustion synthesis, *Ceramics International* 2014 12603–12607.
- XVI. Voltšihhin, N.; Hussainova, I., Antonov, M., Abrasion of WC based hardmetals, *3rd European Conference on Tribology and 4th Vienna International Conference on Nano-Technology, ECOTRIB*, Vienna, Austria 2011, 229–232.

ACKNOWLEDGEMENTS

I would like to express my special thanks to my supervisor Dr.Sci. Irina Hussainova, for her support, guidance and encouragement, which made this work possible. I would also to thank my second supervisor PhD. Maksim Antonov for helping and advising in various technical aspects and practical questions and support of this work. I am deeply grateful to the staff of Tallinn University of Technology for their shared experience, fruitful and always enjoyable working atmosphere. I would like to thank my colleagues for their contribution to the publications.

I am very grateful and appreciate all the colleagues from the international cooperation, which became a part of this work and without whom this work would not be possible. I would like to thank Professor Simo-Peka Hannula from the Aalto University in Finland for giving me the opportunity of working in his team and to use some advanced equipment. Also MSc Erkin Cura from the Prof. Hannula research group who kindly helped me to gain valuable experience while performing different experiments.

I would like to express my great thank to Dr. Miguel A. Rodriguez from the Instituto de Ceramica y Vidrio in Spain for giving me the possibility of working under his supervision in a highly developed ceramic production oriented laboratory.

Estonian Science Foundation (grants numbers ETF8850, ETF8211, SF0140062s08 and AR12133) is acknowledged for supporting this research. The research work on basalt addition into the ceramic matrix was carried out during the course of study in the frame of ETF8850 and the main results are reported in the paper V. This work has been also partially supported by graduate school „Functional materials and technologies“, receiving funding from the European Social Fund under project 1.2.0401.09-0079 and Archimedes Foundation.

I would like to thank my family and friends for their continuous direct and indirect support, patience, understanding and encouragement at different stages of the present work.

Finally, I would like to express my obeisance to the Destiny for giving me the possibility of becoming a young scientist and obtaining PhD degree.

ABSTRACT

Design and technology of oxides-containing ceramic-based composites

Ceramics and ceramic-based composites are materials of the future without any doubt. Ceramics have low density and very high strength characteristics. Ceramics have high resistance to oxidation, they are chemically inert in many harsh environments and withstand elevated temperatures, because of their high melting temperatures. All the named properties are being the result of the covalent bonding of the ceramic materials. Another side of the covalent bonding in the ceramics is that these materials are brittle and because of their high melting point they are difficult to fabricate. They break immediately as soon as maximum fracture load value is obtained.

Powder metallurgy (PM) is one of the best methods for the production of ceramic-based materials. It gives an ability to produce different material compositions and introduce properties improving additives during the precursor powder preparation stage.

In current study PM was used for the production and development of the ceramic-based composite materials. Carbides, oxides and metals were taken as the main composing elements. Three main compositions were produced in present study and yttria-stabilized tetragonal zirconia (YTZ) was used as a main additional or compositional component in all of the produced materials. It was decided to study the properties of such materials as WC-Ni-ZrO₂, ZrC-ZrO₂ and ZrO₂-Al₂O₃. Production and development consisted in fabrication of the designed compositions with different sintering techniques because sintering was considered as one of the main and most influencing stage of PM.

Four main sintering technologies were used in present study: three conventional sintering techniques (ambient sintering in high temperature furnace, vacuum pressureless sintering (VPS) and hot isostatic pressing (HIP)) and one non-conventional but rapidly developing and promising technique called spark plasma sintering (SPS).

The aim of this research was to produce new types of ceramic-based composite materials with high level of densification and high mechanical properties by the means of different sintering techniques and to compare the properties and microstructural characteristics between those technologies in order to reveal best suitable method for given material group.

The research has shown that SPS technique is more preferable for the production of the materials, which need to be produced with sintering temperatures lower than conventional consolidation temperatures. Also when grain growth of the ceramics need to be kept minimal, SPS is more preferable due to shorter sintering time. However, sintering of the ZrC-ZrO₂ composite has shown that named mechanical and microstructural parameters will be the same in both SPS and VPS cases.

KOKKUVÕTE

Oksiide sisaldava komposiitkeraamika tehnoloogia

Keraamika ja keraamikal põhinevad komposiidid on huvipakkuvad materjalid tänu nende madalale tihedusele, kõrgetele tugevusnäitajatele ja heale vastupanule oksüdeerumisele. Keraamika on keemiliselt inertne paljudes agressiivsetes keskkondades ja peab vastu kõrgendatud temperatuuridele. Kõik nimetatud omadused on keraamika korral tagatud aatomitevaheliste kovalentsete sidemetega, samas kovalentsetest sidemetest tuleneb negatiivne pool – nende haprus. Keraamika puruneb kiirelt, samaaegselt kui pinge saavutab oma maksimaalse väärtuse. Samas on ka keraamika valmistamisel (paagutamisel) osakeste vaheliste sidemete tekitamiseks vaja palju energiat.

Pulbermetallurgia (PM) on üks parimatest viisidest keraamiliste materjalide valmistamiseks. See annab võimaluse erineva koostisega materjalide tootmiseks ja võimaldab saada eriomadusi, kasutades parendavaid lisandeid.

Uuringu põhieesmärgiks oli valmistada uut tüüpi komposiitkeraamika, mis on pooride ja teiste defektide vaba, parendatud mehaaniliste omadustega, kasutades erinevaid paagutustehnoloogiaid. Võrreldakse erinevate paagutustehnoloogiate teel saadud materjalide omadusi ja mikrostruktuurseid karakteristikuid, leidmaks sobivaim paagutusmeetod antud materjaligrupi tootmiseks.

Käesolevas töös on kasutatud PM tehnoloogiat selleks, et arendada ja valmistada keraamilisi komposiitmaterjale. Põhikomponentideks on võetud karbiidid, oksiidid ja metallid. Töös on uuritud kolme erineva koostisega ja tsirkooniumdioksiidi (ZrO_2) lisandiga komposiitkeraamikat. Eesmärgiks oli uurida WC-Ni-ZrO₂, ZrC-ZrO₂ ja ZrO₂-Al₂O₃ komposiitkeraamika omadusi. Omaduste parandamiseks uuriti komposiitkeraamika erinevaid paagutustehnoloogiaid: kolme traditsioonilist meetodit (kõrgetemperatuurne paagutamine õhus, paagutamine vaakumis, kuumisostaatiline pressimine) ja üht mittetraditsioonilist aga kiiresti arenevat ja perspektiivset paagutustehnoloogiat – plasmäsädepaagutust (*spark plasma sintering, SPS*).

Uuringute tulemusena selgitati välja, et plasmäsädepaagutusmeetod on sobivam materjalidele, kui on oluline madalam paagutustemperatuur ja lühiajalisem paagutuskestvus võrreldes traditsiooniliste paagutusmeetoditega. Plasmäsädepaagutus võimaldab saada WC-Ni-ZrO₂ komposiitkeraamika korral peeneteralisema materjali ja paremad sitkusnäitajad; Al₂O₃ kiududega armeeritud ZrO₂ keraamika korral vältida kiudude lagunemist ja sellest tulenevalt parandada materjali sitkust. ZrC-ZrO₂ komposiitkeraamika korral mehaanilised omadused on samasugused nii plasmäsäde- kui vaakumpaagutuse kasutamisel.

CURRICULUM VITAE

1. Personal data

Name	Nikolai Voltšihhin
Date and place of birth	14.01.1985, Kohtla-Järve
E-mail address	<u>nikolai.voltšihhin@ttu.ee</u>

2. Education

Educational institution	Graduation year	Education (Programme/degree)
Tallinn University of Technology	2010	Development and Production Engineering / Master
Tallinn University of Technology	2007	Development and Production Engineering / Bachelor
Kohtla-Järve Vene Gümnaasium	2004	Secondary education

3. Language competence/skills (fluent, average, basic skills)

Language	Level
Russian	Native
Estonian	Fluent
English	Fluent

4. Special courses

Name of the course	Educational and research
PM Sintering - Advanced Processes and Materials	EPMA European Powder Metallurgy Association 03.2013
International Training Programme on laboratory quality management systems	National Institute of Training and Standardization; 02.2014
Towards comprehensive Control of Wear	TWC Tampere; 10.2010
2012 Aalto University	Joint research 02– 05.2014
Instituto de Cerámica y Vidrio del CSIC	Joint research 04.2014

5. Professional employment

Period	Organisation	Position
09.2011 – 08.2012	Tallinn University of Technology	Engineer
09.2012 – 08.2013	Tallinn University of Technology	Researcher
09.2013 – ...	E-Profiil AS	Welding Engineer

ELULOOKIRJELDUS

1. Isikuandmed

Ees- ja perekonnanimi
Sünniaeg ja -koht
Kodakondsus
E-posti aadress

Nikolai Voltšihhin
14.01.1985 Kohtla-Järve
Eesti
nikolai.voltšihhin@ttu.ee

2. Hariduskäik

Õppeasutus (nimetus lõpetamise ajal)	Lõpetamise aeg	Haridus (kraad/eriala)
Tallinna Tehnikaülikool (TTÜ)	2010	Magister, Tootearendus ja tootmistehnika
Tallinna Tehnikaülikool (TTÜ)	2007	Bakalaureus, Tootearendus ja tootmistehnika
Kohtla-Järve Vene Gümnaasium	2004	Keskharidus

3. Keelteoskus (alg-, kesk- või kõrgtase)

Keel	Tase
Vene	Emakeel
Eesti	Väga hea
Inglise	Väga hea

4. Täiendusõpe

Kursuse nimi	Täiendusõppe korraldaja nimetus
PM Sintering - Advanced Processes and Materials	EPMA European Powder Metallurgy Association; 03.2013
International Training Programme on laboratory quality management systems	National Institute of Training and Standardization; 02.2014
Towards Comprehensive Control of Wear	TWC Tampere; 10.2010
2012 Aalto University	Joint research 4 month
Instituto de Cerámica y Vidrio del CSIC	Joint research 2 weeks; 04.2014

5. Teenistuskäik

Töötamise aeg	Tööandja nimetus	Ametikoht
09.2011 – 08.2012	Tallinna Tehnikaülikool	Insener
09.2012 – 08.2013	Tallinna Tehnikaülikool	Teadur
09.2013 – ...	E-Profil AS	Keevitusinsener

PUBLICATIONS

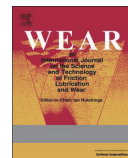
- I. Hussainova, I., Antonov, M., **Voltšihhin, N.**, Kübarsepp, J., Wear behavior of Co-free hardmetals doped by zirconia and produced by conventional PM and SPS routines. *Wear* 312 (2014) 83–90.

DOI: <http://dx.doi.org/10.1016/j.wear.2014.01.014>



Contents lists available at ScienceDirect

Wear

journal homepage: www.elsevier.com/locate/wear

Wear behavior of Co-free hardmetals doped by zirconia and produced by conventional PM and SPS routines



Irina Hussainova*, Maksim Antonov, Nikolai Voltsihhin, Jakob Kübarsepp

Department of Materials Engineering, Tallinn University of Technology, Ehitajate 5, 19086 Tallinn, Estonia

ARTICLE INFO

Article history:

Received 24 September 2013

Received in revised form

20 January 2014

Accepted 22 January 2014

Available online 14 February 2014

Keywords:

Cemented carbides

Co-free hardmetals

Erosion

Abrasion

Spark plasma sintering

Zirconia

ABSTRACT

In this work, the microstructural features and mechanical properties of Co-free hardmetals doped by 3 mol% yttria stabilized tetragonal zirconia and densified by means of conventional vacuum pressureless sintering as well as spark plasma sintering were studied. Influence of dispersed zirconia clusters on mechanical behavior and erosive and abrasive wear resistance of hardmetals with 6 wt% of stabilized ZrO₂ was investigated. It was shown that zirconia transformability affects the wear performance of the composites. For utilization of the mechanism of transformation toughening some essential requirements such as grain size and grain size distribution should be met. Simultaneous increase in fracture toughness due to stress induced transformation toughening of tetragonal zirconia with increase in hardness due to grain growth inhibition during processing allows considering the cemented carbides doped by zirconia as promising tribomaterials.

© 2014 Elsevier B.V. All rights reserved.

1. Introduction

Processing and mechanical behavior of various types of cemented carbides has been extensively studied over the last decade; however, to extend the service life of cemented carbides and enhance their reliability under severe conditions, novel compositions have been continuously developed and their wear behavior evaluated. Tungsten carbides based composites are one of the most widely used industrial materials due to their unique combination of mechanical, physical and chemical properties. These materials represent the aggregates of hard WC particles bonded with cobalt or nickel and usually produced by a liquid-phase sintering. Most of the WC–Co applications, starting from cutting tools through dies to teeth on gravel extractors, require high wear and oxidation resistance and tolerance to impact loading. Poor thermal stability of cobalt and insufficient corrosion–oxidation resistance limit the applications of such kind of hardmetals as structural components where high temperature mechanical properties, acceptable fracture toughness and wear resistance are required. Therefore, in recent decades research interests have been focused on improvement of composites reliability and durability [1–6]. One of the approaches is a partial substitution of WC particles by other non-oxide compounds and/or using grain growth inhibitor [7,8]. The alternative way to improve durability is

modifying the cobalt binder phase by doping with nickel, iron, etc. Substantial research efforts have been directed towards sintering of nanosized tungsten carbide based composites attempting considerable improvement in the mechanical properties of the hardmetals [9]. Indeed, there are strong indications of dramatic shift in mechanical behavior of nano-structured and/or ultra-fine grained materials [1,5]. However, there is no ultimate picture yet on advantage of nano-structures considering their fracture toughness. Attempt to incorporate zirconium dioxide into the WC matrix to substitute binder metal has recently met with the success in fabrication of WC–ZrO₂ composites with superior properties and excellent chemical stability [1,4,5]. Along with high flexural strength of about 1 GPa and fracture toughness of about 10 MPa m^{1/2}, zirconia also possesses a relatively high hardness and wear resistance [10]. These properties have led to the use of zirconia-based components in a number of engineering applications such as automobile engine parts, wire drawing dies and cutting tools [11].

Transformation toughening of materials based on the martensitic phase transformation in ZrO₂ systems has been widely studied [6,10,11] and results demonstrated a potential for exploitation of stabilized tetragonal zirconia as a toughening agent in different ceramic matrices. However, one of the most effective methods to increase the fracture toughness of ceramics and improve materials reliability is incorporating a ductile metallic phase. Ceramic–metal composites (cermets or hardmetals) can represent such kind of matrix for zirconia incorporation not only for increase in toughness but also for improvement in wear

* Corresponding author. Tel.: 372 6203371.

resistance through increase in hardness by inhibiting carbide grains growth and hindering cracks propagation. The attempts to incorporate ZrO_2 into low binder containing or binderless cermets seem to be a promising way in development of engineering materials tolerant to impact loading.

The method of the composite fabrication, i.e. processing parameters, plays a crucial role for developing the materials properties. The wear behavior of cemented carbides is directly related to its chemical composition and microstructure. The wear resistance of these materials generally increases by the reduction of binder metal content and by decreasing the grain size. The ongoing research is focused on the development of sintering techniques that allow full densification of WC-based hardmetals at lower sintering temperature and/or within a shorter thermal cycle time, such as hot pressing [6,12], microwave sintering [13] or spark plasma sintering (SPS) [14]. From a practical point of view, the essential requirement to the processing route obtains the uniform distribution of phases throughout a composite and a dense material with low residual flaw population. Wettability of the constituents, therefore, should be carefully considered. Due to relatively better wettability between zirconium dioxide and nickel as well as nickel better oxidation resistance as compared to cobalt, the composites of tungsten carbide with nickel binder metal were assessed in the present work. The tribological performance of the cemented carbides with and without zirconia additives and fabricated by two different methods (conventional vacuum sintering and spark plasma sintering) is the main objective of the study on the composites in erosive and abrasive media.

2. Materials and experimental procedure

2.1. Materials

Cemented carbides with 6–12 wt% of binder metal have found a wide application in industry. In the present work, the composites with 8 wt% of nickel was chosen as a reference material. Because influence of metal content on wear performance of hardmetals is comprehensively documented [15–21], the variations in binder content were not considered as a goal of this study. The amount of yttria stabilized zirconia of 6 wt% was chosen as being quite enough for exploitation and investigation of the mechanism of transformation toughening while small enough not to unfavorably influence the hardness of the composites. WC powder with average particles size of $0.9\ \mu\text{m}$ and 99% of purity was provided by Wolfram GmbH, Austria. The commercially available nickel powder of 99.7% purity and average grain size of $7\ \mu\text{m}$ was used as a binder metal. 6 wt% of a commercial 3 mol% yttria stabilized tetragonal zirconia powder ($< 100\ \text{nm}$, 99.9% purity, Alfa Aesar, Germany) was mixed with the precursor powders to produce the WC–Y– ZrO_2 –Ni hardmetal. To eliminate unfavorable η -phase formation during sintering 0.2 wt% of free carbon was added to the mixture as described elsewhere [12]. The powders were mixed in ethanol with PEG (Polyethylene glycol) plasticizer in a rotary ball mill for 72 h using 6 mm diameter WC–Co milling balls. The

contamination from the WC–Co balls was minimized by a low energy mode of mixing.

2.2. Processing

Milled and dried powder blends were subjected to a cold pressing at 8.5 MPa to obtain green compacts with a green density of about 55% of theoretical density. Green bodies have been held at $500\ ^\circ\text{C}$ in hydrogen for 30 min to burn plasticizers off.

Two different techniques, namely vacuum pressureless sintering (VPS) and spark plasma sintering (SPS), also known as field assisted sintering or pulsed electric current sintering, were used in this study for powders densification.

Retention of the metastable tetragonal polymorph of zirconia is critically dependent on the sintering conditions and is affected by the sintering temperature largely. Based on the previous results [6,12] the sintering temperature for the composites processing has been chosen as $1450\ ^\circ\text{C}$ for VPS and $1275\ ^\circ\text{C}$ for SPS routines. The procedure of the specimens' fabrication is sketched in Fig. 1.

The SPS technology allows us to densify WC–Co materials at much lower temperatures as compared to conventional pressureless sintering.

The spark plasma sintering (FCT HP D 25-2, Germany) was performed in vacuum at the conditions of electric current pulse duration of 10 ms and pause of 5 ms. The powders were poured into a cylindrical graphite die and sintered at $1275\ ^\circ\text{C}$ and pressure of 50 MPa for 1 min.

The main purposes of the consolidation routes are to ensure a uniform distribution of tetragonal inclusions within a matrix and to retain the majority of the zirconia grains in metastable tetragonal polymorph.

2.3. Characterization

Prior to the investigations, the specimens were grounded and smoothly polished with diamond paste to obtain optically reflecting surfaces.

The microstructure and grain size of the constituent phases were examined with scanning electron microscopy (SEM, Leo Supra-35) equipped with energy dispersive spectroscopy (EDS – TM-1000) analyzer. Grain size was described by the spherical equivalent diameter.

X-ray diffraction (XRD; Siemens, Bruker D5005) analysis was conducted to identify phases in the initial powder and crystalline phases after sintering and erosion/abrasion tests. Specimens were irradiated with Cu $K\alpha$ -radiation at 40 kV in a scanning range 2θ from 20° to 80° with a step size of 0.04° . The integrated intensities of the (101) tetragonal peak and (111) and (111) monoclinic peaks were measured and volume fraction of the monoclinic polymorph was calculated using the Porter and Heuer method corrected for the monoclinic–tetragonal system [22].

The sintered density was measured by the Archimedes technique using water as the immersion medium. Hardness was measured on an Indentec 5030 SK V Vickers hardness tester with an indentation load of 10 kg. The reported Vickers hardness, HV_{10} , for each composition is the mean and standard deviation of 10 indents.

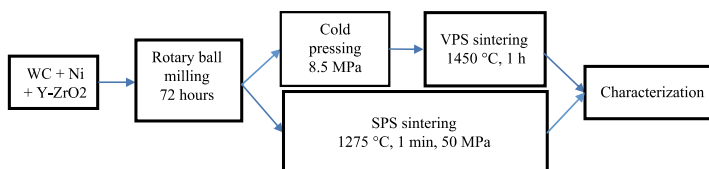


Fig. 1. Sketch of the composites processing.

The indentation toughness approach was chosen as the easiest and effective way to estimate fracture toughness of the composites. The indentation fracture toughness, K_{IC} , was calculated from the length of radial cracks emanating from the corners of the Vickers indentation imprints using the well-known Palmqvist approach. Load of 50 kg on the indenter resulted in quite well developed cracks that would mitigate any surface effects of the indentation. The c/a ratio (c – half-crack length of a radial crack, and a – half-diagonal length of an indent) is less than 3 in most cases; therefore, a developed crack system may be considered as the Palmqvist system. The surface cracks initiated by the indenter were measured using optical microscopy that gives suitable contrast on the surface for accurate measurements of the crack lengths. The reported values are the mean and standard deviation of at least six indentations. It should be noted that the single-edge V-notch beam (SEVNB) route provides more reliable values of the fracture toughness as compared to the indentation fracture toughness, which often gives the overestimated values. However, difficulties in the sample preparation limit SEVNB method adaptability.

Erosion testing was conducted with the help of conventional four-channel particles accelerator [16], which consists of a feeder to give a controlled in-feed of particles, a rotating disc with six radial channels to accelerate the particles and a target holding system. During operation, particles were continuously fed into the central hole of the rotating disc, accelerated through several radial ceramic channels by the centrifugal force and ejected from the open end of the acceleration tubes. The specimen targets are located around the disc on adjustable holding systems. Silica particles traveling at velocities of 50–80 ms^{-1} at a normal incident angle were used as erodents in this study. Tests were conducted at room temperature and the erosion rate was determined as volume loss of the target material per mass of the erodent particle.

Minimum of four erosion rate measurements were made for each test condition and material. Subsequently, the results were averaged.

Abrasive testing was performed using the rubber-rimmed rotary wheel machine according to the modified ASTM 65–94 method with reduced diameter of the wheel disk for testing small sized specimens and cutting down expenses during development stage of a new material [17]. Abrasion test results are reported as volume loss in cubic millimeters per load and distance ($\text{mm}^3 \text{N}^{-1} \text{m}^{-1}$) for the specified test conditions are summarized in Table 1. The wear tests were repeated at least 3 times and average values are stated throughout the paper.

3. Results and discussion

3.1. Microstructural analysis

The XRD patterns as well as SEM image of the precursor mixture are shown in Fig. 2.

The two main microstructural features of hardmetals, which greatly influence the wear resistance of the materials, are the binder content and the carbide grain size that largely affect the mechanical properties and, therefore, tribological performance [18–21]. The shape of carbide grains in the conventionally sintered WC–Co hardmetals is usually a truncated triangular prism and influenced by the binder metals and/or additives. In the composites developed during this study, three types of the WC grains have been detected: small amount of standard triangular shaped grains, some amount of rectangular shaped grains, while most of the WC grains were relatively equiaxial (Fig. 3). The shape change could be related to the effect of zirconia on the interface energy of the system. In the SEM images the dark spots represent zirconia particles; gray areas show nickel binder and bright regions are carbides.

Vacuum pressureless sintered materials revealed insignificant grain growth during heat treatment and bimodal final distribution of the WC grains composed of two groups: $\leq 1 \mu\text{m}$ and $\geq 2.5 \mu\text{m}$. Most of the WC grains are equiaxed and separated by a thin layer of nickel. Therefore, the addition of another ceramic phase suppresses the formation of undesirable triangular WC grains.

From Fig. 3a, zirconia is in well-dispersed clusters of uniform size distribution ranging between 0.2 and 3 μm . The ultrafine zirconia powders ($\sim 100 \text{nm}$) possess very high surface to volume ratio. In order to minimize the total interfacial energy of the system, the large surface area provides a strong driving force for the powder particles to form agglomerates. These agglomerates determine the final clusters size in the bulk composites.

The density data revealed the near theoretical densification (over 99% of theoretical density) of the product that pointed to the fact that WC–Ni–Y/ZrO₂ hybrid material may be successfully

Table 1
Abrasive test conditions.

Specification	Description
Scheme	Block-on-wheel
Wheel	\varnothing 80 mm, width 8 mm, steel covered by chlorobutyl rubber
Abrasive	SiO ₂ , particle size 0.1–0.3 mm, HV=1100, feeding rate 300 g min^{-1}
Circumferential velocity	1 m s^{-1}
Number of rotations	1500 turns
Force against specimen	5 kg (47 N)
Atmosphere	Air, relative humidity 50 \pm 10%
Temperature	Room temperature

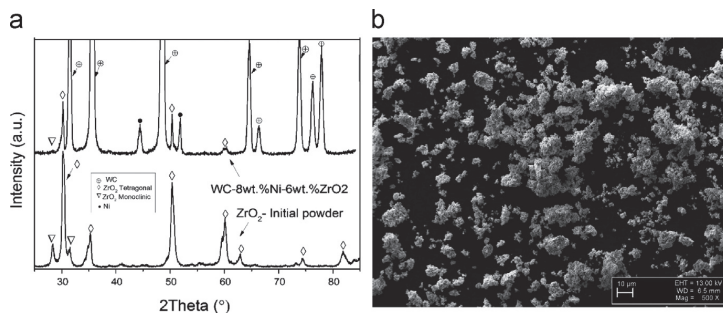


Fig. 2. (a) XRD patterns of the initial zirconia powder and precursor powder blend; (b) SEM micrograph of the precursor powder.

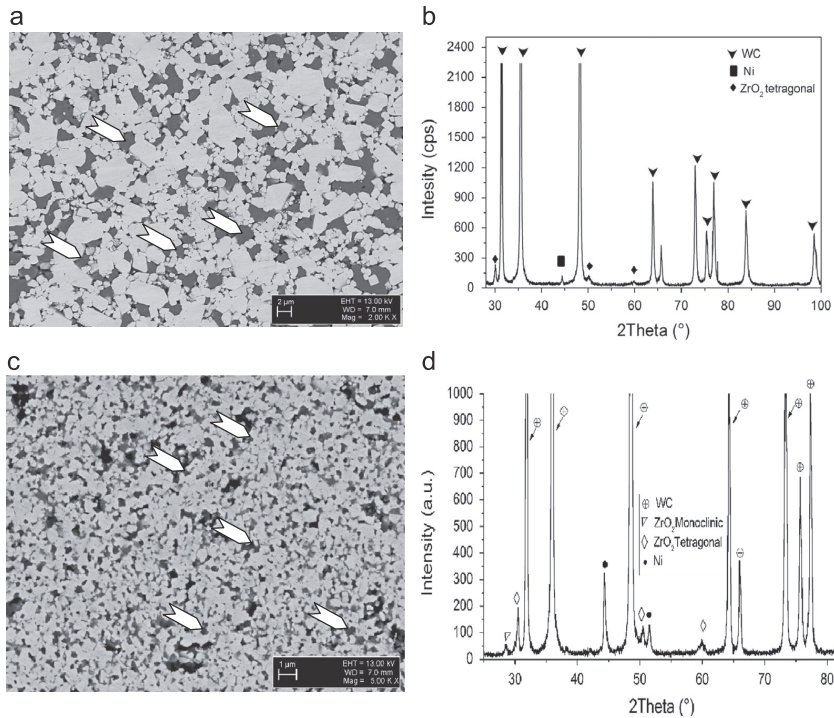


Fig. 3. (a) SEM image of the pressureless sintered WC–Ni–Y/ZrO₂ and (b) the XRD pattern; (c) SEM images of the SPSed WC–Ni–Y/ZrO₂ and (d) the XRD pattern. White arrows point at zirconia clusters.

produced with the help of pressureless sintering at 1450 °C. Another important observation is the presence of t-ZrO₂ in the sintered material. The XRD pattern recorded from the polished surface of the material and shown in Fig. 3b shows no spurious phases, while some monoclinic zirconia is present along with its tetragonal modification. This suggests that the metastable tetragonal phase can be retained during processing and may contribute to the increase in fracture toughness.

Application of a high electric current for SPS allows consolidating powders to full density much faster and at lower temperatures as compared to conventional methods of powder metallurgy. The microstructure can be considered as an ultra-fine grained one with the WC grain size in the sub-micron range, which is about the particle size of the precursor WC powder (~0.9 μm). This result implies minimal grain growth during processing. Therefore, it may be concluded that rapid sintering process and dispersion of ZrO₂ particles are useful in suppressing the WC grain growth. The effect of oxides on grain growth is still quite questionable and requires further evaluation.

XRD patterns recorded from the polished surfaces of the processed samples are presented in Fig. 3c. Within the limits of XRD detection, no phases other than WC, tetragonal and monoclinic zirconia, and Ni could be recorded from the corresponding patterns. This suggests that no sintering reaction occurred to any noticeable extent during the processing; Y/ZrO₂ is retained in its metastable tetragonal polymorph in the present processing scheme and, therefore, can contribute to increase in fracture toughness of the composite.

The martensitic transformation from the tetragonal to the monoclinic structure is strongly influenced by zirconia grain size

and size distribution throughout a composite [5,10,23]. Retention of the metastable tetragonal phase is further maximized by maintaining the grain size of the zirconia below an “upper” critical grain size value, when particles are the subjects of the spontaneous transformation, while above a “lower” critical size when particles are overstabilized for any transformation. From a practical point of view, the essential requirements are retaining of controlled metastability of the tetragonal phase at the service temperature and uniform distribution of the zirconia additives with the appropriate size as well as a low residual flaws population.

Pressureless sintered composites contain the zirconia agglomerates of relatively wide size distribution ranging between 0.1 and 2.5 μm (Fig. 3). The SEM examination also revealed the presence of nanocrystalline zirconia particles of 30–60 nm entrapped within micron WC grains.

Ytria stabilized zirconia grains are much smaller in the spark plasma sintered specimens. Zirconia grains can also be determined as ultra-fine sized although zirconia particles are highly agglomerated and present clusters of uniform size distribution ranging between 0.05 and 0.5 μm and most of them are located between fine carbide grains surrounded by binder metal.

A thermodynamic formulation for the critical size of inclusions to be transformed in a constrained matrix dc can be expressed through the process of “competition” in a change of a surface free energy and a chemical free energy during martensitic t→m transformation of the zirconia particle. The thorough theoretical consideration of the problem is out of scope of the present paper; however, rough analysis performed by the authors in [24] by comparison of Gibbs energies of the composite materials with

inclusions in different phase states gives an estimation of the critical radius of the 3 mol% yttria stabilized zirconia particles to be around 1 μm .

3.2. Mechanical properties

The mechanical properties of the composites developed are listed in Table 2. Hardness and fracture toughness are two of the most important mechanical properties of tribo-materials. Many materials characteristics such as wear resistance, for example, are more or less affected by these two parameters. As expected, quite high Vickers hardness was achieved in the fine grained cermets as reported in Table 2. Conventional hardmetals of 8–12 wt% of binder metal (Co or Ni) possess hardness in a very wide range starting from as low as about $HV_{10}=1000$ and achieving as high value as 1600 depending on many factors including carbide grain size, porosity, and so on [25,26]. It is well known that the hardness of the ultra-fine grained and nano-grained materials is significantly higher ($\sim 1500\text{--}2000$) and increases with decrease in WC grains size [9,26].

The volume change accompanying transformation creates a compressive strain field around a crack tip to oppose crack propagation, while the strain energy associated with any net shear component of the transformation strain in the transformation zone contributes an effective increase in the energy of fracture [27]. Additional contributions to toughness may result from micro-cracking associated with accommodation of the transformation shape strain and from crack deflection within the transformation zone ahead of the crack. Usually ceramic materials display a very limited amount of local plasticity; therefore, some amount of ductile binder metal can help in preventing secondary spallation in the matrix. In addition, bridging crack surfaces by ductile ligaments may contribute to the materials fracture toughness.

Indentation fracture toughness of the composites developed is somewhat higher as compared to published data for conventional and even nanocrystalline cemented carbides with the same amount of metal binder [9,25]. It has been shown that the crack does not advance exactly along the interfaces in conventional WC–Co/Ni hardmetals but proceeds in the binder, forming closely

spaced shallow dimples in material [9]. For conventional bulk WC–Co/Ni hardmetals, the fracture toughness is a function of a mean free path λ between the WC grains. A finer grain size usually results in smaller λ at a given constant volume fraction of binder and smaller plastic zone, and therefore, lower fracture toughness. For ultra-fine grained hardmetals the effect of the plastic mechanisms of binder metal will no doubt be reduced [9]. The mean free path is estimated to be about 320 nm and 100 nm in VPSed and SPSeD composites, respectively. The degree of contiguity greatly influences the properties of composites, particularly if the properties of the constituent phases differ significantly. Generally, as the contiguity increases, hardness increases and fracture toughness decreases. Continuity between both WC grains and WC–Y/ZrO₂ grains was estimated to be 0.66 for VPSed material and 0.68 for SPSeD one. Therefore, some increase in fracture toughness of VPSed hardmetal can be expected from synergetic effect of the crack bridging/plasticity of the metal binder as well as the stress activated phase transformation.

However, it should be noticed that because the fracture toughness data listed in Table 1 were measured indirectly using the Palmqvist method and converted to the K_{IC} values, it is not evident that these values can be reproduced using the standard fracture toughness testing methods such as the short-rod method (ASTM-B771) or the SENB method (ASTM-E399).

Fig. 4 shows the SEM micrographs of the indentation cracks propagating in the composites. The crack propagates predominantly along grain boundaries indicating an intergranular character of cracking; zirconia grains also tend to deflect the crack. Further, when the crack propagates along the tetragonal grains, some crack closure can be observed pointing to the possible grain transformation due to the crack stress field. Therefore, the multiplicative interactions such as crack deflection and stopping combined with binder plasticity are evident and can be considered as operating toughening mechanisms in the composites.

3.3. Wear resistance

Quantitative results of the erosion and three-body abrasion of the cermets tested are given in Table 3.

Table 2
Mechanical properties of the WC–Ni–Y–ZrO₂ hardmetals.

Material	VPS _{WC–Ni}	VPS _{WC–Y–ZrO₂–Ni}	SPS _{WC–Y–ZrO₂–Ni}
Relative density (%)	~ 98	~ 99	~ 98
Average WC grain size (μm)	~ 3.0	Bi-modal	~ 0.9
Hardness (HV_{10})	1650 ± 77	1770 ± 53	1755 ± 36
IFT, K_{IC} ($\text{MPa m}^{1/2}$)	11.1 ± 3.8	15.03 ± 4.1	11.35 ± 3.3

Table 3
Wear rates of the materials studied.

Grade	Erosion rate ($\text{mm}^3/\text{kg}; 50 \text{ ms}^{-1}$)	Erosion rate ($\text{mm}^3/\text{kg}; 80 \text{ ms}^{-1}$)	Abrasion rate ($\text{mm}^3/\text{Nm} \times 10^{-5}$)
VPS _{WC–Ni}	2.72 ± 0.33	6.42 ± 0.53	15.0 ± 2.3
VPS _{WC–Y–ZrO₂–Ni}	0.64 ± 0.2	1.44 ± 0.33	9.4 ± 1.2
SPS _{WC–Y–ZrO₂–Ni}	1.51 ± 0.26	2.86 ± 0.28	8.8 ± 0.9

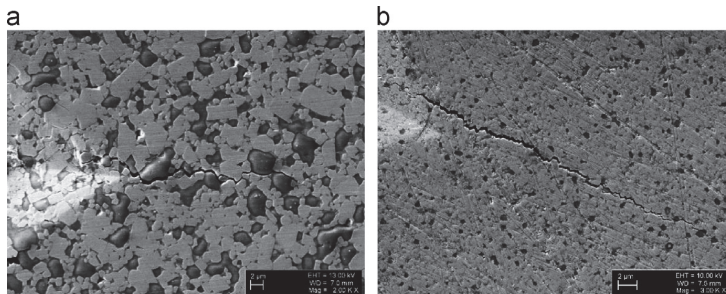


Fig. 4. SEM micrographs of the indentation cracks on the surface of (a) pressureless sintered WC–Ni–Y–ZrO₂ and (b) spark plasma sintered WC–Ni–Y–ZrO₂.

3.3.1. Erosion

The erosion rate of WC–Ni–Y/ZrO₂ hybrids is lower as compared to erosion rate of the conventional WC–Ni hardmetal. It is well proved that the erosion rate of the cemented carbides increases with increasing WC grain size or, in other words, with decreasing hardness [25,28]. However, many other characteristics, such as fracture toughness and residual porosity, should be taken into account when erosion resistance is evaluated [3,29]. Among materials tested, the reference WC–Ni hardmetal exhibited the lowest mechanical performance in terms of porosity, hardness and toughness; therefore, its lowest wear resistance is quite expected at both velocities of the erosive particle impact (Table 3 and Fig. 5). Assuming a wear resistance is related to hardness and fracture toughness following the relationship $\propto K_{IC}^m H^n$, (where the exponents m and n have negative values and vary according to the manner in

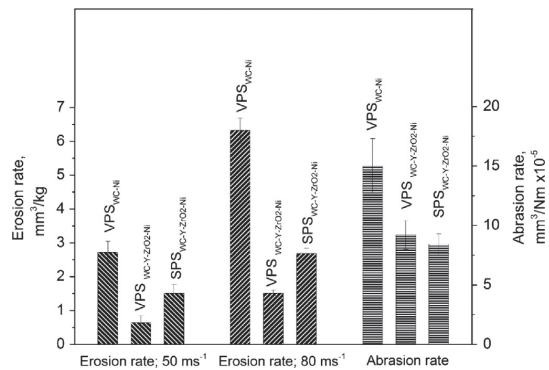


Fig. 5. Erosion rates of the hardmetals tested.

which material is removed; C is a constant of proportionality taking into consideration test conditions), the erosion performance of pressureless sintered hardmetal should be the best one. Indeed, the VPSed grade shows the highest wear resistance and, therefore, the effect of phase transformation toughening is somewhat masked. The worn surfaces of the composites were examined to determine the wear mechanisms and zirconia transformability. The SEM micrographs, displayed in Fig. 6, give some views onto the surfaces damaged by silica particles traveling at the velocity of 80 ms⁻¹.

The surfaces exposed to impact of the erosive particles appear to be severely damaged and deficient with the binder metal. Scars of plastic deformation in the carbide grains, cracking of some large grains and grains separation along WC–WC and WC–Ni interfaces combined with depletion and washout of the binder phase around the carbides lead to the weakening of the materials and, as a consequence, to removal of the unsupported carbides. Very similar mechanisms of erosion wear for WC–Co hardmetals are reported in [30], for example. The role of tetragonal zirconia grains is not so clearly understood from the micrographs; some limited intergranular cracking between WC and Y/ZrO₂ can be observed (Fig. 6). However, almost no transgranular crack propagation through the zirconia clusters (except very large agglomerates) was observed. In all probabilities, zirconium dioxide particles undergo the phase transformation under applied load. Stress-induced transformation consumes crack propagation energy relieving the stress concentration. The resulting volumetric expansion closes traction along the crack reducing the driving force for its propagation. Transformation would result in volumetric expansions along the three axes of the individual lattice directions of crystals that would be randomly oriented. Some crack deflection or crack arresting near zirconia particle could occur to dissipate some of the fracture energy. Depletion of the protective binder remains unsupported or weakly bonded with carbides; zirconia grains are removed from the surface as a whole.

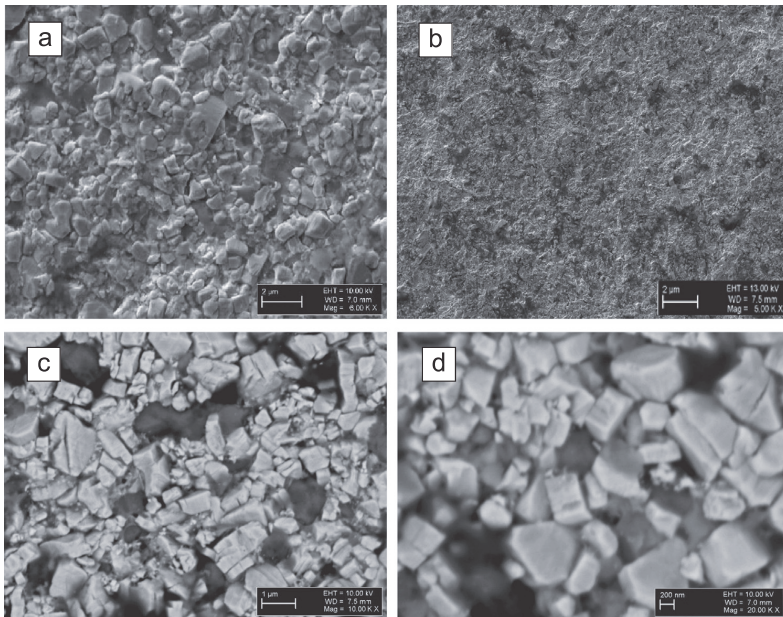


Fig. 6. SEM micrographs of the worn surfaces: (a, c) surface of VPSed composite at different magnifications and (b, d) surface of SPSed composite at different magnifications.

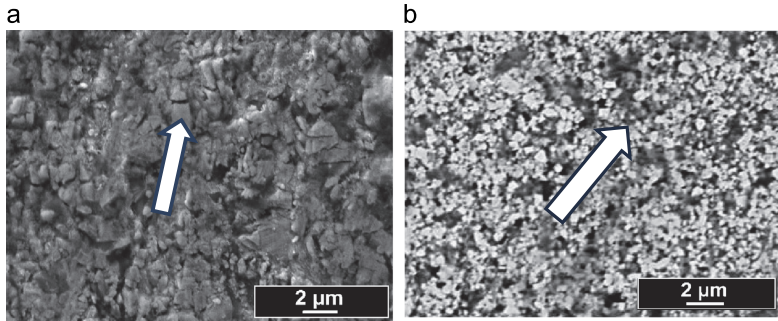


Fig. 7. SEM images of the specimens subjected to abrasive wear: (a) pressureless sintered WC-Ni-Y/ZrO₂ and (b) spark plasma sintered WC-Ni-Y/ZrO₂.

Table 4
Tetragonal zirconia transformability.

Material	VPS _{WC-Y-ZrO₂-Ni}	SPS _{WC-Y-ZrO₂-Ni}
m-Y-ZrO ₂ (as-sintered) (%)	9.6 ± 1.5	7.9 ± 1.2
m-Y-ZrO ₂ (eroded at 50 ms ⁻¹) (%)	36 ± 5.5	27.5 ± 3.7
t-Y-ZrO ₂ transformability (erosion)	~40	~29
m-Y-ZrO ₂ (eroded at 80 ms ⁻¹) (%)	56.8 ± 4	38.4 ± 5.7
t-Y-ZrO ₂ transformability (erosion)	~63	~41
m-Y-ZrO ₂ (abraded) (%)	48.4 ± 4.6	54.9 ± 3.5
t-Y-ZrO ₂ transformability (abrasion)	~53	~60

3.3.2. Abrasion

Fig. 7 shows the damage generated on the surface by silica particles during abrasion tests. For consistency, the SEM examinations were undertaken at the center of the wear scar [30] and the direction of abrasive motion is shown by an arrow.

Extrusion and depletion of the binder phase occur very quickly. The binder metal loss weakens the mechanical strength and structural integrity of the surface layer. Fine carbide grains can therefore be easily detached from the surface by a subsequent event. The micrograph of the VPSed hardmetal reveals a severely fragmented carbide structure; fine carbide grains in SPSed composite seem to wash away of the surface. In both cases at the initial stage of abrasive wear, abrasive particles selectively remove the binder phase leading to the formation of small pits with intergranular facets. The removal of the binder-phase leads to the lowering of fracture strength and development of plastic strain within the surface layers of the sintered hardmetal [30]. The strain developed is relieved by the formation of cracks within the carbide grains along their slip planes [17,31] and possible phase transformation of the tetragonal zirconia exerted to high contact stress during the initial entrainment resulting in maximum strain.

3.3.3. Effect of tetragonal zirconia transformability

To prove (or disprove) the possible effect of phase transformation on the erosive performance of the composites, the XRD analysis of as-sintered and damaged surfaces was carried out.

The amount of the monoclinic phase at fracture surfaces determines the extension of t→m transformation. Diffraction peaks from monoclinic zirconia can hardly be detected in the as-sintered specimen (Fig. 3). XRD observation of the worn surface shows lowering of intensity of the tetragonal zirconia peaks due to partial transformation into the monoclinic phase during erosion wear. Table 4 presents fraction of monoclinic yttria stabilized zirconia and transformability of its tetragonal polymorph, which is defined as the volume percent of t-Y/ZrO₂ in the composite before and after testing.

Low amount of monoclinic zirconia is indicative of an insufficient energy transmitted from the silica particles traveling at the velocity of 50 ms⁻¹ during the erosion test for the transformation of the tetragonal zirconia; however, when subjected to impact at 80 ms⁻¹ the transformability of the tetragonal zirconia is increased. Therefore, the effect of possible phase transformation toughening in the hardmetals doped by zirconia can be stated for the conditions of high energy impacts of the erodent particles. However, much work needs to be carried out before making any specific conclusions because the effect of phase transformation toughening can be masked by relatively higher density and hardness of the VPSed hardmetal as compared to other materials. Abrasion resistance of the SPSed composite is a bit higher as compared to other materials despite lower fracture toughness; for such kind of test conditions, the transformability of zirconia is the highest. This fact may suggest the positive effect of zirconia transformation on abrasion resistance of the hardmetals.

The stress state under which the tetragonal phase of yttria stabilized zirconia undergoes martensitic phase transformation at different conditions of loading remains to be further tested. However, the development of the advanced structures of WC-Ni hardmetals with enhanced mechanical properties and wear resistance can be fulfilled by doping of the hardmetal matrix by oxide ceramic particles.

4. Conclusions

Simultaneous increase in fracture toughness due to possible stress induced transformation toughening of tetragonal zirconia with increase in hardness due to grain growth inhibition during processing allows considering the cemented carbides doped by zirconia as promising tribomaterials. Optimized technological process is of utmost importance in cemented carbides production and utilization of mechanisms of transformation toughening. However, to make more specific conclusions about the effect of zirconia transformability on the wear performance of composites, further research is needed.

Wear of doped cemented carbides is mainly controlled by binder plasticity, strength of interparticle interfaces, cracking tolerance (fracture toughness) of the individual WC grains, and zirconia transformability.

Acknowledgments

The authors would like to acknowledge Ms. R. Traksmaa and Ph.D. M. Viljus from Materials Research Centre, TUT, for the help with XRD and SEM analysis; and Prof. S-P. Hannula and Ms. Erkin Cura

from AALTO University Foundation, Finland, for their help in SPS processing and useful discussion on the composite fabrication, Estonian Science Foundation under Grant nos. 8211 and 8850, Estonian Ministry of Education and Research under target financing (Project T062) as well as Science Academy of Finland (Grant no. 259596) are deeply appreciated for the financial support of this study.

References

- [1] O. Malek, B. Lauwers, Y. Perez, P. De Baets, J. Vleugels, Processing of ultrafine ZrO₂ toughened WC composites, *J. Eur. Ceram. Soc.* 29 (2009) 3371–3378.
- [2] Z.H. Qiao, X.F. Ma, W. Zhao, Fabrication, microstructure and mechanical properties of novel cemented hard alloy obtained by mechanical alloying and hot-pressing sintering, *Mater. Sci. Eng. A* 460 (15) (2007) 46–49.
- [3] I. Hussainova, M. Antonov, A. Zikin, Erosive wear of advanced composites based on WC, *Tribol. Int.* 46 (2012) 254–260.
- [4] B. Basu, T. Venkateswaran, D. Sarkar, Pressureless sintering and tribological properties of WC–ZrO₂ composites, *J. Eur. Ceram. Soc.* 25 (9) (2005) 1603–1610.
- [5] D. Jiang, O. der Biest, J. Vleugels, ZrO₂–WC nanocomposites with superior properties, *J. Eur. Ceram. Soc.* 27 (2007) 1247–1251.
- [6] I. Hussainova, M. Antonov, N. Voltsihhin, Assessment of zirconia doped hardmetals as tribomaterials, *Wear* 271 (2011) 1909–1915.
- [7] T. Viatte, S. Bolognini, T. Cutard, G. Feusier, D. Mari, W. Benoit, Investigation into the potential of a composite combining toughness and plastic deformation resistance, *Int. J. Refract. Met. Hard Mater.* 17 (1999) 79.
- [8] S.G. Huang, O. Van der Biest, J. Vleugels, VC-doped WC–NbC–Co hardmetals, *Mater. Sci. Eng. A* 488 (2008) 420–427.
- [9] Z. Zak Fang, X. Wang, T. Ryu, K.S. Hwang, H.Y. Sohn, Synthesis, sintering and mechanical properties of nanocrystalline cemented tungsten carbide, *Int. J. Refract. Met. Hard Mater.* 27 (2009) 288–299.
- [10] R.H.J. Hannink, P.M. Kelly, B.C. Muddle, Transformation toughening in zirconia-containing ceramics, *J. Am. Ceram. Soc.* 83 (3) (2000) 461–487.
- [11] B. Basu, Toughening of yttria-stabilized tetragonal zirconia ceramics, *Int. Mater. Rev.* 50 (4) (2005) 239–256.
- [12] N. Voltsihhin, I. Hussainova, M.E. Cura, S-P. Hannula, R. Traksmaa, Densification and microstructure development in zirconia toughened hardmetals, *Key Eng. Mater.* 527 (2013) 50–55.
- [13] E. Breval, J.P. Cheng, D.K. Agrawal, P. Gigl, M. Dennis, R. Roy, et al., Comparison between microwave and conventional sintering of WC/Co composites, *Mater. Sci. Eng. A* 391 (2005) 285–295.
- [14] S.I. Cha, S.H. Hong, B.K. Kim, Spark plasma sintering behaviour of nanocrystalline WC–10Co cemented carbide powders, *Mater. Sci. Eng. A* 351 (2003) 31–38.
- [15] I. Hussainova, M. Antonov, Assessment of cermets performance in erosive media, *Int. J. Mater. Prod. Technol.* 28 (2007) 361–376.
- [16] T. Deng, M.S.A. Bradley, M.S. Bingley, An investigation of particle dynamics within a centrifugal accelerator type erosion tester, *Wear* 247 (2001) 55–65.
- [17] M. Antonov, I. Hussainova, R. Veinthal, J. Pirso, Effect of temperature and load on three-body abrasion of cermets and steel, *Tribol. Int.* 46 (2012) 261–268.
- [18] X. Ren, H. Miao, Z. Peng, A review of cemented carbides for rock drilling, *Int. J. Refract. Met. Hard Mater.* 39 (2013) 61–77.
- [19] I. Hussainova, Microstructure and erosive wear in ceramic-based composites, *Wear* 258 (1–4) (2005) 357–365.
- [20] H. Saito, A. Iwabuchi, T. Shimizu, Effect of Co content and WC grain size on wear of WC cemented carbides, *Wear* 261 (2) (2006) 126–132.
- [21] H. Reshetnyak, J. Kübarsepp, Resistance of hardmetals to fracture, *Powder Metall.* 41 (3) (1998) 211–216.
- [22] H. Toraya, M. Yoshimura, S. Somiya, Calibration curve for quantitative analysis of the monoclinic–tetragonal ZrO₂ system by X-ray diffraction, *J. Am. Ceram. Soc.* 67 (1984) C-119.
- [23] A. Suresh, M.J. Mayo, Crystalline and grain size-dependent phase transformations in yttria-doped zirconia, *J. Am. Ceram. Soc.* 86 (2) (2003) 360–362.
- [24] A. Freidin, R. Filippov, I. Hussainova, E. Vilchevskaja, Critical radius in the effect of transformation toughening of zirconia doped ceramics and cermets, *Key Eng. Mater.* 527 (2012) 68–73.
- [25] Y. Wang, M. Heush, S. Lay, C. Allibert, Microstructure evolution in the cemented carbides WC–Co, *Phys. Status Solidi A* 193 (2002) 271–283.
- [26] K. Jia, T.E. Fisher, B. Gallois, Microstructure, hardness and toughness of nanostructured and conventional WC–Co composites, *Nanostruct. Mater.* 10 (5) (1998) 875–891.
- [27] A.G. Evans, R.M. Cannon, Toughening of brittle solids by martensitic transformations, *Acta Metall.* 34 (5) (1986) 761–800.
- [28] M.G. Gee, A. Gant, B. Roebuck, Wear mechanisms in abrasion and erosion of WC/Co and related hardmetals, *Wear* 263 (2007) 137–148.
- [29] I. Hussainova, Microstructural design of ceramic–metal composites for tribological application, *Key Eng. Mater.* 334–335 (2007) 125–128.
- [30] M.R. Thakare, J.A. Wharton, R.J.K. Wood, C. Menger, Effect of abrasive particle size and the influence of microstructure on the wear mechanisms in wear-resistant materials, *Wear* 276–277 (2012) 16–28.
- [31] M. Gee, C. Phatak, R. Darling, Determination of wear mechanisms by stepwise erosion and stereological analysis, *Wear* 258 (1–4) (2005) 412–425.

- II. **Voltšihhin, N.**, Hussainova, I., Cura, E., Hannula, S-P., Traksmäa, R.,
Densification and microstructure development in zirconia toughened
hardmetals. Key Engineering Materials 527 (2013) 50–55.

DOI: <http://dx.doi.org/10.1016/j.ceramint.2013.12.063>

Densification and Microstructure Development in Zirconia Toughened Hardmetals

Nikolai Voltsihhin^{1,a}, Irina Hussainova^{1,b}, M. Erkin Cura^{2,c},
Simo-Pekka Hannula^{2,d} and Rainer Traksmäa^{3,e}.

¹Department of Materials Engineering, Tallinn University of Technology, Ehitajate tee 5, 19086 Tallinn, Estonia

²Department of Materials Science and Engineering, Aalto University, P.O.Box 16200, FI-00076 Aalto, Finland

³Materials Research Centre Technology, Tallinn University of Technology Ehitajate tee 5, 19086 Tallinn, Estonia

^anikolai.voltsihhin@ttu.ee, ^birina.hussainova@ttu.ee, ^cerkin.cura@aalto.fi,

^dsimo-pekka.hannula@aalto.fi, ^erainer.traksmaa@ttu.ee.

Keywords: Zirconia, wear, cermet, sintering, SPS, XRD.

Abstract. Different process methods and parameters together with different amount of additives were used to fabricate WC-Ni-ZrO₂ hardmetals with mechanical properties aiming at improved performance under erosive wear. XRD observation showed the presence of tetragonal zirconia in the cermet matrix after processing. The best erosion resistance with erosion rate of about 0.7 mm³/kg was demonstrated by the specimen produced either by vacuum sintering or SPS and added by 0.2 wt% of free carbon. This cermet has also demonstrated the highest hardness of 17.7 GPa.

Introduction

Zirconia, ZrO₂, is considered as one of the most important ceramic materials in modern technologies [1,2]. ZrO₂-based ceramic alloys are known as the strongest and toughest single phase-ceramic oxides yet produced [3]. Polymorphism, which gives ability to undergo crystal lattice transformation from cubic to tetragonal and from tetragonal to monoclinic phase, makes this material interesting for scientific studies and industrial applications.

The present study deals with zirconia containing hardmetals. The most commonly exploited dispersed-zirconia ceramic system is ZrO₂-toughened Al₂O₃ (ZTA) that is utilized for grinding media, metal cutting tools and biomedical applications [4]. The present paper is focused on fabrication and testing of conventional WC – 8wt.%Ni (the matrix material) alloyed by partially-stabilized zirconia (PSZ) in amount of 6 wt.%. To produce composite with microstructural parameters sufficient for activation of the transformation toughening mechanism the processing flaws should be kept to a minimum [5].

In order to clarify the influence of processing parameters on microstructure and mechanical properties of the composites different techniques were used. Although milling and mixing parameters have great influence on final properties of sintered parts (i.e. high energy attritor can provoke spontaneous *t* → *m* transformation of zirconia), the final properties and microstructural parameters are defined during the sintering process.

The major challenge is the restriction of grain growth during processing. The promising approach for improving densification at lower temperatures and shorter dwell times as compared to conventional sintering routines is using spark plasma sintering (SPS) [6]. The microstructure obtained by SPS differs from the microstructure of conventionally sintered composites, such as vacuum pressureless sintering (VPS), for example, [7-9]. Because of structural sensitivity of many mechanical properties, the effect of different sintering routes requires comprehensive understanding.

Experimental

Composites were fabricated from the blends of commercially available powders of WC (Wolfram GmbH, Austria), Ni and PSZ (3 mol % yttria stabilized zirconia) (TOSOH, Japan) with initial particles sizes of 0.9-1.1 μm , 5-7 μm and around 29 nm, respectively. Some amount of carbon (0.2, 0.4 and 1 wt.%) in the form of graphite was added to the initial compositions. The purpose of adding C was to eliminate the formation of η -phase [7, 10]. The procedure of specimen fabrication is sketched in Fig. 1. Two different milling techniques as well as two different sintering routines were used.

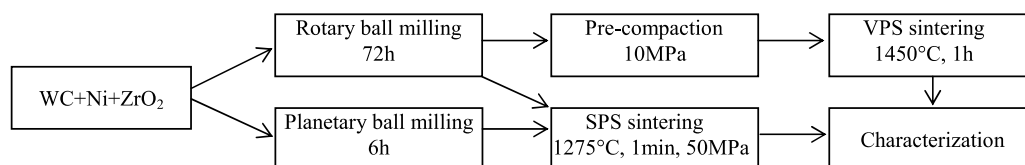


Fig. 1. Schematic presentation of the main processes of fabrication

After sintering the densities of the composites were determined by Archimedes method. The Vickers hardness was measured by Indentec 5030 SKV with a load of 20 kg according to ISO 6507. Fracture toughness was evaluated with the help of IFT (indentation fracture toughness) approach from the Vickers indent imprint. Toughness evaluation was made for Palmquist crack system on the base of equations given elsewhere [11, 12]. The microstructure of the sintered compacts was investigated by SEM (Zeiss EVO MA-15) and the phase structure was identified by X-ray diffraction (XRD) with $\text{Cu-K}\alpha$ radiation.

Solid particle erosion of the composites was studied with the help of a conventional centrifugal four-channel accelerator [13]. The main idea of the erosion test was not only to define the wear resistance of the composites produced by different methods, but also to activate phase transformation in zirconia particles and therefore observe its effect. The erosion tests have been performed using abrasive silica particles with size range 0.1-0.3mm at impact angle of 90° and particle velocity of 50 ms^{-1} . Tests were conducted at room temperature and the erosion rate was determined as volume loss of the target material per mass of the erodent particle.

Results

XRD analysis. The initial commercial 3 mol% Y_2O_3 partially- stabilized zirconia powder, as-mixed powders, sintered bulk samples and eroded surfaces were analyzed by XRD.

The initial zirconia powder showed the presence of about 90% of tetragonal and 10% of monoclinic phases (Fig. 2a). The XRD analysis of the milled powders also revealed the presence of tetragonal zirconia (Fig. 2b). Tetragonal zirconia was thus retained in the blend after milling. Reason for successful milling and avoiding spontaneous transformation from tetragonal to monoclinic is assumed to be the addition of ethanol as a process control agent PCA, thus making cold welding processes less pronounced and impossible to impose stress necessary for transformation of zirconia. Previous studies [14] have shown that dry milling in planetary ball mill can provoke zirconia transition from one crystallographic system into another one.

XRD patterns showed no evidence of detectable phase transformation after the sintering with either method (Fig. 2). In SPS relatively high mechanical pressure and Joule heating have not considerably influenced transformation from tetragonal to monoclinic polymorph, neither the addition of extra carbon to the initial composition has not had any significant effect on the state of zirconia.

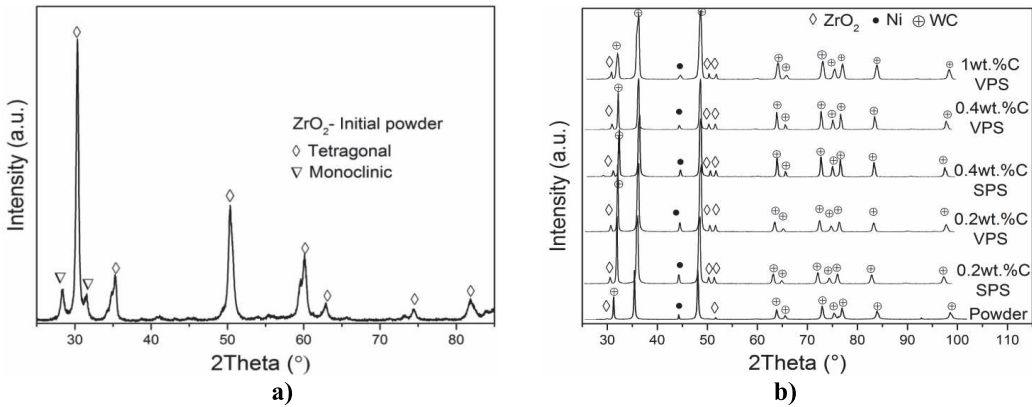


Fig. 2. XRD patterns of a) initial ZrO_2 powder and b) powder and samples after processing.

Microstructure. Microstructure of the produced specimens varied significantly depending on the sintering route, carbon content and method of mixing.

The images in Figs. 3a and b represent microstructures of SPSed specimens at $1275^\circ C$ while milled by different methods. It can be clearly observed that grain structure of the grade milled for 72 hours is finer than that milled in planetary ball mill for 6 hours at 350 rpm.

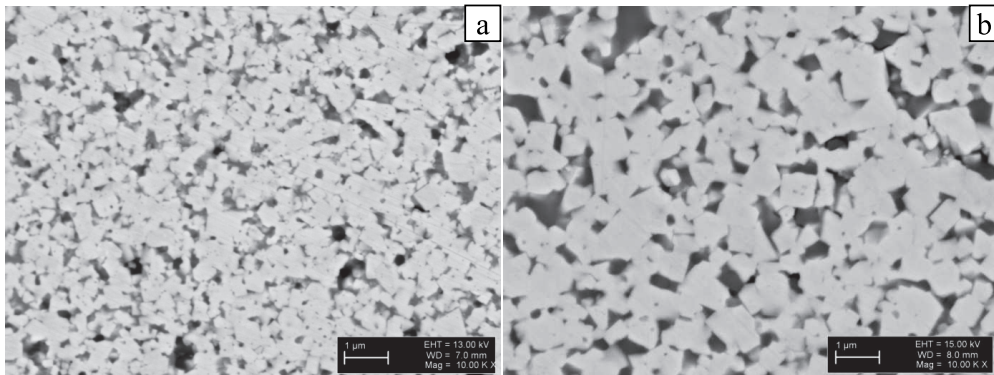


Fig. 3. a) Rotary ball milled for 72 h; b) Planetary ball milled for 6 h.

Fig. 4 demonstrates micrographs taken from the surfaces of the composites produced by different sintering techniques and containing various carbon additions. Microstructures in Fig. 4a, b and c were produced with VPS and have 0.2, 0.4 and 1 wt.% C, respectively. In the micrographs discontinuous grain growth as a result of increasing carbon amount, was observed. However, this is not the case for SPSed materials, which grain growth is minimal for all specimens, even for the highest carbon addition (see details in [7]).

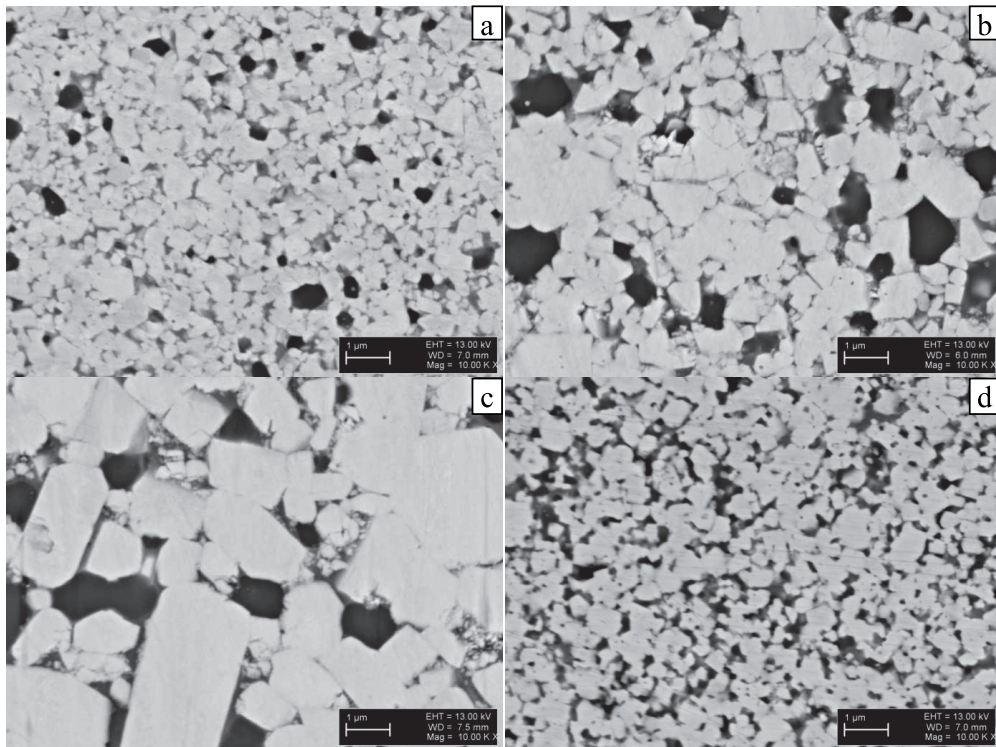


Fig. 4. a) VPS 0.2 wt.% C; b) VPS 0.4 wt.% C; c) VPS 1 wt.% C; d) SPS 1 wt.% C

Mechanical properties and erosion resistance. Density, hardness and fracture toughness of the specimens are listed in Table 1. Grades with 0.2 wt.% C have higher hardness and density as compared to the grades with 0.4 or 1 wt.% C. However, the fracture toughness of these composites is somewhat lower than that of the composites with 0.4 or 1 wt.% C.

Table 1. Properties of the samples produced by different techniques

C [wt.%]	Milling Method	Sintering Method	Density [g/cm^3]	Hardness [GPa]	Fracture toughness K_{IC} [$\text{MPa}\cdot\text{m}^{1/2}$]
0.2	Planetary ball mill	SPS	13.25	14.9±0.27	-
0.2	Rotary ball mill	VPS	13.7	17.71±0.53	9.6±2.14
0.2	Rotary ball mill	SPS	13.56	16.89±0.36	9.2±0.9
0.4	Rotary ball mill	VPS	12.78	14.55±0.3	11.7±0.96
0.4	Rotary ball mill	SPS	12.54	13.54±0.27	10.5±0.75
1	Rotary ball mill	VPS	12.71	12.74±0.15	13.11±1.15
1	Rotary ball mill	SPS	12.78	14.78±0.29	9.06±1.22

Fig. 5 represents erosion rates of the grades doped by different carbon content and sintered with different techniques. As it could be predicted, materials with lower carbon content and accordingly higher hardness showed lower erosion rates than grades having higher carbon content and lower hardness. Despite the fact that grades with higher extra carbon have higher fracture toughness (Table 1), which is a critical parameter for wear resistance of brittle materials [15,16], their wear rate is higher than grades with lower fracture toughness. Having the highest density VPS produced specimen has also the highest hardness and wear resistance despite of relatively low value of IFT. It should be mentioned that low energy loading does not allow transformation of zirconia to occur, therefore, the fact of transformation toughening is masked by other processes during propagation of the crack from the Vickers indent corner.

No straight dependence of erosion rate on sintering technique can be defined. For 0.2 wt.% C added grades the VPSed specimen had slightly higher erosion resistance than the sample fabricated with SPS. However, it should be noted that the difference is in the range of system/measurements accuracy and also can reflect higher porosity of the SPSed specimen. The same behaviour is observed for 0.4 wt.% C doped cermets, while the erosion rate difference was higher between methods of production. For the 1 wt.% C cermets the wear resistance is higher for the SPSed specimen. Its lower wear rate is most probably related to ultra-fine grain structure (Fig. 4d) and high hardness.

XRD observation of the worn surface shows lowering of intensity of the tetragonal zirconia peaks due to partial transformation into the monoclinic phase during erosion wear (Fig. 5b). Low amount of monoclinic zirconia is indicative of an insufficient energy transmitted from the silica particles traveling during erosion test for the transformation of the tetragonal zirconia. Therefore, the effect of possible phase transformation toughening in the hardmetals doped by zirconia is masked by the relatively low energy impacts of the erodent particles.

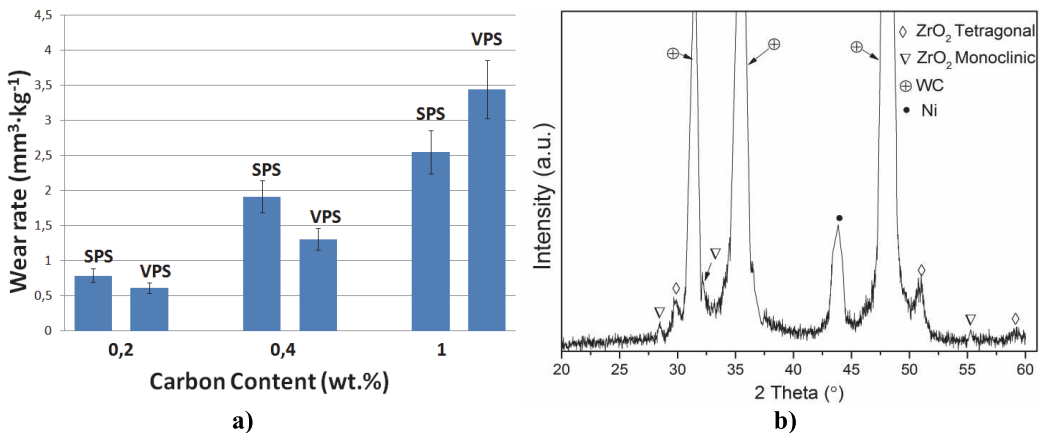


Fig. 5. a) Erosion rates of the grades tested, b) XRD pattern of an eroded surface

Conclusion

In this study hardmetals with the additions of partially stabilized zirconia as a hypothetical toughening agent and extra carbon were fabricated using different powders mixing methods and sintering routines. XRD observations confirmed the presence of the tetragonal zirconia in powder mixtures and composites after sintering, which indicates that processing did not cause spontaneous transformation of zirconia. As XRD observation after erosion tests did not show the presence of high amount of monoclinic polymorphs of zirconia on the worn surface suggesting that the erosion test conditions were not severe enough to cause transformation. The erosion rate of the tested specimens varied with carbon content and the best wear resistance of $\sim 0.7 \text{ mm}^3 \cdot \text{kg}^{-1}$ was demonstrated by the specimens with 0.2 wt.% C and produced by either SPS or VPS.

Acknowledgement

Estonian Science Foundation under grant No. 8211 and graduate school “Functional materials and technologies“, receiving funding from the European Social Fund under project 1.2.0401.09-0079 in Estonia and Academy of Finland under grant No. 259596 are acknowledged for financial support of this research.

References

- [1] A. Heuer, L.W. Hobbs, Science and technology of zirconia, Advances in ceramics, Vol. 3 American Ceramic Society, Westerville, 1981.
- [2] S. Somiya, N. Yamamoto, H. Yanagina (Eds.), Advances in ceramics, Vols. 24A and 24B American Ceramic Society, Westerville, 1988.
- [3] R.H. Hannink, P.M. Kelly, B.C. Muddle, Transformation toughening in zirconia-containing Ceramics. *J. Am. Ceram. Soc.* 83 (2000) 461 – 487.
- [4] F. F. Lange, Transformation Toughening, Part 5: Effect of temperature and alloy on fracture toughness, *J. Mater. Sci.* 17 (1982) 255 – 262.
- [5] D. J. Green, R. H. J. Hannink, M. V. Swain, Transformation toughening of ceramics. CRC Press, Boca Raton, 1989.
- [6] M. Tokita, Mechanism of spark plasma sintering, *Ceramics*, 21 (2010) 605 – 608.
- [7] M.E. Cura, N. Voltsihhin, I. Hussainova, M. Viljus, S-P. Hannula, Effect of carbon content on sinterability and properties of ZrO₂ doped WC-cermets, in: T. Otto (Ed.), Proceedings of the 8th international conference of DAAAM Baltic industrial engineering, Tallinn, 2012, pp. 771 – 776.
- [8] N. Voltsihhin, M.E. Cura, I. Hussainova, S-P. Hannula, Sintering routes for zirconia doped hardmetals, in: T. Otto (Ed.), Proceedings of the 8th international conference of DAAAM Baltic industrial engineering, Tallinn, 2012, pp. 765 – 770.
- [9] I. Hussainova, A. Smirnov, M. Antonov, Mechanical characterization and wear performance of WC-ZrO₂-Ni cermets produced by hot isostatic pressing. *Adv. Mat. Res.* 214 (2011) 344 – 348.
- [10] S. Kim, S-K. Han, J-K. Park, H-E. Kim, Variation of WC grain shape with carbon content in the WC-Co alloys during liquid-phase sintering, *Scripta Mater.* 48 (2003) 635 – 639.
- [11] A. G. Evans, T. R. Wilshaw, Quasi-static solid particle damage in brittle solids. I. Observations, analysis and implications. *Acta Metall.* 24 (1976) 939 – 956.
- [12] A. G. Evans, E. A. Charles, Fracture toughness determinations by indentation. *J. Am. Ceram. Soc.* 59 (1976) 371 – 372.
- [13] I. Hussainova, M. Antonov, Assessment of cermets performance in erosive media, *Int. J. Mater. Prod. Technol.* 28 (2007) 361 – 376.
- [14] Hussainova, I.; Antonov, M.; Voltsihhin, N. (2011) Assessment of zirconia doped hardmetals as tribomaterials. *Wear*, 271 (2011) 1909 – 1915.
- [15] A. Evans, M. Golden, M. Rosenblatt, Impact damage in brittle materials. *Proc. R. Soc. London Ser.* 361 (1978) 343–353.
- [16] H. Reshetnyak, J. Kubarsepp, Resistance of hardmetals to fracture. *Powder Metallurgy*, 41 (1998) 211 – 216.

Engineering Materials and Tribology

10.4028/www.scientific.net/KEM.527

Densification and Microstructure Development in Zirconia Toughened Hardmetals

10.4028/www.scientific.net/KEM.527.50

DOI References

[3] R.H. Hannink, P.M. Kelly, B.C. Muddle, Transformation toughening in zirconia-containing Ceramics. *J. Am. Ceram. Soc.* 83 (2000) 461 – 487.

<http://dx.doi.org/10.1111/j.1151-2916.2000.tb01221.x>

[10] S. Kim, S-K. Han, J-K. Park, H-E. Kim, Variation of WC grain shape with carbon content in the WC–Co alloys during liquid-phase sintering, *Scripta Mater.* 48 (2003) 635 – 639.

[http://dx.doi.org/10.1016/S1359-6462\(02\)00464-5](http://dx.doi.org/10.1016/S1359-6462(02)00464-5)

[11] A. G. Evans, T. R. Wilshaw, Quasi-static solid particle damage in brittle solids. I. Observations, analysis and implications. *Acta Metall.* 24 (1976) 939 – 956.

[http://dx.doi.org/10.1016/0001-6160\(76\)90042-0](http://dx.doi.org/10.1016/0001-6160(76)90042-0)

[12] A. G. Evans, E. A. Charles, Fracture toughness determinations by indentation. *J. Am. Ceram. Soc.* 59 (1976) 371 – 372.

<http://dx.doi.org/10.1111/j.1151-2916.1976.tb10991.x>

[13] I. Hussainova, M. Antonov, Assessment of cermets performance in erosive media, *Int. J. Mater. Prod. Technol.* 28 (2007) 361 – 376.

<http://dx.doi.org/10.1504/IJMPT.2007.013085>

- III. Hussainova, I., **Voltšihhin, N.**, Cura, E., Hannula, S-P., Densification and characterization of spark plasma sintered ZrC–ZrO₂ composites. Materials Science & Engineering A 597 (2014) 75–81.

DOI: <http://dx.doi.org/10.1016/j.msea.2013.12.058>



Densification and characterization of spark plasma sintered ZrC–ZrO₂ composites



Irina Hussainova^{a,*}, Nikolai Voltšihhin^a, Erkin Cura^b, Simo-Pekka Hannula^b

^a Department of Materials Engineering, Tallinn University of Technology, Ehitajate 5, 19086 Tallinn, Estonia

^b Department of Materials Science and Engineering, Aalto University, School of Chemical Technology, POB 16200, Aalto 00076, Finland

ARTICLE INFO

Article history:

Received 26 August 2013

Received in revised form

11 December 2013

Accepted 12 December 2013

Available online 22 December 2013

Keywords:

Zirconia

Zirconium carbide

Spark plasma sintering

Microstructure

Mechanical properties

ABSTRACT

ZrC based composites alloyed by nanosized tetragonal 3 mol% yttria stabilized zirconia were produced with spark plasma sintering to > 98% of the theoretical density by sintering at 1900 °C under pressure of 50 MPa for 10 min. The volume fraction of stabilized zirconia varied from 25 to 40 vol% in the precursor powder blend. Room temperature hardness and modulus of elasticity of the compacts were in the range reported earlier for similar materials densified by pressureless sintering, while indentation fracture toughness was around 7 MPa m^{1/2}. Structural analysis indicated formation of oxycarbides of various stoichiometries.

© 2013 Elsevier B.V. All rights reserved.

1. Introduction

Zirconium carbide (ZrC) is one of the ultra-high temperature materials (melting point is about 3530 °C) commercially adopted in tool bits for cutting tools and can be suitable for many other applications such as crucibles, re-entry vehicles, jet engines or supersonic vehicles where low density and high-temperature load-bearing capability constitute the most important requirements [1,2]. Due to the presence of metallic bonding, ZrC has thermal and electrical conductivity that is comparable to the zirconium metal. High hardness (~25 GPa) and modulus (~390 GPa) combined with a relatively low density (6.63 g cm⁻³) makes this material particularly attractive for tribological applications. Zirconium carbide was densified to 98% of relative density by conventional hot pressing at 2300 °C applied for 60 min under the pressure of 40 MPa [3]. However, low sinterability of powders and poor fracture toughness of bulks (≤ 4 MPa m^{1/2}) limit the wide application of ceramics based on ZrC. One of the promising approaches for improving sinterability and material reliability includes the use of sintering additives. For example, the use of molybdenum as a binder agent for liquid-phase sintering of ZrC–Mo cermets has resulted in mechanically enhanced bulk materials [4,5]. The addition of zirconium diboride was reported to enhance the densification of ZrC-based composites of low porosity level

(2–4%) [6]. Silvestroni et al. observed formation of binary phases of ZrC–MoSi₂ and ternary phases of ZrC–HfC–MoSi₂ and ZrC–ZrB₂–MoSi₂ [6]. New phases such as (Zr, Hf)C solid solutions, SiC and Zr–Mo–Si secondary phases were detected after a heat treatment at 1900–1950 °C in 60 min. The room temperature mechanical properties of these materials were comparable to properties of ZrC bulks produced by the pressure-assisted technique. Fracture toughness values in the range of 3.5–4.0 MPa m^{1/2} give no evidence of significant toughening in the composites. In [7], yttria stabilized zirconium dioxide was tested as sintering additive for zirconium carbide consolidation. The mixtures of ZrC with 20–40 wt% ZrO₂ were sintered to near theoretical density at temperatures ≥ 2000 °C and dwell time ≥ 1 h. The final microstructure consisted of a dispersed zirconia in continuous oxycarbide matrix. Zirconium carbide exhibits a rock salt structure (*Fm*–*3m* space group), in which the oxygen can either be incorporated into the vacant sites or be partially substituted by carbon. It is believed that formation of defective oxycarbides enhances the diffusion and densification in carbide matrix [7,8]. Formation of ZrC_xO_y compounds in the ZrC–ZrO₂ system at temperatures around 2000 °C was outlined in [9] and maximum solubility of oxygen in zirconium carbide at this temperature was found not to exceed 15 at%. The composites of ZrC_xO_y–ZrO₂ sintered at 1800–2000 °C in an argon atmosphere in a graphite tube furnace possessed a four-point bending strength of 220–320 MPa and a fracture toughness of 4–5.8 MPa m^{1/2} [7]. The moderately high fracture toughness of 4–5.8 MPa m^{1/2} was associated with the presence of tetragonal

* Corresponding author. Tel.: + 3726203371.

E-mail address: irina.hussainova@ttu.ee (I. Hussainova).

zirconia, which induced toughening through residual stresses and possible transformation of zirconia grains.

Utilization of zirconia (ZrO_2) as a ceramic sintering additive has been extensively studied for the last few decades [10–13]. Moreover, among oxide ceramics, tetragonal zirconia polycrystals (TZP) have an excellent combination of strength and toughness, wear resistance, as well as high chemical and corrosion resistance [10]. Due to the stress-induced martensitic phase transformation of the metastable tetragonal phase to the monoclinic polymorph ($t \rightarrow m$), zirconia is expected to increase the fracture toughness of composites [14,15]. Factors controlling the transformation include the size, charge and amount of stabilizer cations [14,15]; the grain size and grain size distribution [12,16]; residual stresses [17]; temperature; oxygen vacancy concentration; thermal expansion anisotropy of the t - ZrO_2 ; and microstructural constraints imposed by inert non-transforming phases [15–19]. The tetragonal phase of ZrO_2 can generally be stabilized by dopants; and yttria (Y_2O_3) is one of the most commonly adopted ones. For example, optimal mechanical properties and electrical conductivity of ZrO_2 -40 vol% WC composites were found for zirconia, which was stabilized with 2 and/or 3 mol% Y_2O_3 [11,20,21]. The presumed successful incorporation of stabilized tetragonal zirconia is expected to increase the fracture toughness of ceramic composites, as well as to improve material performance at tribological conditions. The processing parameters influence zirconia polymorphism and, therefore, the recent developments have focused on technologies that allow retaining tetragonal zirconia after sintering for possible phase transformation toughening of the material containing t - ZrO_2 [10,21–23].

With field-assisted sintering, also known as spark plasma sintering (SPS) or pulsed electric current sintering, which employs a pulsed DC current, it is possible to consolidate powders to full density much faster and at lower temperatures than with traditional methods such as pressureless sintering and hot pressing [21–23]. In particular, the SPS method has potential to maintain the nano and sub-microstructure in nanopowder-based materials after consolidation [22]. The present study focuses on (i) densification behavior of the ZrC - ZrO_2 composite system by spark plasma sintering; and (ii) mechanical characterization of the sintered bulks.

2. Experimental procedure

2.1. Materials and processing

Commercially available zirconium carbide (ZrC) powder (particle size around 3.5 μm ; Strategic Metal Investments Ltd., Canada) was mixed with 25 and 40 vol% partially 3 mol% yttria stabilized tetragonal zirconia (t - ZrO_2) nanopowder of 99% purity (average primary particle size 30 nm and agglomerate size about 0.2 μm ; Tosoh, Japan). The blend was milled in a planetary ball milling device (Fritsch, Pulverisette 6 classic) with ZrO_2 balls (\varnothing 10 mm) and a ball-to-powder ratio of 4:1 for 6 h at 300 rpm in ethanol.

Spark plasma sintering (FCT HPD 25-2 GmbH with vertically positioned pyrometer for temperature control) was performed in vacuum at 1600–1900 °C. A pulsed electric current with pulse duration of 10 ms and pause time of 5 ms was applied throughout all sintering cycles. The powder blend was poured into a cylindrical graphite die with an inner diameter of 20 mm and sintered for 10 min. The heating rate was set at 100 °C/min up to the sintering temperature and the cooling rate was \sim 200 °C/min. The relatively low heating rate was applied since a high heating rate can cause temperature gradients and subsequently sintering inhomogeneity, leading to non-uniform microstructural and mechanical properties of the sintered parts [3,21,22]. ZrC -YTZ composites were densified by means of a solid state sintering,

which is a common procedure for producing high temperature ceramics and composites. Densification at the solid state is controlled by diffusion and a large part of the densification in SPS occurs already during heating. Slow heating rate enhances the densification. The applied pressure of 50 MPa was adjusted to the powder at room temperature and kept constant throughout the experiment. The load was applied at the beginning of the sintering process because high green density is favorable for better densification rate by reducing the pores prior to the densification during heating. Graphite papers were employed to separate the powder from the graphite die/punch set-up.

2.2. Material characterization

Specimen density was measured by means of Archimedes' method with distilled water as an immersing medium. The bulk Vickers hardness was estimated with Indentec 5030 SKV at the load of 98.1 N applied for 15 s according to ISO 6507. Modulus of elasticity was measured with the indentation technique as described in [25] according to EN ISO 14577 (ZHU Zwicki-Line Z2.5). The indentation fracture toughness (IFT) was calculated by resorting to the both Palmqvist and Median crack systems [26]. The surface cracks initiated by the indent were measured with SEM microscopy (TM Hitachi 1000, Japan). A large load of 50 kg on the indenter was applied to drive the well-distinguished surface cracks and mitigate any surface effects. The reported hardness and fracture toughness constitute the mean and standard deviation values of 10 indentations.

The microstructure of the polished samples was examined by means of Scanning Electron Microscopy (SEM, Hitachi S-4700, Japan). The chemical compositions of the powder mixtures and bulk samples were analyzed with the help of X-ray diffraction analysis (XRD, Philips PW3830 X-ray Generator, 4 kW, Cu-Anode) using CuK_{α} radiation at the accelerating voltage of 40 kV and a filament current of 30 mA with a scan step size of 0.02° and a count time of 0.4 s at each step. X-ray diffraction was applied for phase identification and calculation of the relative monoclinic and tetragonal ZrO_2 phase content following the method of Toraya et al. [26]. The transformability of a ceramic is defined as the difference in m - ZrO_2 content detected from fractured and polished surfaces.

3. Results and discussion

3.1. Precursor powders

A survey of the yttria stabilized zirconia (YTZ) peaks indicates that in the precursor powder, zirconia was in its tetragonal polymorph and the powder blend mixed in ethanol showed insignificant t - m phase transformation (Fig. 1) during processing. The mixing of the carbide-oxide blend revealed no notable solid-state reactions between ZrC and YTZ; XRD investigation indicated the presence of tetragonal yttria stabilized zirconia and cubic zirconium carbide as the major phases in the precursor.

In essence, powder particles can be considered hierarchically structured agglomerates of nano-sized zirconia dispersed between and/or on the surface of zirconium carbides, Fig. 2. Therefore, bi-modal pore size distribution is expected in the final product because the densification of agglomerates is easier than elimination of inter-agglomerate pores.

3.2. Densification

Near full densification of ZrC - ZrO_2 composite by means of pressureless sintering at temperatures higher than 2000 °C was

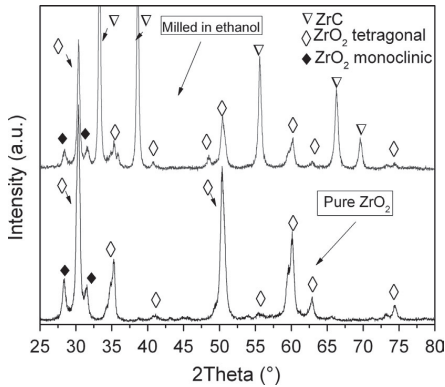


Fig. 1. XRD patterns of zirconia precursor powder and ZrC–YTZ composite powders.

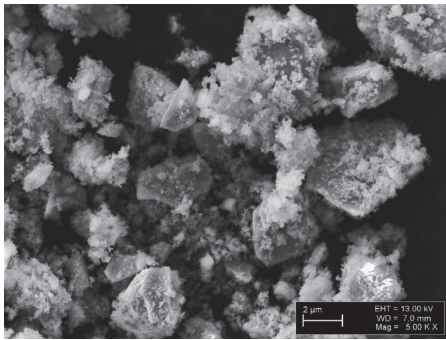


Fig. 2. SEM micrograph of the precursor powder of ZrC–40 vol% YTZ composition.

reported in [7]. SPS is a consolidation method, in which mechanical pressure is combined with electric and thermal fields to enhance interparticle bonding and densification [21]. The densification curves of the ZrC–YTZ powder compacts are presented in Fig. 3, which demonstrates the movement of the upper electrode during the process as a function of sintering time. When the pressure is applied at room temperature, the displacement is positive and the powder is compressed to its green density (stage 1). The displacement at heating is in the opposite direction due to expansion of the graphite molds (stage 2). No substantial densification was observed below 1000 °C. Rapid shrinkage of the composite compacts started during the heating from 1000 to 1700 °C (stage 3). Incorporation of a nanocrystalline ZrO₂ sinter additive reduces the sintering temperature required for achieving near theoretical density of WC-based ceramic composites [24]; the similar mechanisms should, in principal, operate for densification of ZrC. The goal was to produce a fully dense composite with optimal mechanical properties. Hence, the attempt to densify the composites was performed at a temperature as low as 1600 °C. Also, pure ZrC powder was sintered as a reference material, revealing that the temperature of 1900 °C applied for 10 min at 50 MPa was insufficient for full material densification.

The onset of densification of ZrC–40 vol% YTZ composition sintered at 1900 °C was almost achieved during the first minutes of the dwell period. However, insignificant piston’s movement was registered during the entire dwell period. ZrC–25 vol% YTZ composition was sintered at the same dwell time and temperature. Densification of this composition started at 1100 °C implying that a

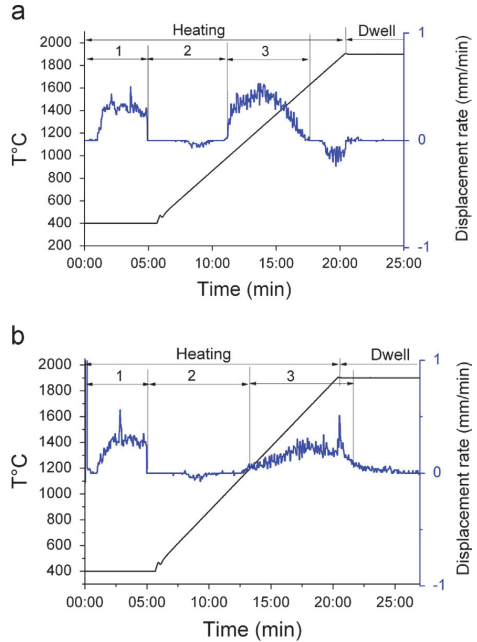


Fig. 3. The densification curves for (a) ZrC–40 vol% YTZ composition and (b) ZrC–25 vol% YTZ composition.

Table 1
Designation and density of the sintered materials.

ZrO ₂ content, vol%	Designation	Temperature, °C	Theoretical density, g/cm ³	Measured density, g/cm ³	Relative density, %
0	ZrC	1900	6.63	6.38	96.2
25	25YTZ	1900	6.43	6.31	98.6
40	40YTZ_1	1900	6.36	6.33	99.5
40	40YTZ_2	1600	6.36	6.2	98

higher temperature is required to fully densify the lower zirconia content material. The densification curves plotted in Fig. 3a and b reveal several large peaks that can be attributed to application of the pressure to a “cold” precursor powder in the mold, and then to the start of a diffusion-aided compaction under heating. The large peak at 1850 °C, Fig. 3b, is due to the overshooting of the set maximum temperature and, consequently, reducing of the applied current.

The calculated theoretical density of the composites (according to the rule of mixtures on the basis of the starting nominal compositions assuming no impurities, no porosity and no reactions and transformations during processing) is 6.43 g/cm³ for ZrC–25 vol% YTZ (grade 25YTZ) and 6.36 g/cm³ for ZrC–40 vol% YTZ. Designation of the grades and the measured densities are summarized in Table 1. Assuming there were no significant phase transformations or spurious phase formation during sintering, densification greater than 98% of the theoretical density by SPS route can be stated. Fine rounded pores are homogeneously distributed mostly along the grain boundaries.

The effectiveness of the SPS route over pressureless sintering is demonstrated by the fact that near full densification of the composites of the same composition requires about 400 °C lower temperatures and only 10 min of holding time in contrast to longer than 1 h.

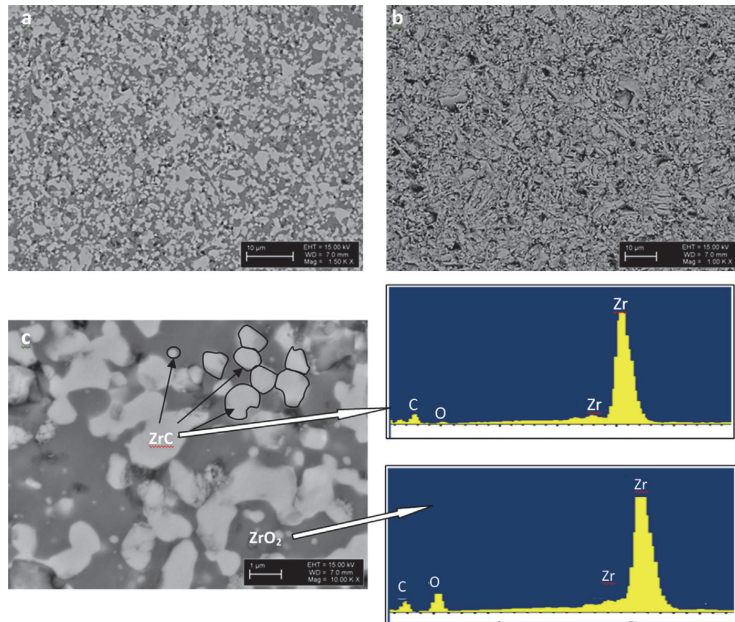


Fig. 4. SEM images of (a) 40 vol% YTZ composite sintered at 1900 °C for 10 min; (b) 25 vol% YTZ composite; and (c) high magnification SEM of 40 vol% YTZ composite with elemental analysis by EDS.

Sintering of pure ZrC requires temperatures higher than 2000 °C. The presence of zirconium dioxide enhances the densification kinetics during SPS treatment. Additional oxygen vacancies influence the mass transfer by diffusion of atoms, and, consequently, the process of sintering [8,21–24]. Another reason for enhancing sintering kinetics can be related to the size effect [24]. Well dispersed nano-sized YTZ particles with a high specific surface area promote a greater grain-boundary diffusion.

3.3. Microstructure and constituent phases

The microstructure of the sintered composites was analyzed by examining the polished surfaces with SEM, as presented in Fig. 4. Two phases are well distinguished on the micrographs: light areas represent ZrC and dark areas yttria stabilized ZrO₂. Zirconia is found in the well-dispersed clusters that increase in size with the increase in YTZ content. Zirconia seems to form an interconnected phase in the composites. The ZrC grain size is difficult to determine because of the inability of chemical or thermal methods to etch the specimens. However, some individual grains can be distinguished (Fig. 4c) and their average size does not exceed the size of the starting ZrC particles, suggesting that ZrC grain growth is minimal during the process of densification; only the average size of YTZ clusters was somewhat smaller in the composite with 40 vol% YTZ. Minimal grain growth is typical for SPS processing [21–23]. The shrinkage between 1000 and 1100 °C, Fig. 3, can be attributed to the densification of ultrafine-sized YTZ aggregates around micro-sized ZrC particles. Minor grain growth (grain growth factor about 1.7) was observed after the spark plasma sintering of pure ZrC, which was densified to 96% of its theoretical density under given conditions.

XRD patterns of the sintered composites are presented in Fig. 5. Tetragonal yttria stabilized zirconia polymorphs are detected on both patterns, assuming the possibility of stress-induced transformation at the tip of the propagating crack caused by loading.

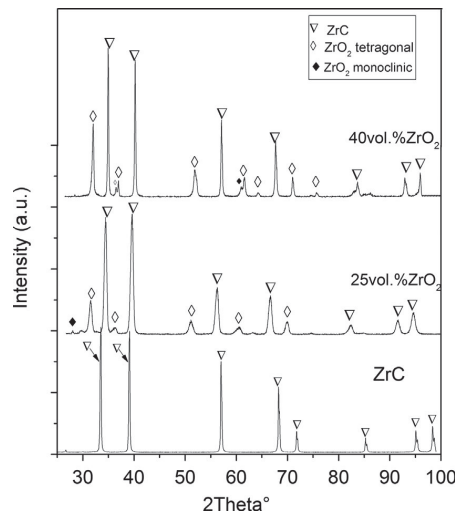


Fig. 5. XRD patterns of the bulk samples.

Tetragonal zirconia was found on the surface of the specimens sintered at both temperatures: 1900 °C and 1600 °C. Dissolved oxygen is known to reduce the lattice parameters in Group IV carbides and ZrC tends to gather oxygen up to several percent when heated. The Zr–C system contains one cubic compound, ZrC; its lattice parameter varies with oxygen contamination, noticeably decreasing from $a=0.4698$ nm for ZrC_{0.97} down to $a=0.4673$ nm for ZrC_{0.69}O_{0.15} [7,8]. Up to 1600 °C, the ZrC phase represents its initial state of ZrC_{0.94} stoichiometry with no detectable change in lattice parameter of 0.4694 nm. A slight decrease in the lattice

parameter to 0.4688 nm (or the displacement of the diffraction peaks toward higher diffraction angles) of ZrC in 25YTZ grade after sintering at 1900 °C suggests the formation of Zr–C–O compound of most probably $ZrC_{0.9}O_{0.1}$ stoichiometry. A decrease in lattice parameter to 0.4680 nm implies formation of oxycarbide matrix of $ZrC_{0.8}C_{0.2}$ in 40YTZ_1.

3.4. Mechanical properties

The mechanical properties are listed in Table 2. The measured Vickers hardness of the spark plasma sintered bulk ZrC is around 20 GPa that is well below the values reported for monolithic zirconium carbide (~25 GPa) [2]. It is well-established that the closed porosity can reduce the hardness exponentially as outlined by Wu and Rice [28]. The hardness correction for porosity can generally be estimated as $H \approx H_0 \times e^{-bP}$, where H is the measured hardness, H_0 is the hardness of the material with no porosity, P is the volume fraction of porosity, and b is a characteristic number for the porosity that is based on shape and distribution [28]. In this case, the b factor of 3 was adopted for the dispersed spherical porosity observed in the microstructure. When the hardness of ZrC was corrected for porosity, H_0 had a value of about 21.8 GPa, which was about 8% greater than the value measured in the present study. If the rule of mixture was followed, the theoretical hardness of the ZrC–40 vol%YTZ specimen should be at least 17.9 GPa due to a high content of zirconia phase (reported hardness of yttria stabilized zirconia ranges from 11 to 13 GPa). However, hardness is also affected by residual porosity, the relatively coarse microstructure and distribution of constituents. The hardness of the ZrC–25 vol%YTZ grade is lower than the hardness of the grade with higher zirconia content. This may be attributed to a lower degree of densification due to a poorer sinterability of the material with higher ZrC content and a short dwell time.

A wide variation of the hardness values around the average value suggests a non-homogeneous phase distribution throughout the material. Also, the oxycarbides of different stoichiometries may have intrinsically different moduli and hardness. Indeed, a significant influence of the chemical composition on the mechanical properties of ZrC_xO_y was demonstrated in [8]. It was revealed that the incorporation of oxygen in zirconium carbide lattice results not only in noticeable enhancement of the densification kinetics but also in decrease in mechanical properties.

The measured moduli of elasticity are summarized in Table 2. The elastic modulus was expected to decrease with increasing zirconia content due to lower modulus of yttria stabilized zirconia adopted in this study (~205 GPa) as compared to ZrC (~392 GPa, [2]). The measured modulus of elasticity of ZrC, however, was lower than reported in [2]. No significant difference in the moduli of composites was revealed; the elastic moduli were between 249 and 260 GPa for the composites tested.

Several models have been developed to predict the modulus of elasticity of multi-phase materials [29,30]. The Hashin and Shtrikman relation [29] draws on the shear and bulk moduli of the

material along with volumetric and stored energy considerations for each phase. A model proposed in [30] combines a volumetric rule of mixtures with phase contiguity. A detailed analysis of the models' predictions is out of scope of this paper, while a description of the approach is given in [31]. It was obtained that the theoretical predictions are in close proximity to a normal volumetric rule of mixture for the composites giving modulus of elasticity 286 GPa for 40 vol%YTZ and 328 GPa for 25 vol%YTZ. The low values of measured hardness and modulus can reflect the influence of the residual porosity, which seems to be larger than that concluded from comparative analysis of the measured and theoretical densities and presence of the monoclinic phase along with tetragonal zirconia, as well as presence of oxycarbides.

Indentation fracture toughness (IFT) of the composites is listed in Table 2. Spark plasma sintered ZrC has the lowest fracture toughness ($\approx 2.5 \text{ MPa m}^{1/2}$) and the 40 vol% YTZ composition has the highest toughness ($\approx 8.9 \text{ MPa m}^{1/2}$). A moderately high standard deviation is indicative of the inhomogeneity in the microstructure and influence of residual porosity on IFT. In comparison to IFT values of HP composites found in literature [5], these values are, nevertheless much higher. The fracture toughness of a hot pressed ZrC was estimated to be as low as $1 \text{ MPa m}^{1/2}$, while fracture toughness of ZrC–40 vol%Mo as high as $6.6 \text{ MPa m}^{1/2}$ in [5].

Increase in IFT for ceramic–metal composites with increasing metal phase content is a well-documented fact [4,32]. In the present work, an increase in IFT may be partially attributed to the presence of tetragonal zirconia. Transformation toughening in zirconia ceramics has been widely studied [14–16,33]. The volume change accompanying the transformation creates a compressive strain field around a crack tip to oppose crack propagation, while

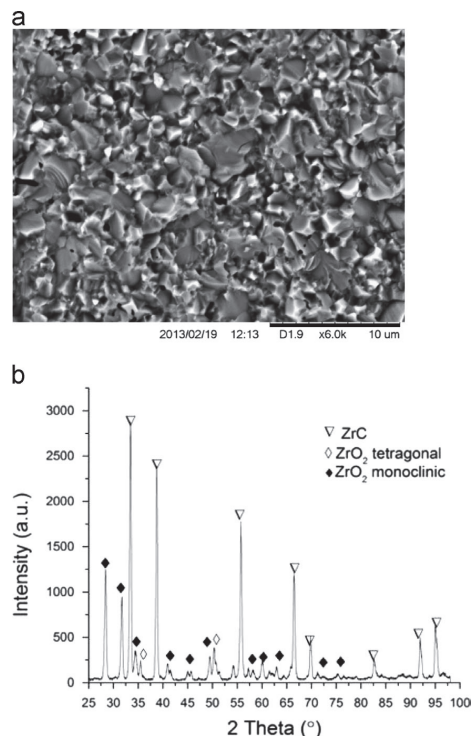


Fig. 6. Representative SEM images of the fractured surface of 25YTZ grade (a); and X-ray diffraction pattern of the fractured surface of 25YTZ grade (b).

Table 2
Mechanical properties of the composites.

Grade	Modulus, GPa	Vickers hardness, GPa	IFT (P*), $\text{MPa m}^{1/2}$	IFT (M**), $\text{MPa m}^{1/2}$
ZrC	363 ± 33	20.2 ± 2.35	2.5 ± 1.3	–
25YTZ	258 ± 25	15.17 ± 0.82	7.24 ± 2.2	8.9 ± 3.2
40YTZ_1	259 ± 23	15.52 ± 0.58	7.33 ± 1.2	8.9 ± 2.9
40YTZ_2	249 ± 28	15.1 ± 1.85	5.83 ± 3	7.1 ± 4

IFT=Indentation fracture toughness.

P* Palmqvist crack.

M** Median crack.

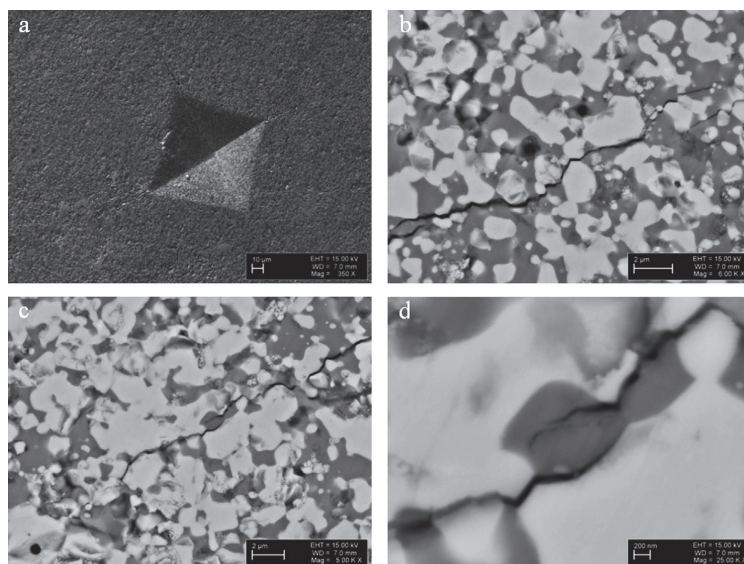


Fig. 7. Representative SEM images of (a) indentation imprint; and (b, c, d) cracks propagating from the corner of indent taken from the surface of the ZrC-40 vol% YTZ composite.

the strain energy associated with any net shear component of the transformation strain in the transformation zone contributes to an effective increase in the energy of fracture [14]. The chemical composition and grain size dictate the t -ZrO₂ transformability. It was estimated that for 3 mol% yttria stabilized zirconia, the critical grain size is about 1 μm [34]. Nevertheless, in multi-phase materials, the critical grain size is also affected by matrix constraint and residual stresses. The matrix constraint is related to modulus of elasticity of the matrix. Materials produced in the present study exhibit a network of zirconia (matrix) instead of well-distributed individual grains. In order to assess material's transformability, the difference in monoclinic phase content on the polished and fractured surfaces, i.e., the fraction of stabilized zirconia transformed into monoclinic phase during fracture, was determined with XRD measurement. The volume fraction of m -ZrO₂ is calculated based on the intensities of the (111) and (11 $\bar{1}$) reflection peaks of monoclinic phase and (111) peak of tetragonal polymorph measured on polished and fractured materials, in accordance with the procedure described in [27]. The level of zirconia transformed was estimated at about 32% for the 40YTZ_1 grade; 26% for 40YTZ_2 grade; and 36% for 25YTZ grade. The transformability of the tetragonal zirconia decreased from 36% in 25 vol%YTZ containing composite down to 32% in the composite with 40 vol% of yttria stabilized zirconia. Reducing transformability in the 40YTZ_1 grade explains the similar values of the indentation fracture toughness of the composites despite the relatively large difference in zirconia content: toughness increases with increase in transformability, indicating that the stress-induced phase transformation can constitute one of the mechanisms responsible for toughening. The representative SEM image and XRD pattern of the fractured surface of 25YTZ grade are shown in Fig. 6.

The toughening mechanism based on mismatch in coefficients of thermal expansion (CTE) can also operate in a multi-phased material. CTE of zirconia (about $10 \times 10^{-6} \text{ }^\circ\text{C}^{-1}$) is higher than that of zirconium carbide (about $6 \times 10^{-6} \text{ }^\circ\text{C}^{-1}$). After cooling to room temperature the zirconia phase is placed in tension and ZrC in compression, which can additionally contribute to fracture toughness, as lower critical stress is needed for transformation of the particle under tensile residual stresses.

Fig. 7 shows the SEM micrographs of the indentation crack propagating from the corners of the Vickers indent. In all probability, the advanced crack transforms some of the zirconia particles occurring in the path of crack tip, leaving behind regions of permanently transformed material. The crack propagates predominantly along the grain boundaries, indicating an intergranular character of cracking; ZrC grains tend to deflect the crack. Therefore, the multiplicative interactions such as crack deflection and branching combined with transformation toughening are evident and can be regarded as operating toughening mechanisms in the composites.

4. Conclusions

Near fully dense and free of impurities ZrC–YTZ composites containing the tetragonal polymorph of zirconia can be obtained within 10 min treatment at 1900 °C under pressure of 50 MPa by means of the SPS technique. Hardness and modulus of elasticity were evaluated to be around 15 GPa and 260 GPa, respectively, while the indentation fracture toughness was measured to be above 7 MPa m^{1/2}. The main toughening mechanisms in the produced composites include the phase transformation from tetragonal to monoclinic polymorph of yttria stabilized zirconia combined with crack deflection and branching. An increase in transformability results in increase in fracture toughness, regardless of the volume fraction of the YTZ phase. The reaction of the zirconium carbide with zirconium dioxide in a vacuum at temperatures in the range of 1600–1900 °C leads to formation of oxycarbides of various stoichiometries. The presence of oxycarbides affects the mechanical properties of the composites; however, this phenomenon requires further investigation.

Acknowledgments

The Estonian Science Foundation under Grants 8211 and T062 as well as the Academy of Finland under Grant no. 259596 are

acknowledged for the financial support of this research. The authors would like to thank PhD M. Viljus and MS R. Traksmaa, both from Materials Research Center, TUT, for their help with microstructural and XRD analysis.

References

- [1] E. Wuchina, E. Opila, M. Opeka, W. Fahrenholtz, I. Talmay, *Electrochem. Soc. Interface* 16 (2007) 30–36.
- [2] H.O. Pierson, *Handbook of Refractory Carbides and Nitrides*, William Andrew Publishing & Noyes, Westwood, 1996.
- [3] P. Barnier, C. Brodhag, F. Thevenot, *J. Mater. Sci.* 21 (1986) 2547–2556.
- [4] S.E. Landwehr, G.E. Hilmas, W.G. Fahrenholtz, T.G. Talmay, H. Wang, *Mater. Sci. Eng.* 497 (2008) 79–86.
- [5] S.E. Landwehr, G.E. Hilmas, W.G. Fahrenholtz, *J. Am. Ceram. Soc.* 91 (2008) 873–878.
- [6] L. Silvestroni, D. Sciti, *J. Mater. Res.* 23 (2008) 1882–1889.
- [7] E. Min-Haga, W.D. Scott, *J. Mater. Sci.* 23 (1988) 2865–2870.
- [8] M. Gendre, A. Maitre, G. Troiliard, *J. Eur. Ceram. Soc.* 31 (2011) 2377–2385.
- [9] T.Y. Kosolapova, V.B. Fedorus, A.D. Panasyuk, G.K. Kozina, Translated from *Poroshk. Metall.* 1 (1972) 60–64.
- [10] K.M. Reddy, A. Mukhopadhyaya, B. Basu, *J. Eur. Ceram. Soc.* 30 (2010) 3363–3375.
- [11] I. Hussainova, M. Antonov, N. Voltsihhin, *Wear* 271 (2011) 1909–1915.
- [12] O. Malek, B. Lauwers, Y. Perez, P. de Baets, J. Vleugels, *J. Eur. Ceram. Soc.* 29 (2009) 3371–3378.
- [13] I. Hussainova, M. Antonov, A. Zikin, *Tribol. Int.* 46 (2012) 254–260.
- [14] R.H.J. Hannink, M.V. Swain, *Annu. Rev. Mater. Sci.* 24 (1994) 359–408.
- [15] B. Basu, J. Vleugels, O. van der Biest, *Mater. Sci. Eng. A* 366 (2004) 338–347.
- [16] B.L. Alfonso, M. Yuichiro, K. Masanori, et al., *Acta Mater.* 50 (2002) 4555–4562.
- [17] A. Krell, A. Teresiak, D. Schläfer, *J. Eur. Ceram. Soc.* 16 (1996) 803–811.
- [18] R.H.J. Hannink, P.M. Kelly, B.C. Muddle, *J. Am. Ceram. Soc.* 83 (2000) 461–487.
- [19] F.F. Lange, *J. Am. Ceram. Soc.* 69 (1986) 240–242.
- [20] D. Jiang, O. Van der Biest, J. Vleugels, *J. Eur. Ceram. Soc.* 27 (2007) 1247–1251.
- [21] S. Grasso, Y. Sakka, G. Maizza, *Sci. Technol. Adv. Mater.* 10 (2009) 053001.
- [22] R. Orru, R. Licheri, A.M. Locci, A. Cincotti, G. Cao, *Mater. Sci. Eng. R* 63 (2009) 127–287.
- [23] D. Sciti, S. Guicciardi, M. Nygren, *Scr. Mater.* 59 (2008) 638–641.
- [24] K. Biswas, A. Mukhopadhyay, B. Basu, K. Chattopadhyay, *J. Mater. Res.* 22 (2007) 1491–1501.
- [25] W.C. Oliver, G.M. Pharr, *J. Mater. Res.* 7 (1992) 1564–1583.
- [26] K. Niihara, *J. Mater. Sci. Lett.* 2 (1983) 221–223.
- [27] H. Toraya, M. Yoshimura, S. Somiya, *J. Am. Ceram. Soc.* 67 (1984) C119–C121.
- [28] C.C. Wu, R.W. Rice, *Ceram. Eng. Sci. Proc.* 6 (1985) 977–994.
- [29] Z. Hashin, S.A. Shtrikman, *J. Mech. Phys. Solids* 10 (1962) 343–352.
- [30] Z. Fan, P. Tsakiroopoulos, A.P. Miodownik, *Mater. Sci. Technol.* 8 (1992) 922–929.
- [31] I. Hussainova, E. Hamed, I. Jasiuk, *Mech. Compos. Mater.* 6 (2011) 667–678.
- [32] I. Hussainova, *Wear* 258 (2005) 357–365.
- [33] D. Casellas, F.L. Cumbreira, F. Sánchez-Bajo, W. Forsling, L. Llanes, M. Anglada, *J. Eur. Ceram. Soc.* 21 (2001) 765–777.
- [34] A. Freidin, R. Filippov, I. Hussainova, E. Vilchevskaja, *Key Eng. Mater.* 527 (2012) 68–73.

IV. **Voltšihhin, N.**, Rodríguez, M., Hussainova, I., Aghayan, M., Low temperature, spark plasma sintering behavior of zirconia added by a novel type of alumina nanofibers. *Ceramics International* 40 (2014) 7235–7244.

DOI: <http://dx.doi.org/10.1016/j.ceramint.2013.12.063>



ELSEVIER



CrossMark

Available online at www.sciencedirect.com

ScienceDirect

Ceramics International 40 (2014) 7235–7244

CERAMICS
INTERNATIONAL

www.elsevier.com/locate/ceramint

Low temperature, spark plasma sintering behavior of zirconia added by a novel type of alumina nanofibers

Nikolai Voltsihhin^{a,*}, Miguel Rodríguez^b, Irina Hussainova^a, Marina Aghayan^a

^aDepartment of Materials Engineering, Tallinn University of Technology, Ehitajate 5, 19086 Tallinn, Estonia

^bInstituto de Cerámica y Vidrio (CSIC), Campus Cantoblanco, 28049 Madrid, Spain

Received 20 August 2013; received in revised form 27 November 2013; accepted 16 December 2013

Available online 27 December 2013

Abstract

A novel type of alumina nanofibers has been used for fabrication of the alumina toughened zirconia composites and the effect of different sintering techniques on the characteristics of the material was studied. ZrO_2 –10 vol% Al_2O_3 composite was consolidated by spark plasma sintering (SPS) in a temperature range from 1000 °C to 1200 °C and by pressureless sintering in air at 1300 °C. Dilatometry sintering of the said composite material was performed in order to assess its sinterability. Al_2O_3 used in fabrication of the composite is a novel type of alumina nanofibers and thus the effect of different sintering techniques on the formation of the material was investigated. Microstructural analysis has revealed that Al_2O_3 nanofibers partially retained their fiber states after being sintered at 1100 °C under SPS conditions while some of the fibers turned into rounded inclusions. Specimens produced by the SPS routine at temperatures of 1100 °C and 1200 °C were consolidated 93% of theoretical density while the same material sintered with the conventional PM method in air had a densification degree of 74%.

© 2013 Elsevier Ltd and Techna Group S.r.l. All rights reserved.

Keywords: Spark plasma sintering; Ceramic composite; Microstructure; Fibers

1. Introduction

Zirconia toughened alumina (ZTA) is one of the most known and widely used ceramic composite materials (CMC) yet produced. This is a material based on alumina which contains different amounts of zirconia added to it as a sintering aid, toughening agent or as both [1–3]. It is also called as the alumina–zirconia composite and is designated as AZ.

In the previous decade, a considerable amount of work has been done on the alumina zirconia ceramic composite system with a particular emphasis on improving the mechanical properties, utilizing the recognized toughening mechanisms [4]. Noted for their mechanical properties, AZ composites are commonly used in structural applications, such as cutting tools, grinding media and in many medical applications. Additionally, AZ composites feature high strength, fracture toughness, elasticity, hardness, and wear resistance, and one

of the main properties of this ceramic is biocompatibility. Usually AZ composites contain 80–95% of alumina and 5–20% zirconia, and this material is called ZTA. However, there are cases where zirconia is used as the main phase and alumina is a doping additive for increasing properties [5]. In this case, the composite is called alumina toughened zirconia (ATZ). It seems that so much is already done and those composites are depleted for scientific studies. However, using new approaches for well-known materials compositions is always of a scientific interest, whether the approach is a new production technique or an improved type of the same constituent material or combination of both.

There are some research already done with this family of materials reinforced by whiskers [6,7]. In order to deepen the understanding of the movement of siliceous phase in YSZ compacts with alumina single crystal rods and facilitate the improvement of grain-boundary conductivity in SOFC electrolytes Knibbe et al. experimented and discussed the mechanism that alumina plays on the sintering behavior of zirconia.

*Corresponding author. Mobile: +372 58451639.

E-mail address: nikolai.voltsihhin@tu.ee (N. Voltsihhin).

Alumina nanofibers (ANFs) have recently been introduced to the market of ceramic materials and therefore have a wide potential. This material can be used as a performance enhancing additive in coatings, polymers, ceramics and other raw materials in order to boost critical physical properties in the end-products. In this study ANFs are applied as potential whiskers like reinforcement for the zirconia matrix. Whiskers reinforcement of ceramics is a well-known technique for increasing mechanical properties of the CMCs [8]. The diameter of the alumina fibers can be of two sizes – 7 and 40 nm. Due to the nanostructure of the fibers and the initial gamma phase they have a large surface area, while being very closely agglomerated together, because of the attraction forces acting in between. This property of the ANFs gives a challenge of accurate dispersion of the nanofibers in the composite. Another property of the fibers is their thermal stability at temperatures of up to 1100 °C after which gamma phase of the fibers will undergo transformation to alpha phase and fibers will decompose into particles [9]. This property makes these fibers useful for refractory applications and at the same time creates a challenge to produce dense ceramic composite materials. The conventional sintering temperature for obtaining near full density material from nanosize zirconia and alumina is in the range of 1300–1500 °C. This is a challenge where non-standard, pressure-assisted sintering technologies, such as hot press (HP) or SPS, should be used [10]. It has already been shown that nanosized aluminum oxide can be sintered at temperatures as low as 1225 °C and that the SPS technology significantly decreases the densification temperature of the materials, especially if they are of nanoscale [11,12].

In this research an attempt to produce near full density material of the ATZ composite with the ANF whiskers thoroughly dispersed into zirconia matrix, at temperatures ranging from 1000 to 1200 °C, with the help of the spark plasma sintering technique was made.

2. Experimental

Partially stabilized zirconia (PSZ) nanosize powder was purchased from TOSOH (Japan) TZ-3Y-E. Average particle size of the powder is ~25 nm. Gamma-alumina nanofibers had the average diameter of 40 nm and length of 4 cm (length/diameter ratio of 10^{-6}). The obtained raw materials were mixed in the amount of 90 vol% of zirconia and 10 vol% of alumina, using the rotary ball mill technique for 24 h in ethanol environment for better dispersion of the fibers. Zirconium oxide grinding balls of 10 mm diameter were used for mixing. After mixing powders were characterized with SEM for the dispersion of fibers in zirconia. For better understanding of the sintering processes such as densification behavior taking place inside this composite dilatometry (Setaram, TMA Setsys 16/18, France) sintering was done at a constant shrinkage rate up to the temperature of 1475 °C. Sintering of the produced powders was done using a SPS furnace (Dr. Sinter, SPS-510CE, Japan) at 100 °C/min, 50 MPa pressure, for 5 min dwell time and using graphite

molds with 10 mm diameter. Three different temperatures were tested: 1000, 1100 and 1200 °C to see the effect of increasing temperature on the densification behavior in the SPS furnace. Sintering in air environment at 1300 °C for 1 h was done, in order to study the properties of the ATZ produced by the conventional sintering technique and to compare them with the SPS sintered ones.

After sintering obtained samples were characterized for density, hardness, elasticity modulus and microstructural properties and X-ray analysis was done for identification of the phase present in the samples. Density was measured using a geometrical approach, hardness was measured with the help of a Vickers tester (Indentec 5030 SKV) under the load of 100 N, and elasticity modulus was measured using ZHU zwicki-Line 2.5/Z2.5 universal hardness testing machines under the load of 100 N, according to [13]. Microstructural characterizations were done using a Zeis EVO MA15 scanning electron microscope. XRD analysis was done using a Bruker (Siemens Bruker D5005 analyzer with $\text{CuK}\alpha$ -radiation).

3. Results and discussion

3.1. Mixing and dispersion of the fibers

As it was already mentioned before, fibers exist in the agglomerated form of huge bundles and that is why one of the most important steps in their processing is their dispersion and separation from each other. Fibers are easily dispersed in different liquids such as water or ethanol; however, after drying nanofibers get attracted to each other and they become agglomerated again. In order to avoid agglomeration and bundle formation after drying each fiber should be separated from one another with a layer of some other material. In Fig. 1 the powder obtained after ethanol mixing can be seen.

Fig. 1a is the common view of the mixed powder and anything can hardly be seen at this magnification. At a higher resolution (Fig. 1b), the picture becomes clearer, and it can be seen that nanosized zirconia is mixed with alumina fibers. Circles in Fig. 1b show the places where alumina fibers are located. From this image it can be concluded that fibers are quite homogeneously distributed with zirconia and most of them are separated from each other, being caught by the groups of zirconia nanoparticles.

High resolution SEM image can be seen in Fig. 1d. It demonstrates a closer view and from this the size of the fibers or whiskers can be measured. The length of the fibers identified from this area of the mixture varies from 300 nm to 2.3 μm , which means that the aspect ratio of whiskers (length/diameter) is spread from 8 to 60. Hence, it can be concluded that there are whiskers of alumina nanofibers having different lengths and located separately from each other in the zirconia matrix. Nevertheless, there are places where fibers are not so well dispersed and they stay in the bundle state having a length of about 3–5 μm while having hundreds and thousands of fibers bonded together with attraction forces (Fig. 1c).

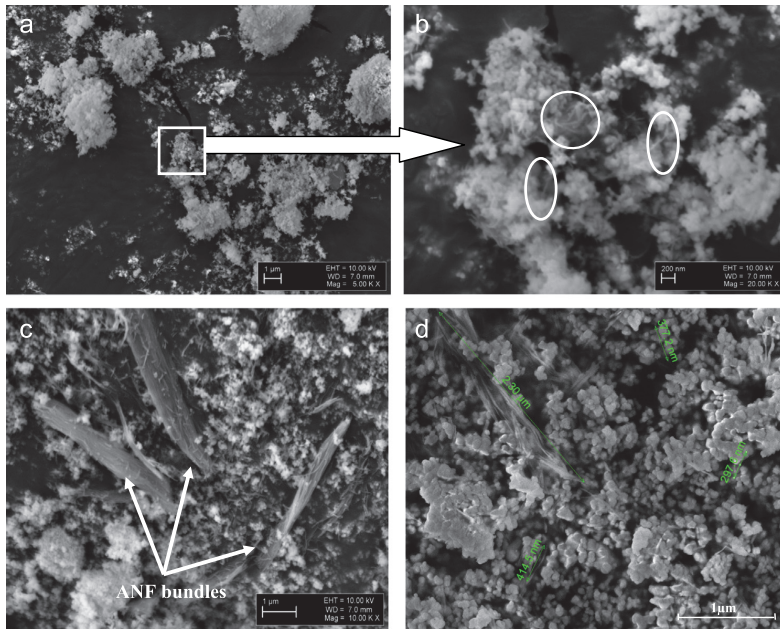


Fig. 1. SEM images of the ATZ powder mixed in ethanol for 24 h.

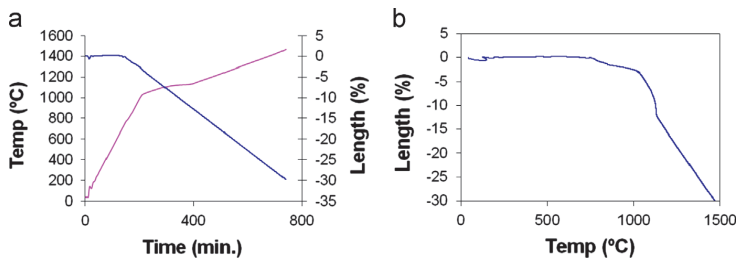


Fig. 2. Dilatometry curves of the ATZ material at a constant shrinkage rate.

3.2. Dilatometry sintering

Dilatometry sintering at a constant shrinkage rate was done in order to see the densification behavior of the powders in pressureless conditions, in order to be able to design a pressureless sintering cycle for this material and to compare the pressureless dilatometry measurements with measurements obtained after spark plasma sintering densification.

There are two graphs representing dilatometry measurements of the alumina toughened zirconia material in Fig. 2, for better understanding of the densification process. Graph “a” represents the original measurement and shrinkage dependence on time and temperature, which can be also named as the heating rate curve as the curve changes in dependence to time. Here the shrinkage curve behaves linearly and an

increase in densification can be understood from the heating rate curve, which slows down to maintain the constant shrinkage rate. Graph “b” shows shrinkage dependence on temperature only, in order to see inconstant movement of the shrinkage curve and its dependence on the temperature. From both of the graphs, the temperature at which densification occurs can be found. In graph “a” heating rate slows down to some extent after 150 min of sintering at a temperature of about 780 °C for few tens of minutes and then, after continuous heating of about 20 min with a lower ramp up to the temperature of about 1070 °C, the heating rate slows down to keep the constant shrinkage rate up to 1200 °C temperature. After 1200 °C the temperature rise becomes faster, indicating end of the main densification step. The same values can be derived from graph “b”. It can be seen that in the temperature

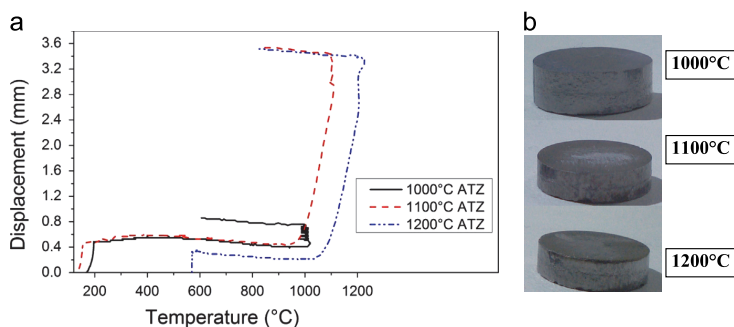


Fig. 3. Displacement curves of the SPS sintering cycles of the ATZ material.

range 0–760 °C the displacement of the material is almost zero. In the temperature interval from 760 °C to 1070 °C displacement occurs smoothly for about 5%. After the temperature of 1070 °C densification occurs sharply up to the end of the heating – 1475 °C, when the shrinkage reaches almost 30%. Therefore, two temperature steps at 780 °C and 1070 °C can be named as the main shrinkage passages. Shrinkage at 780 °C is insignificant and most probably occurs due to monoclinic to tetragonal thermal phase transformation of PSZ which has a small amount of monoclinic phase initially. The second shrinkage step is more considerable and can include few processes. One can be prolongation of zirconia transformation, because it can be seen in Fig. 2b that the shrinkage starts at 780 °C and gradually goes to the next shrinkage step. Another process that can take place at the temperature of 1070 °C is the beginning of densification activity of zirconia nanoparticles and alumina nanofibers. It is a known fact that lower the size of the particles, higher is their surface energy and more readily they will form bonds with each other. It has already been shown before that composite ceramics with this specific grade of PSZ will start to densify at about the same temperature at which densification occurs in the present study [14]. Another reason for such a rapid shrinkage can be attributed to the beginning of gamma to alpha phase transformation of ANFs, which can be explained by the very high local temperature gradients, exceeding critical values in some regions of the samples, where nanofibers cannot resist the transformation processes. Even though densification starts at a temperature as low as 1070 °C it continues up to the end of the measurement. It can be seen that temperature increase and ramp finish at about 1475 °C, while shrinkage curve is still in motion in both graphs (a and b). The most possible reason for this shrinkage is that densification of zirconia and alumina continues. Transforming into alpha phase after 1200 °C, it can have a densification range from 1250 °C to 1500 °C [15].

3.3. Low temperature, spark plasma sintering

Even though the densification beginning temperature derived from dilatometry can be as low as 1070 °C it is not enough to get a densified material with conventional sintering

in air. The temperature to obtain a dense body for the pressureless sintering of the zirconia should be at least 1300 °C, which is defined by the producer. However using the SPS technique allows sintering of the materials to a high density at lower temperatures than conventional sintering [16]. Another advantage of SPS sintering is that, it allows obtaining the online data of pistons motion and thus, to depict densification curve of the sintered material under certain conditions and get the basic understanding of this material's sinterability behavior.

The three pistons displacement lines depicted in Fig. 3 stand for different sintering temperatures at which the samples were produced. In case of 1000 °C sintering the displacement is going on at the temperature of about 1000 °C. However, this displacement is insignificant and 0.2 mm of punching movement can be hardly called as densification. In case of 1100 °C the densification starts to occur at 1000 °C as in the case with 1000 °C sintering and it goes up to the end of sintering. Here the densification is significant and the punch travel distance is about 3 mm. Electrodes displacement reaches the maximum in the beginning of the dwell period and then densification becomes insignificant. Therefore, 5 min of dwelling should be enough to reach the maximum possible density at this particular temperature and prolonged dwell time experiments are not needed. In case of 1200 °C sintering temperature, densification occurs somehow later (at higher temperature) than in the previous sintering and goes up to 1200 °C. The main reason for such a behavior is the difference in measuring methods of the temperature during the sintering process. In case of 1000 °C and 1100 °C experiments, temperature was measured using a thermocouple while in case of 1200 °C the temperature for thermocouple measuring is too high, and a pyrometer was used instead. Hence it can be concluded from the graphs that temperature error between pyrometer and thermocouple measurements is about 70 °C in the case of sintering of studied experiments. The shrinkage is again quite noticeable, while not much more than in the case of 1100 °C experiment. The difference of the sintered samples can be seen from Fig. 3b. Sample sintered at 1000 °C is almost two times thicker than the samples sintered at 1100 °C and 1200 °C.

Taking into account the error of the 1200 °C experiment measurement it can be concluded that the densification step takes place at a temperature between 1000 °C and 1200 °C.

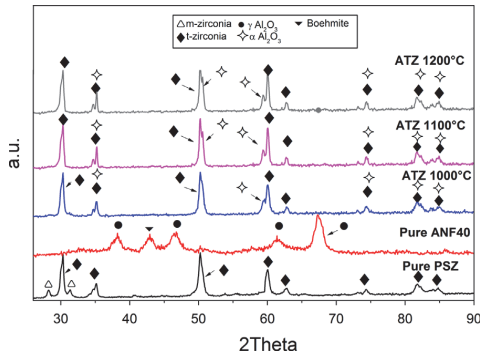


Fig. 4. XRD pattern of the materials studied in this research.

The results obtained by the dilatometry measurement also show the main densification step in this interval of temperatures. It can be assumed again that nanoparticles of zirconia completely densify at this temperature, while it is not clear whether it is possible for alumina fibers to densify at this low temperature. The densification behavior shows the ability to produce specimens with high density at temperatures as low as 1100 °C.

3.4. Microstructure and phase analysis of the sintered samples

The main idea behind low temperature sintering is to produce high density material while retaining the gamma alumina phase of the fibers, or at least retaining alumina in its fiber form.

The graph in Fig. 4 shows five different XRD patterns of the materials studied. ATZ 1000 °C and ATZ 1100 °C patterns look very similar to the pure PSZ pattern. However there are some distinctions. For instance, the peaks at 29° and 31°, representing some amount of the monoclinic polymorph of zirconia on the pure PSZ pattern, cannot be found on both 1000 °C and 1100 °C patterns. Consequently, monoclinic zirconia completely transforms into a tetragonal polymorph at temperatures lower than 1000 °C when the SPS sintering approach is used. This agrees with the measurements obtained from dilatometry sintering. A small difference can be found on the 1100 °C pattern which cannot be observed for pure zirconia and the 1000 °C pattern. The peak at 50° appears double, which points to the presence of the second phase inside this peak. This peak stands for both: tetragonal zirconia and alpha alumina. This is also observed for other peaks. Some of the alpha alumina peaks lay closely together with tetragonal zirconia peaks and, as a result, coincide in the diagram. Therefore, the peaks which stand for both tetragonal zirconia and alpha alumina were doubly marked on the graph. Thereby, the presence of these peaks confirms the alpha alumina formation in the sintered samples. No gamma alumina and boehmite peaks present on the XRD pattern of pure ANF40

could be observed for either 1000 °C or 1100 °C SPS sintered samples, which gives an evidence of full gamma alumina and boehmite transformation into alpha alumina. However, the reason for that could be low amount of gamma phase left in the composite and as a result its low intensity. This also proves the results of research in which alpha alumina forms at temperatures lower than 1100 °C under SPS conditions. This can be confirmed by the peak at 60° which stands alone on the pure ZrO₂ pattern and then doubles when sintered with ANFs at 1000 °C and 1100 °C. All these phenomena of low temperature transformation of monoclinic zirconia into tetragonal and gamma alumina into alpha alumina should be attributed to the specific conditions of SPS sintering, such as Joule heating, high pressures and rapid sintering, and special effects between the grain surfaces (local heatings with increased diffusivities). It must also be considered that the measured temperature is on the surface of the pressing die. At these very high heating rates, there would be a thermal gradient that can also help to explain the differences in phase transformation temperatures.

On the basis of the XRD results, it can be predicted that ANFs have lost their fiber form and appear in particulate view. Nevertheless, the SEM observation of the polished surface was done and images of the specimens sintered at different temperatures can be seen in Fig. 5.

The left column of the images in Fig. 5a, c, and e shows the common view of the microstructure of each specimen sintered at different temperatures. The right-side images depict micrographs of the closer look on the microstructure. The common view shows the presence of the ANF bundles in the samples produced at 1000 °C and 1100 °C, while it cannot be so clearly understood at 1200 °C. At a closer look on the 1000 °C sintered microstructure different sizes of the ANF bundles can be seen. One huge bundle, of about 8 μm in length surrounded by smaller bundles and single whiskers embedded into the zirconia matrix, can be seen. Zirconia is consolidated slightly higher than green density, which can be derived from the friable view of the microstructure. It can also be concluded from Fig. 3b, in which the 1000 °C sample has a densification of only some tens of millimeters and the sample itself is almost as thick as the green body. However the fibers are retained after being sintered at this temperature whether in view of bundles like whiskers or single fiber whiskers, even though XRD observation has shown that there is no more gamma alumina at this temperature and all of the alumina is transformed into alpha form.

Fig. 5c and d shows the microstructure of the specimen sintered at 1100 °C. As it was analyzed from the densification curves of the sintering cycle the temperature of 1100 °C resulted in noticeable shrinkage and densification of the sample. From Fig. 5d it can be seen that the zirconia powder is mostly densified and we cannot see any free rounded particles of zirconia like it is in the case of 1000 °C sintered specimen. Dispersion of alumina in the zirconia matrix changes along with densification of the material in general and neck formations increase between zirconia particles in particular. While densifying and moving under pistons pressure the flow of zirconia particles is pushing the alumina inclusions in different directions and thus changing locations of alumina particles. Therefore, dispersion of alumina in 1100 °C sintered

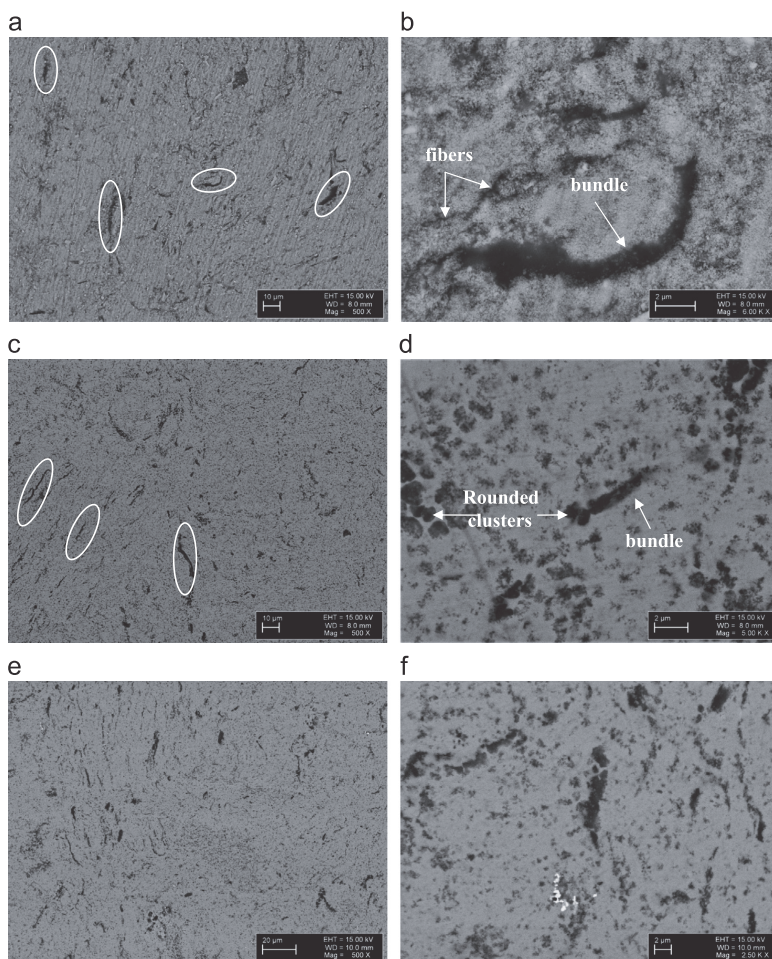


Fig. 5. SEM images of the specimens sintered at different temperatures. (a and b) 1000 °C, (c and d) 1100 °C, and (e and f) 1200 °C.

samples is more homogeneous than in the case of 1000 °C microstructure. From the general view in Fig. 5c it can be seen that bundles of fibers are retained after this kind of shrinkage during severe SPS process. While looking closer into the microstructure reveals that not all the fibers are retained and a major part of them is changed into rounded oxide clusters after sintering. It is difficult to estimate the amount of transformed alumina from the SEM images.

In the sample sintered at 1200 °C, state of the bundles and fibers cannot be clearly distinguished. A better understanding of processes taking place during transformation of ANF can be revealed from the closer look of 1100 °C and 1200 °C samples which can be seen in Fig. 6. This figure shows the states of the ANF in the zirconia matrix and demonstrates possible processes going on in the composite during sintering. It can be seen that in both 1100 °C and 1200 °C sintered cases there are transformed ANF bundles in the form of rounded clusters

and untransformed fibers, whether in the form of bundles or agglomerates of fibers or in the form of separate fibers. Of course, single fibers can be hardly distinguished, because of their small sizes and interaction with the zirconia matrix. Nevertheless, bent and curved single fibers can be noticed. There can be several reasons for the curvature of the single fibers and some of those reasons are brought in Fig. 6c where the possible process of densification parameters influence on the fibers is sketched.

The main factors affecting the behavior of the whiskers-like fibers and bundles of alumina are shown in Fig. 6c under step 1. There are factors that can be identified as acting from outside, such as: zirconia matrix contraction forces (acting from all the sides when densification and neck formation between zirconia nanoparticles occurs), temperature gradients (which are unpredictable in the SPS technique and can have differences of about 100 °C at different locations of the

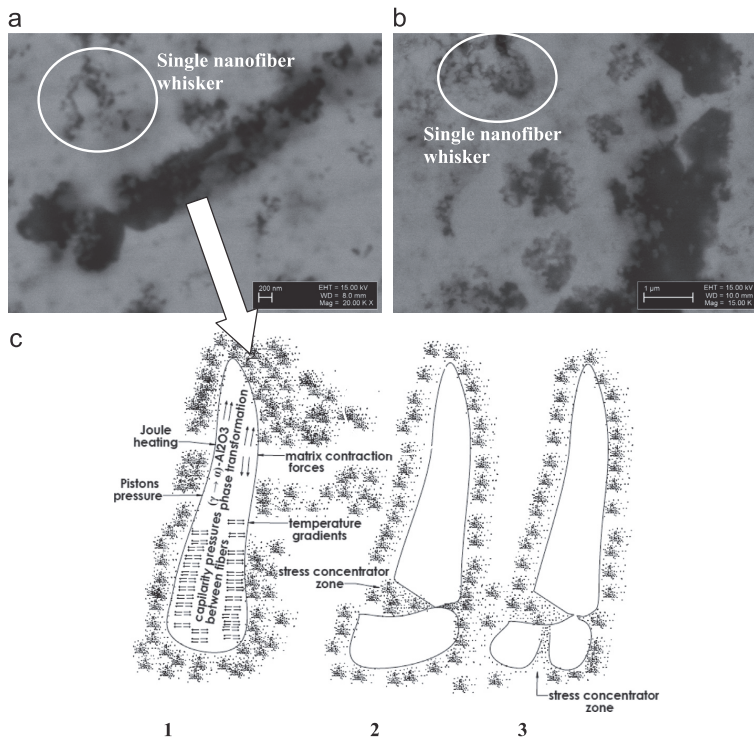


Fig. 6. (a and b) Higher magnification view of the images (d) and (f) of Fig. 5 and (c) depicted draw of the possible processes taking place in composite during the sintering cycle.

samples due to rapid resistive heating), Joule heating and the constant pressure, which is applied during the entire sintering processes [11,17]. There are other processes that take place in the ANF material during the sintering process and those can be identified as processes acting from inside, because they take place inside the alumina material itself. These $\gamma \rightarrow \alpha$ alumina transformations occur due to reduction of the surface area and capillarity pressures acting between the fibers in the bundles and between fibers and the zirconia matrix. It has also been reported that alumina has a solid solubility of 0.2–0.3 wt% from 1200 to 1600 °C [7]. This process can also take place during both SPS and air sintering. It has been reported that current increases the diffusivity and thus enhances the densification mechanisms [18,19]. Therefore, the above mentioned mechanisms are possible during the short SPS cycle.

All of these factors influence the rearrangement of the atoms inside the ANF, changing the geometry of the single fibers and causing breakage of the bundles followed by deformation of the broken part and left part of the bundle. It is assumed that in the stress concentrated place at the end of the bundle deformation of the single fibers causes the breakage of the bundle part and the particles of the zirconia matrix immediately propagate into the freed space in order to minimize the free energy (Fig. 6c step 2). Then, the part divided from the main bundle and having high stresses already inside of it breaks under the influence of the same

conditions that led it to that state earlier. Therefore, step after step, bundles get broken and deformed and single fibers get geometrically curved into particle like inclusions, which can be seen in the microstructure of the ATZ sample.

The same processes will take place during conventional air sintering, except for Joule heating and pistons pressure forces acting inside the material. However, the temperature of the air sintering is 100 °C higher than the maximum SPS experiment temperature, and at this temperature the transformations taking place in the fiber bundles are much faster than those at lower temperatures, because $\gamma \rightarrow \alpha$ alumina transformation temperature is 1200 °C. As a result, no fiber bundles or single fibers in the samples sintered at this temperature can be observed (Fig. 7). All of them are transformed into rounded clusters due to high temperature gradients.

To get a clear idea about the distribution of the bundles and fibers inside the sample and to see the state of the ANFs inside the bulk body, the SEM analysis of the fractured cross-section of the ATZ 1100 °C sample was done. In Fig. 8, micrographs of the fractured cross-section of the sample can be seen.

Fibers are distributed evenly throughout the whole sample, which points out the homogenous mixing of the composite. ANF fibers are embedded into the zirconia matrix and have different lengths and thicknesses. Some of them are tens of microns in length and few micrometers thick. However, most

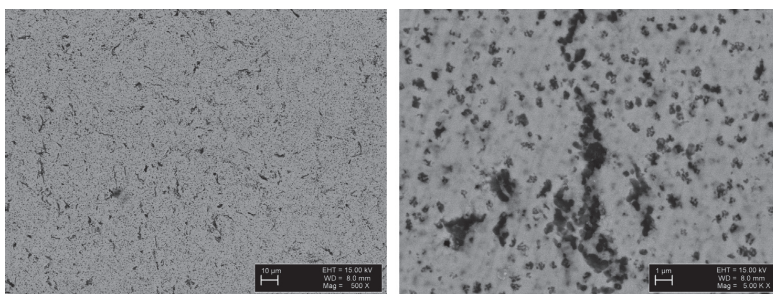


Fig. 7. Microstructure micrographs of the sample sintered at 1300 °C in air.

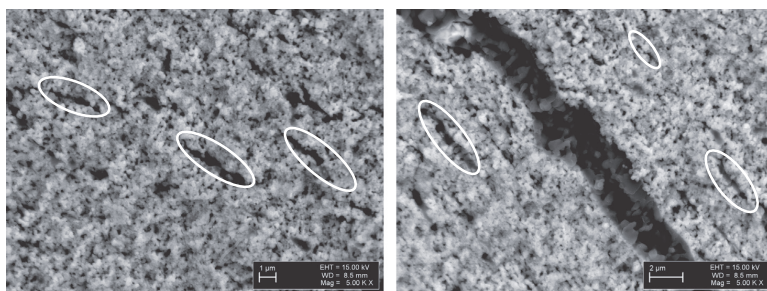


Fig. 8. Fractured cross-section of the ATZ composite sintered at 1100 °C.

Table 1
Properties of the produced specimens.

Specimen (°C)	Density (g/cm ³)	Densification (%)	Hardness (HV10)	Modulus of elasticity (GPa)
1000 SPS	3.17	54	72 ± 5	–
1100 SPS	5.47	93	1035 ± 60	128 ± 24
1200 SPS	5.47	93	754 ± 15	148 ± 18
1300 air	4.35	74	543 ± 25	91 ± 15

of them look the same as on the polished surface. The orientation of the bundles seems to be ordered in one direction. The direction of the bundle alignment is normal to the pistons movement pressure, which is applied in the SPS process. It is difficult to understand which are the pores in the cross-section and which are the alumina inclusions. The elongated inclusions shown in Fig. 8 were identified by the EDS as aluminum and oxygen, which is alumina. However, it is not possible to make precise EDS measurement from the nanosize inclusion that can be seen on the micrograph. Even though, no pores could be seen on the polished surface of the sample, in fractured surface small rounded inclusions look like closed pores, which indicates the undensified state of the sample.

3.5. Properties of the produced specimens

To define the functional suitability of the produced specimens for different applications their properties were measured. The results obtained from the measurements can be seen in Table 1.

As it could be predicted the density of the sample sintered at 1000 °C is very low and can be compared to the density of the green sample pressed at high pressures. The density of the samples sintered at higher temperatures is almost two times higher and crosses the 90% densification level, at which closed porosity is dominant. 93% densification is a low densification degree for the ATZ type of ceramics, but high enough to lead the material to the state of closed porosity. However, this is the first high dense body obtained with ANF material, in which ANFs partially stay in the whiskers state. Density of the sample sintered at 1300 °C in air is much lower than the density of the SPS samples sintered at lower temperatures. The reason for the higher densification degree of the SPS compacts is due to the impact of pressure, Joule heating, and an electrical field diffusion effect which combine together with a high pistons pressure during densification [20].

Values of hardness and elasticity modulus are little bit contradictory for the 1100 °C and 1200 °C samples. The 1100 °C specimen has higher hardness while lower modulus, than the 1200 °C one. Even though 1100 °C specimen has higher

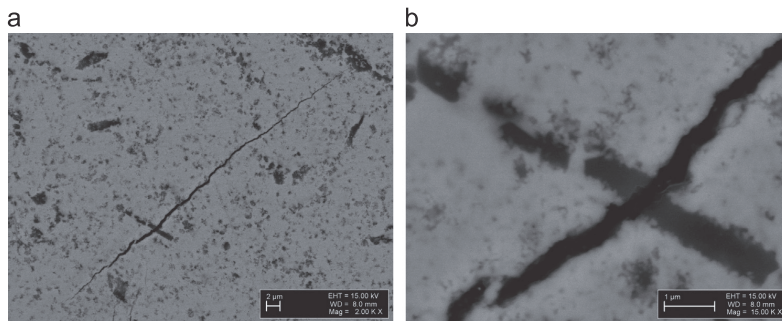


Fig. 9. Crack propagating the matrix and whisker-like ANF inclusion.

hardness it also has high standard deviation, which points to the microstructure inhomogeneity, while the 1200 °C SPSed sample has much lower standard deviation and more predictable behavior. Difference in modulus is not as high as in the case of hardness. Nevertheless, contradictions in these two properties give an idea that the lower temperature sintered specimen has higher hardness but is not as stiff as the higher temperature sintered material. Lower hardness of the 1200 °C sintered specimen can be attributed to the higher amount of ANFs $\alpha \rightarrow \gamma$ phase transformations and their geometrical deformations from whiskers to rounded clusters. It has also been mentioned that alumina starts to dissolve partially (0.2–0.3 wt%) in zirconia from 1200–600 °C, which means that there are additive transformations starting from 1200 °C. These changes influence the microstructure formation and if all the transition processes have not taken place during the sintering cycle, response of the material to the load can be unpredictable. As hardness is very closely related to the strength of the bonding inside the material the weakened interfaces in the case of the 1200 °C specimen result in lowered hardness. The difference in modulus values between the 1100 °C and 1200 °C samples are not as significant as in the case of hardness, indicating that stress–strain behavior of both samples is similar. Hardness and modulus of the sample sintered in air is lower than in the SPSed ones.

One of the ideas of introducing tough whiskers into particulate matrix is to increase its ability to oppose fracture propagation. In Fig. 9, the crack obtained from the Vickers indentation measurement moving through the matrix and then passing through the whisker-like bundle of ANFs can be seen. It should be noticed that movement of the crack is not affected by the ANF inclusion and no crack stopping mechanism takes place, neither crack bridging nor deflection.

The crack prolongs further after meeting the bundle of alumina. This behavior shows that bundles of the ANFs do not act as toughening agents and this could be attributed to the high porosity level between fibers inside the bundle. Another reason for this kind of behavior can be fiber transformation into particle-like inclusion. Nevertheless, it does not mean that random separate fibers located in the matrix will behave the same and that bundle will not have a positive effect on the strength of the composite under the elastic behavior conditions.

4. Conclusion

In this research an ATZ composite containing 10 vol% of novel type γ -ANFs was produced with the help of low temperature SPS sintering and conventional air sintering. Densification behavior of the composite was studied on the densification curves, obtained from the dilatometer and SPS furnaces.

It was shown that the SPS technique allows producing a 93% dense material at 1100 °C and 1200 °C, while conventional air sintering gives density of 74% at 1300 °C.

SEM analysis of the produced specimens' microstructures has shown that ANF bundles and separate fibers are partially in the form of whiskers and partially in the form of rounded transformed clusters. XRD analysis indicates the presence of α -alumina even after sintering at temperatures of 1000 °C under SPS conditions, showing low transformability temperature of nanostructured γ -alumina under SPS conditions. Measurement of the mechanical properties of the specimens has shown that the 1100 °C specimen has noticeably higher hardness (1035 HV10) than the one sintered at 1200 °C (754 HV10), even though the 1200 °C sample has 20 GPa higher elasticity modulus of 148 GPa. Specimen sintered in air had density and hardness lower than both the 1100 °C and 1200 °C specimens.

The whisker-like structure obtained in this study gives a reason for further development of this type of material and finding other ways of dispersing fibers and densifying them to a higher degree.

Acknowledgments

This work was performed within the framework of the research of the Tallinn University of Technology under Grant 8211 and Project AR12133 and the Spanish Science and Technology Agency (CICYT) through the Projects MAT 2010-17753 and MAT 2010-C21088-C03. Authors acknowledge the Archimedes foundation under the Kristjan Jaak scholarship program for funding a part of the research. This work also has been partially supported by graduate school "Functional materials and technologies" which received funding

from the European Social Fund under Project 1.2.0401.09-0079 in Estonia. Authors would also like to thank M. Viljus and R. Traksmaa for their help in making SEM and XRD observations.

References

- [1] H.P. Cahoon, C.J. Cristensen, Sintering and grain growth of alpha-alumina, *J. Am. Ceram. Soc.* 39 (1956) 337–344.
- [2] A.H. De Azua, J. Chevaliera, G. Fantozzia, M. Schehlb, R. Torrecillasb, Crack growth resistance of alumina, zirconia and zirconia toughened alumina ceramics for joint prostheses, *Biomaterials* 23 (2002) 937–945.
- [3] R. Benzaid, J. Chevalier, M. Saa daoui, G. Fantozzi, M. Nawa, L.A. Diaz, R. Torrecillas, Fracture toughness, strength and slow crack growth in a ceria stabilized zirconia–alumina nanocomposite for medical applications, *Biomaterials* 29 (2008) 3636–3641.
- [4] J. Wang, R. Stevens, Review zirconia-toughened alumina (ZTA) ceramics, *J. Mater. Sci.* 24 (1989) 3421–3440.
- [5] P. Bansal Narottam, R. Choi Sung, Processing of Alumina-Toughened Zirconia Composites, National Aeronautics and Space Administration Glenn Research Center, Cleveland, 2003.
- [6] J. Corrochanoa, C. Cerecedob, V. Valcárcelb, M. Lieblich, F. Guitiánb, Whiskers of Al_2O_3 as reinforcement of a powder metallurgical 6061 aluminium matrix composite, *Mater. Lett.* 62 (2008) 103–105.
- [7] R. Knibbe, G.J. Aachterlonie, T. Mori, A. Lashtabeg, J. Drennan, Glass-phase movement in yttria-stabilized zirconia/alumina composites, *J. Am. Ceram. Soc.* 93 (2010) 1494–1500.
- [8] C. Wang, H. Yong, Z. Hongxiang, The effect of whisker orientation in SiC whisker-reinforced Si_3N_4 ceramic matrix composites, *J. Eur. Ceram. Soc.* 19 (1999) 1903–1909.
- [9] M. Aghayan, I. Hussainova, M. Gasik, M. Kutuzov, M. Friman, Coupled thermal analysis of novel alumina nanofibers with ultrahigh aspect ratio, *Thermochim. Acta* 574 (2013) 140–144.
- [10] M. Suárez, A. Fernández, J.L. Menéndez, R. Torrecillas, H.U. Kessel, et al., Challenges and opportunities for spark plasma sintering: a key technology for a new generation of materials, in: B. Ertuğ (Ed.), *Sintering Applications*, InTech, Rijeka, 2013, pp. 320–338.
- [11] E. Kannisto, E. Cura, E. Levänen, S.-P. Hannula, Mechanical properties of alumina based nanocomposites, *Key Eng. Mater.* 527 (2012) 101–106.
- [12] N. Voltsihhin, I. Hussainova, E. Cura, S.-P. Hannula, R. Traksmaa, Densification and microstructure development in zirconia toughened hardmetals, *Key Eng. Mater.* 527 (2012) 50–55.
- [13] DIN 50359, Testing of metallic materials – universal hardness testing – Part 1, 1997, p. 10.
- [14] N. Voltsihhin, I. Hussainova, M. Viljus, Influence of precursor zirconium carbide powders on the properties of the spark plasma sintered ceramic composite materials, *Ceram. Eng. Sci. Proc.* 34 (2013).
- [15] J. Tarazonaa, J.Y. Heb, T. Butlerb, F. Castroa, J. Echeberria, Sinter-HIP of a-alumina powders with sub-micron grain sizes, *J. Eur. Ceram. Soc.* 22 (2002) 1801–1809.
- [16] N. Voltsihhin, E. Cura, I. Hussainova, S.-P. Hannula, Sintering routes for zirconia doped hardmetals, in: T. Otto (Ed.), *Proceedings of the 8th International Conference of DAAAM Baltic Industrial Engineering*, Tallinn, 2012, pp. 765–770.
- [17] A. Zavaliangos, J. Zhang, M. Krammer, J.R. Groza, Temperature evolution during field activated sintering, *Mater. Sci. Eng. A: Struct.* 379 (2004) 218–228.
- [18] E.A. Olevisky, S. Kandukuri, L. Froyen, Consolidation enhancement in spark-plasma sintering: impact of high heating rates, *J. Appl. Phys.* 102 (2007) 114913.
- [19] J. Zhao, J.E. Garay, U. Anselmi-Tamburini, Z.A. Munir, Directional electromigration-enhanced inter-diffusion in the Cu–Ni system, *J. Appl. Phys.* 102 (2007) 114902.
- [20] J.E. Garay, Current-activated, pressure-assisted densification of materials, *Ann. Rev. Mater. Res.* 40 (2010) 445–468.

**DISSERTATIONS DEFENDED AT
TALLINN UNIVERSITY OF TECHNOLOGY ON
*MECHANICAL ENGINEERING***

1. **Jakob Kübarsepp**. Steel-Bonded Hardmetals. 1992.
2. **Jakub Kõo**. Determination of Residual Stresses in Coatings & Coated Parts. 1994.
3. **Mart Tamre**. Tribocharacteristics of Journal Bearings Unlocated Axis. 1995.
4. **Paul Kallas**. Abrasive Erosion of Powder Materials. 1996.
5. **Jüri Pirso**. Titanium and Chromium Carbide Based Cermets. 1996.
6. **Heinrich Reshetnyak**. Hard Metals Serviceability in Sheet Metal Forming Operations. 1996.
7. **Arvi Kruusing**. Magnetic Microdevices and Their Fabrication methods. 1997.
8. **Roberto Carmona Davila**. Some Contributions to the Quality Control in Motor Car Industry. 1999.
9. **Harri Annuka**. Characterization and Application of TiC-Based Iron Alloys Bonded Cermets. 1999.
10. **Irina Hussainova**. Investigation of Particle-Wall Collision and Erosion Prediction. 1999.
11. **Edi Kulderknup**. Reliability and Uncertainty of Quality Measurement. 2000.
12. **Vitali Podgurski**. Laser Ablation and Thermal Evaporation of Thin Films and Structures. 2001.
13. **Igor Penkov**. Strength Investigation of Threaded Joints Under Static and Dynamic Loading. 2001.
14. **Martin Eerme**. Structural Modelling of Engineering Products and Realisation of Computer-Based Environment for Product Development. 2001.
15. **Toivo Tähemaa**. Assurance of Synergy and Competitive Dependability at Non-Safety-Critical Mechatronics Systems design. 2002.
16. **Jüri Resev**. Virtual Differential as Torque Distribution Control Unit in Automotive Propulsion Systems. 2002.
17. **Toomas Pihl**. Powder Coatings for Abrasive Wear. 2002.
18. **Sergei Letunovitš**. Tribology of Fine-Grained Cermets. 2003.
19. **Tatyana Karaulova**. Development of the Modelling Tool for the Analysis of the Production Process and its Entities for the SME. 2004.
20. **Grigori Nekrassov**. Development of an Intelligent Integrated Environment for Computer. 2004.
21. **Sergei Zimakov**. Novel Wear Resistant WC-Based Thermal Sprayed Coatings. 2004.

22. **Irina Preis.** Fatigue Performance and Mechanical Reliability of Cemented Carbides. 2004.
23. **Medhat Hussainov.** Effect of Solid Particles on Turbulence of Gas in Two-Phase Flows. 2005.
24. **Frid Kaljas.** Synergy-Based Approach to Design of the Interdisciplinary Systems. 2005.
25. **Dmitri Neshumayev.** Experimental and Numerical Investigation of Combined Heat Transfer Enhancement Technique in Gas-Heated Channels. 2005.
26. **Renno Veinthal.** Characterization and Modelling of Erosion Wear of Powder Composite Materials and Coatings. 2005.
27. **Sergei Tisler.** Deposition of Solid Particles from Aerosol Flow in Laminar Flat-Plate Boundary Layer. 2006.
28. **Tauno Otto.** Models for Monitoring of Technological Processes and Production Systems. 2006.
29. **Maksim Antonov.** Assessment of Cermets Performance in Aggressive Media. 2006.
30. **Tatjana Barashkova.** Research of the Effect of Correlation at the Measurement of Alternating Voltage. 2006.
31. **Jaan Kers.** Recycling of Composite Plastics. 2006.
32. **Raivo Sell.** Model Based Mechatronic Systems Modeling Methodology in Conceptual Design Stage. 2007.
33. **Hans Rämmal.** Experimental Methods for Sound Propagation Studies in Automotive Duct Systems. 2007.
34. **Meelis Pohlak.** Rapid Prototyping of Sheet Metal Components with Incremental Sheet Forming Technology. 2007.
35. **Priidu Peetsalu.** Microstructural Aspects of Thermal Sprayed WC-Co Coatings and Ni-Cr Coated Steels. 2007.
36. **Lauri Kollo.** Sinter/HIP Technology of TiC-Based Cermets. 2007.
37. **Andrei Dedov.** Assessment of Metal Condition and Remaining Life of In-service Power Plant Components Operating at High Temperature. 2007.
38. **Fjodor Sergejev.** Investigation of the Fatigue Mechanics Aspects of PM Hardmetals and Cermets. 2007.
39. **Eduard Ševtšenko.** Intelligent Decision Support System for the Network of Collaborative SME-s. 2007.
40. **Rünno Lumiste.** Networks and Innovation in Machinery and Electronics Industry and Enterprises (Estonian Case Studies). 2008.
41. **Kristo Karjust.** Integrated Product Development and Production Technology of Large Composite Plastic Products. 2008.
42. **Mart Saarna.** Fatigue Characteristics of PM Steels. 2008.

43. **Eduard Kimmari**. Exothermically Synthesized B₄C-Al Composites for Dry Sliding. 2008.
44. **Indrek Abiline**. Calibration Methods of Coating Thickness Gauges. 2008.
45. **Tiit Hindreus**. Synergy-Based Approach to Quality Assurance. 2009.
46. **Karl Raba**. Uncertainty Focused Product Improvement Models. 2009.
47. **Riho Tarbe**. Abrasive Impact Wear: Tester, Wear and Grindability Studies. 2009.
48. **Kristjan Juhani**. Reactive Sintered Chromium and Titanium Carbide-Based Cermets. 2009.
49. **Nadežda Dementjeva**. Energy Planning Model Analysis and Their Adaptability for Estonian Energy Sector. 2009.
50. **Igor Krupenski**. Numerical Simulation of Two-Phase Turbulent Flows in Ash Circulating Fluidized Bed. 2010.
51. **Aleksandr Hlebnikov**. The Analysis of Efficiency and Optimization of District Heating Networks in Estonia. 2010.
52. **Andres Petritšenko**. Vibration of Ladder Frames. 2010.
53. **Renee Joost**. Novel Methods for Hardmetal Production and Recycling. 2010.
54. **Andre Gregor**. Hard PVD Coatings for Tooling. 2010.
55. **Tõnu Roosaar**. Wear Performance of WC- and TiC-Based Ceramic-Metallic Composites. 2010.
56. **Alina Sivitski**. Sliding Wear of PVD Hard Coatings: Fatigue and Measurement Aspects. 2010.
57. **Sergei Kramanenko**. Fractal Approach for Multiple Project Management in Manufacturing Enterprises. 2010.
58. **Eduard Latõsov**. Model for the Analysis of Combined Heat and Power Production. 2011.
59. **Jürgen Riim**. Calibration Methods of Coating Thickness Standards. 2011.
60. **Andrei Surzhenkov**. Duplex Treatment of Steel Surface. 2011.
61. **Steffen Dahms**. Diffusion Welding of Different Materials. 2011.
62. **Birthe Matsi**. Research of Innovation Capacity Monitoring Methodology for Engineering Industry. 2011.
63. **Peeter Ross**. Data Sharing and Shared Workflow in Medical Imaging. 2011.
64. **Siim Link**. Reactivity of Woody and Herbaceous Biomass Chars. 2011.
65. **Kristjan Plamus**. The Impact of Oil Shale Calorific Value on CFB Boiler Thermal Efficiency and Environment. 2012.
66. **Aleksei Tšinjan**. Performance of Tool Materials in Blanking. 2012.
67. **Martinš Sarkans**. Synergy Deployment at Early Evaluation of Modularity of the Multi-Agent Production Systems. 2012.

68. **Sven Seiler**. Laboratory as a Service – A Holistic Framework for Remote and Virtual Labs. 2012.
69. **Tarmo Velsker**. Design Optimization of Steel and Glass Structures. 2012.
70. **Madis Tiik**. Access Rights and Organizational Management in Implementation of Estonian Electronic Health Record System. 2012.
71. **Marina Kostina**. Reliability Management of Manufacturing Processes in Machinery Enterprises. 2012.
72. **Robert Hudjakov**. Long-Range Navigation for Unmanned Off-Road Ground Vehicle. 2012.
73. **Arkadi Zikin**. Advanced Multiphase Tribo-Functional PTA Hardfacings. 2013.
74. **Alar Konist**. Environmental Aspects of Oil Shale Power Production. 2013.
75. **Inge Roos**. Methodology for Calculating CO₂ Emissions from Estonian Shale Oil Industry. 2013.
76. **Dmitri Shvarts**. Global 3D Map Merging Methods for Robot Navigation. 2013.
77. **Kaia Lõun**. Company's Strategy Based Formation of e-Workplace Performance in the Engineering Industry. 2013.
78. **Maido Hiiemaa**. Motion Planner for Skid-Steer Unmanned Ground Vehicle. 2013.
79. **Dmitri Goljandin**. Disintegrator Milling System Development and Milling Technologies of Different Materials. 2013.
80. **Dmitri Aleksandrov**. Light-Weight Multicopter Structural Design for Energy Saving. 2013.
81. **Henrik Herranen**. Design Optimization of Smart Composite Structures with Embedded Devices. 2014.
82. **Heiki Tiikoja**. Experimental Acoustic Characterization of Automotive Inlet and Exhaust System. 2014.
83. **Jelena Priss**. High Temperature Corrosion and Abrasive Wear of Boiler Steels. 2014.
84. **Aare Aruniit**. Thermoreactive Polymer Composite with High Particulate Filler Content. 2014.
85. **Dmitri Gornostajev**. Development of the Calculation Method for Barge Hull. 2014.
86. **Liina Lind**. Wear of PVD Coatings on Fineblanking Punches. 2014.